NAVAL POSTGRADUATE SCHOOL

MONTEREY, CALIFORNIA

DISSERTATION

CROSS-SHORE EXCHANGE ON NATURAL BEACHES

by

Jenna A. Brown

September 2014

Dissertation Supervisor: Jamie H. MacMahan

Approved for public release; distribution is unlimited

THIS PAGE INTENTIONALLY LEFT BLANK

REPORT DOCUMENTATION PAGE

Form Approved OMB No. 0704-0188

1. AGENCY USE ONLY *(Leave blank)*	**2. REPORT DATE** September 2014	**3. REPORT TYPE AND DATES COVERED** Dissertation

4. TITLE AND SUBTITLE
CROSS-SHORE EXCHANGE ON NATURAL BEACHES

5. FUNDING NUMBERS

6. AUTHOR(S) Jenna A. Brown

7. PERFORMING ORGANIZATION NAME(S) AND ADDRESS(ES)
Naval Postgraduate School
Monterey, CA 93943-5000

8. PERFORMING ORGANIZATION REPORT NUMBER

9. SPONSORING /MONITORING AGENCY NAME(S) AND ADDRESS(ES)
N/A

10. SPONSORING/MONITORING AGENCY REPORT NUMBER

11. SUPPLEMENTARY NOTES The views expressed in this thesis are those of the author and do not reflect the official policy or position of the Department of Defense or the U.S. Government. IRB Protocol number ____N/A____.

12a. DISTRIBUTION / AVAILABILITY STATEMENT
Approved for public release; distribution is unlimited

12b. DISTRIBUTION CODE

13. ABSTRACT (maximum 200 words)
The cross-shore exchange of material is examined on beaches of varying morphology and hydrodynamics. On a dissipative, rip-channeled beach in Monterey, California, field measurements of the rip current vertical structure reveal depth-uniform flows inside the surf zone, and surface-dominated flows with rotation over depth outside the surf zone. Aperiodic, very low frequency pulsations in the near-surface velocity were found to control the mean rip current flow. Observations of Lagrangian surface drifters released on the inner shelf resulted in a new theory of material transport on a rip-channeled beach, where rip current pulses episodically expel material offshore through rip channels, and momentum-driven surfzone circulations pull the material back onshore over shoals to satisfy a mass balance, with no material being completely removed from the nearshore system. Advection and diffusion processes on a steep, reflective beach at Carmel River State Beach, California, are also investigated using measurements of the temporal and spatial evolution of dye released in the surf zone. A net offshore transport did exist, and the mixing and transport processes inside and outside the surf zone were independent. Overall, this work provides new insights into the fate of material transported between the surf zone and inner shelf on natural beaches.

14. SUBJECT TERMS cross-shore exchange; rip current; steep beach; Eulerian; Lagrangian; drifters; dye; mixing; transport; dispersion; diffusion; advection	**15. NUMBER OF PAGES** 161
	16. PRICE CODE

17. SECURITY CLASSIFICATION OF REPORT	**18. SECURITY CLASSIFICATION OF THIS PAGE**	**19. SECURITY CLASSIFICATION OF ABSTRACT**	**20. LIMITATION OF ABSTRACT**
Unclassified	Unclassified	Unclassified	UU

NSN 7540-01-280-5500

Standard Form 298 (Rev. 2-89)
Prescribed by ANSI Std. 239-18

THIS PAGE INTENTIONALLY LEFT BLANK

Approved for public release; distribution is unlimited

CROSS-SHORE EXCHANGE ON NATURAL BEACHES

Jenna A. Brown
Civilian, Department of Defense
B.S., The Ohio State University, 2006
M.S., University of Delaware, 2009

Submitted in partial fulfillment of the
requirements for the degree of

DOCTOR OF PHILOSOPHY IN PHYSICAL OCEANOGRAPHY

from the

NAVAL POSTGRADUATE SCHOOL
September 2014

Author: Jenna A. Brown

Approved by:

Jamie H. MacMahan Professor of Oceanography Dissertation Supervisor	Ad J. H. M. Reniers Professor of Coastal Engineering
Edward B. Thornton Professor of Oceanography (Emer.)	Timothy P. Stanton Research Professor of Oceanography
Jeffrey Paduan Professor of Oceanography	Wendell A. Nuss Professor of Meteorology

Approved by: Peter Chu, Chair, Department of Oceanography

Approved by: Douglas Moses, Vice Provost for Academic Affairs

THIS PAGE INTENTIONALLY LEFT BLANK

ABSTRACT

The cross-shore exchange of material is examined on beaches of varying morphology and hydrodynamics. On a dissipative, rip-channeled beach in Monterey, California, field measurements of the rip current vertical structure reveal depth-uniform flows inside the surf zone, and surface-dominated flows with rotation over depth outside the surf zone. Aperiodic, very low frequency pulsations in the near-surface velocity were found to control the mean rip current flow. Observations of Lagrangian surface drifters released on the inner shelf resulted in a new theory of material transport on a rip-channeled beach, where rip current pulses episodically expel material offshore through rip channels, and momentum-driven surfzone circulations pull the material back onshore over shoals to satisfy a mass balance, with no material being completely removed from the nearshore system. Advection and diffusion processes on a steep, reflective beach at Carmel River State Beach, California, are also investigated using measurements of the temporal and spatial evolution of dye released in the surf zone. A net offshore transport did exist, and the mixing and transport processes inside and outside the surf zone were independent. Overall, this work provides new insights into the fate of material transported between the surf zone and inner shelf on natural beaches.

THIS PAGE INTENTIONALLY LEFT BLANK

TABLE OF CONTENTS

LIST OF FIGURES

LIST OF TABLES

THIS PAGE INTENTIONALLY LEFT BLANK

LIST OF ACRONYMS AND ABBREVIATIONS

1-D	one-dimensional
2-D	two-dimensional
3-D	three-dimensional
3HRLT	three-hour low tide (3-hour time window, centered on low tide)
ADCP	acoustic Doppler current profiler
ADV	acoustic Doppler velocimeter
CTD	conductivity, temperature, and depth
CRSB	Carmel River State Beach
dof	degrees of freedom
EMCM	Electromagnetic current meter
GPS	Global Positioning System
hr	hours
Hz	hertz
IG	infragravity
km	kilometers
LCS	Lagrangian Coherent Structure
m	meters
min	minutes
MSL	mean sea level
NDBC	National Data Buoy Center
NOS	National Ocean Service
O( )	on the order of... (used to denote approximate magnitude)

pdf	probability distribution function
RCEX	Rip Current EXperiment
rms	root-mean-square
s	seconds
SS	sea-swell
SZE	surf zone eddy
VLF	very low frequency

ACKNOWLEDGMENTS

I would like to express my sincere and heartfelt thanks to my advisor, Jamie MacMahan, for his patience and guidance and endless support over the past eight years. You have given me the opportunity to travel the world and play at the beach, and you have helped me find my passion. Thank you for being a wonderful advisor and a good friend. I look forward to working together in the future.

I would also like to give my genuine thanks to my co-advisor, Ad Reniers, for his guidance and support throughout my academic career. Thank you for your patience and for sharing your vast knowledge of numerical modeling and nearshore processes with me. Thank you for welcoming me into your home and your family on my trips to Miami, I appreciate you as a mentor and a friend.

It has been an honor to have Ed Thornton as a mentor; I appreciate your honest advice and encouragement. Thank you for all of the time you spent editing my papers, your red ink and expertise has greatly improved the overall quality of my research.

Edie Gallagher, you are like a big sister to me, and I will always look to you for advice, both work- and life-related. I hope we have many more good times together in the future.

I have to thank everyone that I have worked in the field with, not only for helping to collect some pretty awesome data sets, but also for making the experience in the field enjoyable and unforgettable.

To my closest friends, thank you for giving me an enjoyable work-life balance! BR, thank you for your strength and encouragement; you are my biggest fan and I hope to make you proud.

Lastly, I would like to thank my parents and family for their continual and absolute support. Mom and Dad, you have always encouraged me to follow my dreams, even all the way to California. You taught me to believe in myself, and it is because of your love and encouragement that I am who I am and have accomplished the things that I today.

THIS PAGE INTENTIONALLY LEFT BLANK

I. INTRODUCTION

The transport of material, including suspended sediment, pollutants, biological matter, and nutrients, across the surf zone and the continental shelf has a significant impact on beach composition, water quality, and ecosystem stability. Pollution in the ocean is an environmental hazard, degrading ecosystems and harming wildlife, as well as a human health hazard. Land-based pollution, including agricultural run-off and fecal matter, enters the ocean in the surf zone by means of run-off, storm drains, and coastal tributaries (Culliton 1998; Schiff et al. 2000; Grant et al. 2001), where it can then be carried offshore into the inner continental shelf. Nutrients are supplied to continental shelf ecosystems, which are some of the most productive on Earth, via cross-shore exchange between the surf zone and the inner shelf (Falkowski et al. 1998). Harmful algae blooms and offshore operational discharges, such as oil, originate on the inner shelf and are transported into the surf zone (Anderson 2009). Cross-shore exchange on natural beaches plays an important role in all of these processes; however, it remains poorly understood.

Onshore and offshore exchange occurs by various processes, depending on beach morphology, beach slope, wave conditions, and resulting current patterns. In this work, cross-shore exchange is investigated on a dissipative, alongshore-inhomogeneous, rip-channeled beach, and on a reflective, alongshore-homogeneous, steep beach. Dissipative beaches are defined as having low-sloping profiles and relatively wide surf zones, where waves break well offshore and continue to lose energy as they travel as spilling breakers onshore. The type of dissipative beach examined in this work is the transverse bar and rip state, where the transverse bars are relatively dissipative and strong rip currents occur in the deeper embayments. Dissipative, sandy beaches are popular recreation sites. Reflective beaches are characterized as having a steep (slope $\geq$ 1/10), usually linear, beach face, and a considerably shallower sloping profile seaward of the step. Steep beaches typically have plunging to surging breakers and very narrow surf zones, sometimes confined to the zone of run-up on the beach face. Reflective beaches commonly include rocky shorelines where biology and organisms commonly dwell.

Understanding the transport and retention of hazardous pollutants and biological matter on these beaches is important for reasons ranging from human health factors to sustaining ecosystems.

The cross-shore exchange of material due to the complex circulation patterns on a dissipative, rip-channeled beach is investigated in Chapters II and III. Rip currents are defined as strong seaward-directed flows and are generally coupled to the underlying beach morphology, characterized by deeper, cross-shore oriented, incised channels in shallower, shore-connected shoals or bars. Rip currents typically occur when waves approach the coast shore-normally, and alongshore perturbations in the bottom topography induce alongshore variations in the depth-induced wave breaking, leading to alongshore gradients in pressure and momentum driving water from the shoals toward the rip channels (Bowen 1969). A nearshore circulation system exists where broader regions of wave-driven, onshore-directed flows over the shoals transition to alongshore-directed feeder currents near the shoreline, which converge at the base of the rip channel and flow seaward as a rip current. Rip currents commonly occur in some variation, on most beaches, and have been observed in nature and studied extensively for many years (e.g., Shepard 1936; Shepard et al. 1941; Smith and Largier 1995; Brander and Short 2001; MacMahan et al. 2005). However, it still remains largely unknown how these currents act as a transport mechanism, both temporally and spatially, between the surf zone and the inner shelf.

The vertical structure of the seaward-flowing rip current can have a significant effect on the volumetric estimates of exchange on rip-channeled beaches, and is examined in Chapter II. Field measurements within the surf zone obtained by MacMahan et al. (2005) indicate the rip current vertical profile is depth-uniform below the wave trough, with a significant amount of vertical shear in the wave crest-trough area due to the presence of waves and onshore Stokes drift countering the offshore rip current flow. These findings support the laboratory investigation performed by Haas and Svendsen (2002) of rip current vertical structure. Inside of the rip channel where waves were breaking, the rip currents were nearly depth-uniform, whereas outside of the surf zone there were strong depth variations in the flow, with strong seaward velocities in the upper

water column and weak seaward or shoreward velocities near the bottom. An extensive set of field measurements obtained at Monterey, California, of vertical profiles of rip current flows inside and outside the surf zone over a range of wave and tide conditions are presented in Chapter II, which supplement the very limited number of existing rip current profile measurements, particularly offshore of the surf zone. The variation of the magnitude and rotation of the rip current flows over depth are examined.

Conventional rip current theory suggests that seaward flowing rip currents are the compensating return flow that balances the shoreward Stokes drift, which continuously transports water into the surf zone. Rip currents have long been believed to extend far offshore, and thereby be a means of continuously transporting material out of the surf zone (Shepard et al. 1941; Inman and Brush 1973). However, MacMahan et al. (2010) deployed a fleet of position-tracking surfzone drifters in different open coast beach rip current systems and obtained spatially synoptic estimates of rip current flow patterns. The results revealed semi-enclosed, large-scale vortices that were contained within the surf zone and largely retained drifters. Smith and Largier (1995) used a sector-scanning Doppler sonar to observe jets of water extending seaward from the surf zone (rip currents) and determined that the rip currents occurred episodically and recurred aperiodically, lasting several minutes each. The estimated flushing time due to the rip currents was on the order of 3 hours.

Rip current surfzone retention and exchange evaluated with a three-dimensional (3-D) numerical model demonstrated the importance of including Stokes drift and very low frequency (VLF) motions to accurately describe the behavior of rip current exits (Reniers et al. 2009; Reniers et al. 2010), where excluding Stokes drift or VLF motions resulted in an over or under estimation, respectively, of drifter exits (Reniers et al. 2009). These studies did not investigate the fate of the material (drifters) that was transported outside the surf zone by the rip currents. Talbot and Bate (1987) obtained qualitative aerial observations of dye released in rip currents and examined exchange rips that discharged dye offshore of the breaker line, which either travelled a short distance past the breaker line and was recycled into the surf zone within seconds, or moved up to 2 km beyond the breaker line and then moved alongshore and sometimes re-entered the surf

zone. MacMahan et al. (2010) found similar results, where drifters that did episodically exit the surf zone were transported about 2 surfzone widths offshore from the shoreline, and occasionally some re-entered the surf zone; drifters that were retained within the surf zone were concentrated in the rip current vortices, and were less likely to be transported offshore due to the coupling of the rip current vortex to the underlying morphology. Reniers et al. (2010) used the 3-D numerical model to produce Lagrangian Coherent Structures (LCSs) within rip current pulse surface velocity fields. LCSs represent transport barriers hidden in the flow that control the motion of passively advected particles in unsteady flows. Examining the LCSs, the occasional drifter exit from the surf zone was shown to be due to VLF eddy motions, which detach from the nearshore rip current circulation cell when the VLFs extend beyond the surf zone. Therefore, VLFs were suggested to form the dominant exchange mechanism between the surf zone and the inner shelf. Field measurements of VLF pulsations in rip current velocity and their effect on the magnitude and vertical structure of the mean rip current flow are investigated in Chapter II.

Material transport and cross-shore exchange are investigated on a rip-channeled beach using field observations of position-tracking drifters and dye as tracers in Chapters III and IV, respectively. Observations of drifters released on the inner shelf of the rip-channeled beach in Monterey, California, are examined in Chapter III. The fate of material that exits the surf zone is evaluated, including the cross-shore extent and the on and offshore movement between the surf zone and inner shelf of the drifters, and it was found that no drifters completely left the nearshore region. A new theory of how material is exchanged within the nearshore region on a rip-channeled beach is presented in Chapter III, where the mass transported offshore by the rip current exits is balanced by the surfzone rip current circulations over the shoals pulling material back into the surf zone. Observations of dye released inside the surf zone on a rip-channeled beach in Destin, Florida, are examined in Chapter IV. *In-situ* measurements of dye concentration in a rip channel reveal VLF pulses in the seaward flowing rip current, and aerial images of the temporal and spatial evolution of the dye reveal the advection and diffusion processes associated with the rip current circulation system and that the dye is not

completely removed from the nearshore system. The combination of the measurements are used to estimate surfzone flushing times, times for surfzone re-entry of material transported offshore, and mass transport quantities for a rip-channeled beach.

The transport mechanisms and exchange behavior on a reflective, alongshore-homogeneous, steep beach is examined in Chapter IV. There is almost no field data on how wave reflection from the beach impacts the cross-shore movement of material. Previous dye tracer studies of surfzone mixing and material transport on wide, dissipative, alongshore-homogeneous beaches with milder beach slopes (Harris et al. 1963; Inman et al. 1971; Boehm 2003; Grant et al. 2005; Clarke et al. 2007) may be applicable to reflective, steep beaches. Dye released in the surf zone dispersed 2-D horizontally by advection and diffusion until the surf zone was saturated (Harris et al. 1963; Inman et al. 1971; Clarke et al. 2007; Clark et al. 2010), then was predominantly advected by the alongshore current and transported alongshore, becoming one-dimensional (1-D) in the alongshore direction (Harris et al. 1963; Inman et al. 1971; Grant et al. 2005; Clarke et al. 2007; Clark et al. 2010). The alongshore volumetric flux of water was found to be 50 times greater than the cross-shore volumetric flux (Grant et al. 2005). The results suggest that most of the material remains within the surf zone and travels alongshore between the shoreline and active wave breaking with only a small amount of cross-shore exchange occurring continuously across the surfzone boundary. By evaluating the surfzone diffusivity, Clark et al. (2010) found that horizontal rotational motions with length-scales of the surfzone width or less are important for cross-shore tracer dispersion in the surf zone. Field measurements of surfzone mixing and transport, and cross-shore exchange across the surfzone boundary on a sandy, steep, reflective beach at Carmel River State Beach, California, are described in Chapter IV for a range of wave and alongshore flow conditions. Fluorescent Rhodamine dye was released as a slug in the surf zone, and the temporal and spatial evolution was measured. The advection and diffusion processes inside the surf zone and across the surfzone boundary are described and estimates of the amount of cross-shore exchange are given.

A summary of the findings from the field investigations of cross-shore exchange on natural beaches is given in Chapter V. The mixing and transport processes on the

dissipative, alongshore-inhomogeneous, rip-channeled beach at Monterey, California, will be contrasted to those on the steep, reflective beach at Carmel River State Beach, California. Overall, the results from this work provide a better understanding of the cross-shore exchange between the surf zone and inner shelf on natural sandy beaches, including new insights into the fate of material transported offshore of the surf zone on dissipative and reflective beaches.

II. VERTICAL STRUCTURE OF RIP CURRENTS

A. INTRODUCTION

Rip currents are commonly known to be a mechanism for transporting material, such as sediments, pollutants, biological matter, and even people, out of the surf zone. Numerous field studies have been performed focusing on the temporal and spatial aspects of rip current transport (Shepard and Inman 1950; Sonu 1972; Talbot and Bate 1987; Brander and Short 2001; MacMahan et al. 2010a; amongst others), with many recent studies using Lagrangian drifters to examine the surface transport associated with rip currents (Johnson and Pattiaratchi 2004b; Spydell et al. 2007; Brown et al. 2009; Austin et al. 2010). In particular, several field experiments were performed at the same field site on a rip-channeled beach at Monterey, California (MacMahan et al. 2004a,b; MacMahan et al. 2005; Brown et al. 2009; MacMahan et al. 2010a), and numerous numerical modeling efforts have focused on simulating results from these experiments (Reniers et al. 2007, 2009, 2010), which have greatly increased the understanding of rip current dynamics. While the horizontal circulation flow pattern and surface transport of rip currents is becoming increasingly better understood, limited field measurements of the vertical structure and sub-surface transport of the rip current as it moves offshore and outside of the surf zone exist, which is critical for accurately describing the three-dimensional (3-D) material transport behavior of rip current circulations.

In this work, field measurements of rip current velocities throughout the water column, both inside and outside of the surf zone, obtained at the same field site at Monterey, California, are evaluated to examine the temporal and depth variation of rip current flows. The results presented here will be given in context to the past work examining the role of very low frequency (VLF) motions as the dominant mechanism responsible for rip current transport out of the surf zone, as well as to previous field and laboratory measurements of the vertical structure of rip currents, which are discussed next. The goal of this work is to evaluate the presence of VLF pulsations and their effect on the mean rip current flow, and to use the measurements of the rip current vertical structure inside and outside the surf zone to describe how material is transported offshore

via rip currents. Ultimately, these findings will contribute to the existing knowledge of rip current exchange.

B. BACKGROUND

1. Rip Current Dynamics

Rip currents are defined as strong seaward-directed flows and are part of a dynamic nearshore circulation system. On open coast beaches, they are generally coupled to the underlying beach morphology, characterized by deeper, cross-shore oriented, incised channels in shallower, shore-connected shoals or bars (MacMahan et al. 2006). Morphologically controlled rip currents occur when waves approach the coast shore-normally, and alongshore perturbations in the bottom topography induce alongshore variations in the depth-induced wave breaking, leading to alongshore gradients in pressure and momentum driving water from the shoals toward the rip channels (Bowen 1969; Haller et al. 2002). A circulation pattern exists where broad regions of wave-driven, onshore-directed flows over the shoals transition to alongshore-directed feeder currents near the shoreline, which converge at the base of the rip channel and flow seaward as a rip current. Mean rip current velocities increase with increasing wave height (Shepard 1936; Shepard et al. 1941; Shepard and Inman 1950; MacMahan et al. 2005), and are tidally modulated, with decreases in tidal elevation resulting in increases in rip current flows (Shepard and Inman 1950; Sonu 1972; Aagard et al. 1997; Brander and Short 2001; MacMahan et al. 2005). The interaction between the seaward-flowing rip current and the incident waves has an influence on the offshore transport, where a negative feedback exists with the waves reducing the strength and offshore extent of the rip current (Yu and Slinn 2003). An understanding of the vertical structure of the rip current is necessary to understand the near-surface wave effects on the vertically varying rip current flow, which influences the vertical structure of the mean cross-shore current (Uchiyama et al. 2010).

Spatially synoptic estimates of rip current circulation and Lagrangian transport by MacMahan et al. (2010a) provided field evidence that rip currents are semi-enclosed, large-scale vortices that are largely contained within the surf zone. The rip current

circulations resulted in a high amount of surfzone retention, with only episodic transport offshore (19% of drifters exited the surf zone per hour, on average). These observations were corroborated by drifter measurements in a laboratory experiment by Castelle et al. (2010) examining rip current circulations forced by irregular, shore-normal incident waves propagated over a moveable bed. Reniers et al. (2009, 2010) found that VLF motions in the rip current flow are the dominant mechanism responsible for the occasional surf zone exit. These energetic motions for frequencies less than 0.004 Hz have been observed in rip current flows in the field on many beaches (Smith and Largier 1995; Brander and Short 2001; MacMahan et al. 2004b), and are mostly confined to the surf zone corresponding to surfzone eddies (SZEs) (MacMahan et al. 2004b). Several mechanisms have been investigated for the generation of VLF motions inside the surf zone, including shear instabilities of the rip current (Haller and Dalrymple 2001; Reniers et al. 2007; Bruneau et al. 2009) and wave group forcing (Reniers et al. 2007; Long and Ozkan-Haller 2009). Using a numerical model, Reniers et al. (2007) input various types of wave forcing (monochromatic, bichromatic, random waves) and found that forcing by directionally broad random waves best explained the high VLF intensity inside the surf zone and rapid decay outside the surf zone observed by MacMahan et al. (2004b). The incident wave energy appeared as random spatial blobs, and the spatially varying breaking waves on the wave group timescale (O(10 minutes)) were responsible for forcing the VLF motions (Reniers et al. 2007; MacMahan et al. 2010a). The VLFs are outside the gravity restoring region in frequency-wavenumber space, indicating they are horizontal vortices (i.e., SZEs). The VLF energy occurs at alongshore wave numbers corresponding to the alongshore spacing of rip channels, suggesting the SZEs are coupled to the underlying bathymetry (MacMahan et al. 2004b). Relaxation within the hydrodynamics allows the entire rip current cells to oscillate in the cross-shore within the surf zone on VLF timescales, but the rip current circulations are topographically controlled in the alongshore by the rip channel spacing, therefore preventing them from migrating freely alongshore (MacMahan et al. 2004b), as they would on a homogeneous-bathymetric beach (Johnson and Pattiaratchi 2006; MacMahan et al. 2010a).

The episodic transport of surface material out of the surf zone by a rip current was examined by Reniers et al. (2010) by evaluating Lagrangian Coherent Structures (LCSs) in the rip current surface velocity field produced by a 3-D numerical model capable of resolving wave groups. LCSs represent transport barriers in the flow that control the motion of passively advected particles. Model predictions of the fate of virtual surface drifters propagated by the Lagrangian velocity field showed that in the rip channels inside the surf zone, the virtual drifters clustered together and travelled seaward at the convergence of counter-rotating VLF SZE pairs. The presence of the VLF motions occasionally caused the rip current to pulse and extend beyond the surf zone. Smith and Largier (1995) observed well-defined jets of water extending episodically seaward from the surf zone, while Reniers et al. (2010) found that material trapped by the LCSs that become detached from the surfzone rip current circulation at the outer surf zone is carried offshore in narrow streaks. The field observations and numerical computations summarized here indicate the episodic, pulsating nature of rip currents and emphasize the importance of VLF motions in forcing rip current transport out of the surf zone. The presence and effect of individual VLF pulsations throughout the water column as the rip current moves offshore will be investigated in this work.

2. Rip Current Vertical Structure

The existing *in-situ* field measurements of the vertical structure of rip currents are limited, and were obtained primarily inside the surf zone (Aagard et al. 1997; Brander and Short 2001; MacMahan et al. 2005). Brander and Short (2001) used bi-directional, ducted impellor current meters to obtain vertical rip current velocity profiles in a rip neck and observed an increase in velocity away from the sea-bed and then a decrease towards the water surface, however measurements were made at only three locations in the water column. MacMahan et al. (2005) used a portable acoustic Doppler current profiler (ADCP) to obtain Eulerian rip current velocity measurements throughout the water column in a rip channel in the surf zone. They found that the vertical rip current profile was depth-uniform below the wave trough, with a significant amount of vertical shear in the wave crest-trough area due to the presence of waves and onshore Stokes drift

opposing the offshore rip current flow. The rip current velocity profile as it moves offshore and outside of the surf zone has not been measured simultaneously in the field.

A laboratory investigation of 3-D rip current flow was performed by Haas and Svendsen (2002), where rip currents were forced by normally-incident, monochromatic waves propagating over an alongshore bar with incised rip channels. The rip current flow was measured with three acoustic Doppler velocimeters (ADVs) positioned at different depths and moved to different horizontal locations during repeated wave runs. A similar laboratory experiment was conducted by Dronen et al. (2002) in a narrow wave tank, where half of an alongshore bar and rip channel system were represented. The laboratory results found that inside the surf zone in the rip channel where waves were breaking, the rip currents were nearly depth-uniform, whereas outside the surf zone there were strong depth variations in the flow, with strong seaward velocities in the upper water column and weak seaward or shoreward velocities near the bottom (Dronen et al. 2002; Haas and Svendsen 2002). The steady monochromatic wave forcing resulted in VLF motions outside the surf zone (Haas and Svendsen 2002) due to shear instability of the rip current jet (Haller and Dalrymple 2001; Reniers et al. 2009). This is a different forcing mechanism than surfzone wave-group induced forcing, which results in an aperiodic pulse that is transported beyond the surf zone, and the resulting rip current vertical structure may differ. Here, field observations of rip current vertical structure under directionally spread random wave conditions are examined.

3. Rip Current Volumetric Transport

The time variation of the vertical structure of rip current flows as they move seaward from the surf zone can have a significant effect on the volumetric estimates of exchange on rip-channeled beaches. Talbot and Bate (1987) used semi-quantitative measurements of dye releases to roughly estimate the flux associated with rip currents that exited the surf zone by assuming vertical uniformity everywhere, and found a half-residence time of 22 minutes for surf zone water. Smith and Largier (1995) observed episodic jets of water that extended seaward from the surf zone (i.e., rip currents) with a sector-scanning Doppler sonar. The rip currents lasted several minutes and transported

water rich in suspended sediments and bubbles offshore, suggesting they could cause a significant amount of exchange between the surf zone and offshore. An estimate of the surfzone flushing time was *O*(3 hours) based on surface rip current velocities estimated by the sonar and assuming the flow spanned the entire water depth. Reniers et al. (2009) estimated a surfzone flushing time of *O*(5 hours) based on the assumption that the surfzone retention of surface drifters (80% retention per hour) decayed exponentially with time. These different estimates were based on different assumptions of the vertical structure of the rip current flow exiting the surf zone. Additionally, the retention/flushing of material such as sediments, algae, larvae, bubbles and organic material are likely retained/flushed at the same rate, however their retention depends on vertical advection (Fujimura et al. 2014). Therefore, an understanding of the transport and vertical mixing associated with rip currents is important.

C. FIELD EXPERIMENT

1. Field Site

Field observations were obtained at Monterey, California, from late April to late May 2007, during the Rip Current Experiment (RCEX). The field site was chosen owing to the year-round persistent rip currents and existing knowledge from previous experiments performed at the site (MacMahan et al. 2004a,b; MacMahan et al. 2005; Brown et al. 2009; MacMahan et al. 2010a). The beach was composed of a relatively steep foreshore (1/10 slope) with straight and parallel contours, flattening out inshore (1/100 slope), with quasi-periodic, *O*(125 m), incised rip channels and continuing with a 1/20 offshore slope and straight and parallel contours seaward of the breaker zone (Figure 1). Feeder channels were present near the shoreline and converged with the incised rip channels. The local coordinate system used in this work is defined as positive offshore and to the south.

2. Wave, Wind, Tide, and Bathymetry Measurements

Offshore waves were measured with an upward-looking ADCP deployed in approximately 13 m water depth, which measured co-located pressure and velocity data. Hourly root-mean-square (rms) wave height, H_{rms}, in the sea-swell frequency band (0.04

$< f <$ 0.25 Hz) was computed by transforming the measured pressure spectrum to sea-surface elevation using linear wave theory (Guza and Thornton 1980). Hourly mean wave period, T_{m01}, in the sea-swell band was computed as the first-order moment of the pressure energy density spectrum and the hourly mean wave angle, θ_{m01}, in the sea-swell band was computed from the velocity auto and cross-spectra (Herbers et al. 1999).

Wind speed and direction data was obtained onshore of the field site atop a 10 m tower and rotated into the local coordinate system. Wind stress was calculated using the method by Large and Pond (1981). Tidal elevation data, referenced to mean sea level (MSL), was obtained from NOAA/NOS tidal station 9413450, located approximately 3 km south of the field site. Bathymetry was measured throughout the experiment using sonar-equipped personal watercraft (MacMahan 2001), a walking person, and an all-terrain vehicle, all equipped with a global positioning system (GPS).

During the 19 day long field investigation, the hourly estimated wave conditions in 13 m water depth (Figure 2) included H_{rms} of 0.2 to 1.2 m, T_{m01} of 6.3 to 12.8 s, and θ_{m01} of -4.2 to 5.9°. Shore-normal incident waves are represented as θ_{mo} = 0°, with positive wave angles approaching from the north. The cross-shore winds were generally onshore, with cross-shore wind stress, τ^{wind}_{x}, of -0.29 to 0.02 N m^{-2}. Spring tides were about 2.5 m and occurred near the end of the experiment.

3. Rip Current Measurements

In-situ measurements of the rip current vertical structure were obtained inside and outside the surf zone with two bottom-mounted ADCPs sampled continuously at 1 Hz (dt = 1 s). The ADCPs were deployed in a cross-shore line in a rip channel inside the surf zone ($ADCP_{in}$) in approximately 2 m water depth and just offshore outside of the surf zone ($ADCP_{out}$) in approximately 4 m water depth (Figure 1). The ADCPs inside (outside) the surf zone were mounted approximately 0.35 (0.5) m above the sea-bed, and measured velocity in a total of 30 (20) measurement cells throughout the water column, with a cell size of 0.2 (0.25) m, with the first velocity measurement taken approximately 0.65 (1.23) m above the sea-bed.

The ADCPs measured co-located pressure and horizontal velocity data. The time-varying water depth, h, at each ADCP was computed as the sum of the measured time-varying pressure, p, and the height of the instrument above the sea-bed. The elevation of each ADCP velocity measurement cell above the sea-bed, d, where $d = 0$ m corresponds to the sea-bed, was computed as the sum of the height of the instrument above the sea-bed, the measurement blanking distance from the sensor head, and the measurement cell size multiplied by the given cell number.

Throughout the experiment, the location of $ADCP_{in}$ actually varied between being inside and outside the surf zone as a function of the tidal elevation and incident wave height. Times when $ADCP_{in}$ was inside the surf zone were determined using the local wave-breaking criterion $H_{rms}/h \geq 0.4$ (Thornton and Guza 1982), which typically occurred during large waves and low tides (Figure 3).

a. Depth-Relative Normalization of Velocity

Velocity data obtained from the upward-looking ADCPs resulted in erroneous measurements above the sea-surface, with the number of measurement cells above the sea-surface varying with time due to the fixed size and number of measurement cells and the time-varying sea-surface elevation. In order to remove these erroneous data, the sea-surface elevation, η, as a function of time was computed from the co-located pressure data using linear wave theory (Dean and Dalrymple 1984). Due to noise in the ADCP velocity measurements near the sea-surface, velocity data in measurement cells greater than the total water depth, $d > h + \eta$, were set to zero.

In order to compare velocity measurements obtained in different water depths (due to different cross-shore instrument locations and different times in the tidal cycle at a single location), the velocity data are presented as a function of depth-normalized height above the sea-bed (d/h), where $d/h = 0$ at the sea-bed and $d/h = 1$ at MSL. Additionally, the horizontal velocity data were rotated into the local coordinate system, such that the cross-shore velocity, u, was shore-normal and positive offshore, and the alongshore velocity, v, was shore-parallel and positive to the south.

D. OBSERVATIONS

1. Mean Rip Current Vertical Structure

The variation in the vertical structure of the mean rip current flow as it moves seaward ultimately controls the amount of volumetric exchange occurring between the surf zone and the inner shelf. The cross-shore variation in the mean rip current velocity profiles measured by $ADCP_{in}$ and $ADCP_{out}$ were examined by computing hourly mean u and v as a function of relative-depth d/h (Figures 3 and 4). The mean cross-shore velocity measured at $ADCP_{in}$ when it was inside the surf zone was depth-uniform and was greater in magnitude than $ADCP_{out}$ at the corresponding time (Figure 3). The mean cross-shore velocity measured at $ADCP_{out}$, and at $ADCP_{in}$ during times when it was outside the surf zone, showed variation throughout the water column with maximum offshore velocities at the surface. The cross-shore rip current flows, both inside and outside the surf zone, were strongest during large wave conditions and low tides (e.g., yeardays 124 and 125), consistent with previous observations (e.g., Shepard and Inman 1950; MacMahan et al 2005). The mean alongshore velocity measured at both $ADCP_{in}$ and $ADCP_{out}$ was relatively depth-uniform (Figure 4), and was smaller in magnitude than the corresponding cross-shore velocity. The difference in vertical structure of u and v outside the surf zone, suggests the alongshore component of the flow is not entirely due to the rip current, but may indicate the presence of inner shelf flows. Additionally, the fact that the alongshore current measured at $ADCP_{out}$ is greater than $ADCP_{in}$ when both were outside the surf zone (i.e., yearday 131) suggest the presence of inner shelf flows driven by pressure gradients, other than the tide.

2. Very Low Frequency Motions in the Rip Current Flow

VLF motions in rip current flows were shown to be the dominant mechanism responsible for exchange between the surf zone and the inner shelf on rip-channeled beaches (Reniers et al. 2009, 2010). The presence and intensity of VLFs throughout the water column is examined in the ADCP measurements inside and outside the surf zone, in order to evaluate depth-variable rip current transport from the surf zone to the inner

shelf. The VLF contribution to the total horizontal instantaneous velocity ($U = \sqrt{u^2 + v^2}$) was examined with the rms VLF total velocity magnitude, $U_{rms,VLF}$, defined by

$$U_{rms,VLF}(z) = \sqrt{\int_{0.0005\,Hz}^{0.004\,Hz} S_{uu}(z,f) + S_{vv}(z,f)\,df}, \quad (1)$$

where S_{uu}(z, f) and S_{vv}(z, f) are the energy density spectra of the cross-shore and alongshore velocities. Spectra were calculated from 3-hour records, with dt = 1 s, to capture the VLF signature in the flow with statistical confidence, using a window length of 1024 s with a Hanning window and 50% overlap, resulting in 56 degrees of freedom and a frequency resolution of 0.00098. Throughout the experiment, the VLF energy appeared to increase with increasing wave energy, both inside and outside the surf zone (Figure 5). During energetic conditions, $U_{rms,VLF}$ at $ADCP_{in}$ was constant throughout the water column, while $U_{rms,VLF}$ at $ADCP_{out}$ was more surface dominated and lesser in magnitude (Figure 5). The reduction in the VLF rip current intensity as it moved offshore is consistent with previous observations (MacMahan et al. 2004b).

For the rest of the analysis, the effect of VLF motions on the strength and vertical structure of the rip current flow is examined by evaluating velocities measured only during low tides, when rip current flows are strongest (e.g., MacMahan et al. 2006), and during weak cross-shore wind conditions ($|\tau^{wind}_x| < 0.05$ N m^{-2}), to ensure only wave-driven flows are examined (Figure 2). A total of thirty instances met these criteria during the experiment. Velocity measured during 3-hour windows, centered on low tides, denoted 3HRLT from here on out, were evaluated in order to ensure approximate stationarity in the flow, and to accurately capture the O(10 minute) VLF component of the flow.

In order to describe the strongest rip current flows, which were depth-uniform at $ADCP_{in}$ when it was inside the surf zone, and surface-dominated when it was outside the surf zone and at $ADCP_{out}$, the VLFs were examined at a given reference level near the surface. The reference levels used in this work corresponded to d/h = 0.7 at $ADCP_{in}$ and d/h = 0.8 at $ADCP_{out}$, which were the uppermost measurement cells within the water column that contained velocity measurements for each entire 3HRLT, and were located

below the lowest wave trough for each given record to eliminate the influence of the surface waves.

The mean $U_{rms,VLF}$ over all 3HRLTs at the near-surface reference level was ~0.10 m s^{-1} at $ADCP_{in}$ and decreased to ~0.04 m s^{-1} at $ADCP_{out}$. In comparison, the mean total velocity U_{mean} over all 3HRLTs at the same near-surface reference level was ~0.27 m s^{-1} at $ADCP_{in}$ and ~0.08 m s^{-1} at $ADCP_{out}$. Therefore, the VLF motions are energetic, both inside and outside the surf zone, and the VLF component of the surface rip current flow accounts for approximately 37% and 50% of the total energy at $ADCP_{in}$ and $ADCP_{out}$.

a. VLF Pulses

In previous rip current field observations, the cross-shore and alongshore velocity time series measured in a rip channel inside the surf zone had significant VLF signals (MacMahan et al. 2004b). The presence of VLF pulsations in the measured rip current flow was examined by low-pass filtering ($f < 0.004$ Hz) the cross-shore and alongshore velocities (u_{VLF}, v_{VLF}) throughout the water column measured by $ADCP_{in}$ and $ADCP_{out}$ for the 3HRLTs. Examples of the u_{VLF} pulses for high, intermediate, and low VLF energy conditions are shown in Figure 6. The pulsating nature of the VLF rip current flow is apparent, where the u_{VLF} intensity varies in time between strong seaward velocities (warm colors in Figure 6) and relatively small or zero cross-shore velocities (cool colors in Figure 6). At $ADCP_{in}$ the pulses can be seen extending throughout the entire water column, while at $ADCP_{out}$ the pulses are predominantly at the surface. The magnitude and number of the VLF pulses decreased with decreasing VLF energy.

The maxima in u_{VLF} measured in the near-surface reference levels are further investigated to evaluate the individual pulses in the rip current flow (Figure 7). For each 3HRLT the total number of VLF pulses, N_{pulse}, was determined as the total number peaks in u_{VLF}, which is assumed to represent the total number of independent VLF observations for that 3HRLT. In order to evaluate the maximum effect of the VLF pulses on the rip current transport, only significant VLF pulses were considered, which are defined as the successive peaks in u_{VLF} above a given threshold. The threshold was determined by considering u_{VLF} measured in the near-surface reference level over all 3HRLTs, as shown

by the frequency distribution in Figure 7. The frequency distribution shows the u_{VLF} signal is composed of a large percentage of small pulses and a small percentage of large pulses. The effect of these strong pulses is of interest here, therefore the threshold used to determine significant VLF pulses was two times the standard deviation above the mean $(\mu + 2\sigma)$. This equated to 0.68 m s^{-1} and 0.19 m s^{-1} for $ADCP_{in}$ and $ADCP_{out}$, which are approximately seven and five times greater than the associated mean $U_{rms,VLF}$. A significant pulse was described by the duration, $T_{sig,pulse}$, defined as the time from when u_{VLF} exceeded the given threshold until it decreased to a value below the threshold, and the amplitude, $A_{sig,pulse}$, defined as the maximum u_{VLF} during the pulse duration (Figure 8).

Examples of the VLF rip current pulsations measured in the reference level during high, intermediate, and low VLF energy conditions are shown in Figure 8. The VLF pulses were found to be aperiodic and varied in amplitude throughout each 3HRLT. It was also observed that the VLF pulses did not occur simultaneously at $ADCP_{in}$ and $ADCP_{out}$, and the number of significant VLF pulses measured at $ADCP_{in}$ did not necessarily equal the number measured at $ADCP_{out}$. During high VLF energy conditions there were numerous significant VLF pulses measured at both $ADCP_{in}$ and $ADCP_{out}$, with many of the pulses lasting for several minutes. As the VLF energy decreased, the magnitude and number of significant VLF pulses decreased. For low VLF energy conditions, the magnitude of the VLF pulses at $ADCP_{in}$ and $ADCP_{out}$ were equal at times, and there were less significant VLF pulses. For example, on yearday 128 there was only one, relatively long significant VLF pulse measured at $ADCP_{out}$. These examples demonstrate the randomness of frequency and magnitude of the significant VLF pulses that occur during all VLF energy levels.

The magnitude, duration, and frequency of the VLF pulses in the cross-shore velocity measured inside and outside the surf zone were evaluated to examine the influence of the VLF pulsations on the mean rip current flow. The VLF rip current flow for each 3HRLT was described by the number of significant VLF pulses ($N_{sig,pulse}$), the mean amplitude of the VLF pulses ($A_{mean,sig,pulse}$), and the fraction of the time that the VLF pulses were occurring, defined as the sum of the individual pulse durations divided

by the 3-hour record length ($\sum T_{sig,pulse}/T_{3-hour}$). The relationship of the VLF pulse characteristics to the offshore wave height is shown in Figure 9, which highlights the increased VLF pulse activity for the more energetic wave conditions. The magnitude of $A_{mean,sig,pulse}$ at $ADCP_{in}$ was always greater than that at $ADCP_{out}$ for each 3HRLT, consistent with the observed decrease in $U_{rms,VLF}$ outside the surf zone. In general, more VLF pulses occurred during larger wave conditions, at both $ADCP_{in}$ and $ADCP_{out}$. However, the number of VLF pulses measured at each ADCP was typically not equal. In fact, during several 3-hour records no significant pulses were measured at $ADCP_{in}$ while they were at $ADCP_{out}$. This may be attributed to the higher threshold set at $ADCP_{in}$, which incorporates measurements from when $ADCP_{in}$ was located both inside and outside the surf zone, which filters out the smaller VLF pulses when $ADCP_{in}$ was outside the surf zone. Examining the duration of the significant VLF pulses, the fraction of each 3-hour record that the pulses were occurring at $ADCP_{in}$ and $ADCP_{out}$ was generally equal, with pulses occurring about 10% of the time on average.

b. VLF Vertical Structure

At each ADCP, the vertical profiles of u_{VLF} corresponding to the each individual significant VLF pulse that occurred during all 3HRLTs were combined and bin-averaged based on the individual pulse amplitude $A_{sig,pulse}$ measured in the surface reference bin. This resulted in the VLF rip current pulse vertical profiles being sorted into similar magnitudes and profile shapes (Figure 10). At $ADCP_{in}$, the u_{VLF} profiles are approximately depth-uniform, and increased in magnitude with increasing $A_{sig,pulse}$. At $ADCP_{out}$, the u_{VLF} profiles are surface-dominated, with an increase in magnitude of the surface flow with increasing $A_{sig,pulse}$. This results in a greater amount of shear in u_{VLF} throughout the water column for larger $A_{sig,pulse}$, as the near-bottom u_{VLF} at $ADCP_{out}$ are statistically similar for all $A_{sig,pulse}$.

The effect of the VLF rip current pulses on the magnitude and vertical structure of the mean rip current flow was also examined by sorting the 3HRLT profiles by various VLF pulse characteristics (Figure 11). Inside the surf zone, the VLF pulses added to the mean background rip current flow, while outside the surf zone there is no mean

background flow so the strength of the VLF pulses controls the strength of the rip current flow. In all cases, the magnitude of the mean rip current cross-shore velocity profile was only a fraction of the measured u_{VLF} profiles. The maximum amplitude of the VLF pulses in the rip current surface velocity $A_{max,sig,pulse}$ that occurred during each 3HRLT was found to distinguish the 3-hour mean rip current strength and vertical profile (Figure 11, column 1). Although the strength of the individual VLF pulses that occurred during a 3-hour record varied, the strength of the maximum VLF pulse for that record, even if it only occurred once, seemed to represent the strength of the corresponding 3-hour mean rip current flow. In general, the mean cross-shore velocity rip current profiles below the wave trough were primarily depth-uniform at $ADCP_{in}$, with stronger flows for times when larger $A_{max,sig,pulse}$ occurred. For smaller $A_{max,sig,pulse}$, the rip current profile weakened and became more surface dominated, and $ADCP_{in}$ was likely outside of the surf zone during those times. At $ADCP_{out}$ the rip current was always surface dominated, however the flows were stronger and there was more shear in the velocity profile for larger $A_{max,sig,pulse}$. The mean Eulerian velocity profiles presented in Figure 11 show the velocity measurements between the wave trough and crest, where the velocity goes to zero in this region at $ADCP_{in}$ and there are some onshore velocities in this region at $ADCP_{out}$. Similar trends were observed when the mean velocity profiles were sorted by the mean VLF pulse amplitude $A_{mean,sig,pulse}$ of each 3-hour record (Figure 11, column 2). These results suggest that although a number of smaller VLF pulses occur during each record, the maximum VLF pulse amplitude ultimately controls the rip current flow magnitude and profile.

The rip current velocity profiles were also sorted based on the total number of significant pulses ($N_{sig,pulse}$) and total significant pulse duration ($\sum T_{sig,pulse}/T_{3-hour}$) per 3-hour record (Figure 11, columns 3 and 4). However, for many of the records only one significant VLF pulse occurred, with the total pulse duration being a very small percentage of the total record, therefore using these characteristics to sort the mean velocity profiles was not helpful.

c. VLF Rotation over Depth

As a rip current pulse moves offshore and changes in magnitude, the direction of the pulse likely also changes. The temporal shifts between the VLF horizontal velocity time series measured as a function of depth at each ADCP is determined by computing the cross-correlation coefficient of *u* measured at each depth with *u* measured in the surface reference level, and similarly for *v*, and evaluating $R(\tau = 0)$ (Figure 12). The statistical significance of the computed correlation values was based on N_{pulse} for each 3HRLT, where only statistically significant values at the 95% significance level are shown in Figure 12. During energetic conditions (e.g., yeardays 123 to 126), the *u* (*v*) was strongly correlated $\left(R(\tau = 0) > 0.75\right)$ throughout the entire water column at $ADCP_{in}$, while the correlation decreased with depth at $ADCP_{out}$, as expected.

In order to evaluate the rotation in the VLF pulses over depth, the mean horizontal VLF velocity vector at multiple depths for each 3HRLT were calculated (Figure 13). At $ADCP_{in}$, minimal rotation was observed throughout the water column (not shown), as expected, due to the depth-uniformity that has been observed there. Therefore, the rip current pulses were correlated over the entire depth at $ADCP_{in}$, with no twisting. At $ADCP_{out}$, the surface $U_{mean,VLF}$ vectors were greater in magnitude and directed more straight offshore, whereas the bottom $U_{mean,VLF}$ vectors were smaller in magnitude and were offset in direction (Figure 13). The angle of rotation between the surface and bottom $U_{mean,VLF}$ vectors varied, with the average difference in angle being ~50°. Therefore, as the rip current moved seaward, the flow near the bottom was less correlated with the surface flow, and there was twisting of the rip current pulse over the depth. Complex correlation analysis was also performed, which gives a measure of the correlation between the total horizontal velocity (given as a complex number) and the angle of displacement between them over the depth (Kundu 1976). Similar results were found, however they are not shown here, as the cross-correlation and rotation of the vectors over depth provides more visual apparent results.

E. DISCUSSION

1. Offshore Movement of VLF Rip Current Pulses

The observations of the magnitude and vertical structure of the mean (Figures 3 and 4) and rms VLF (Figure 5) velocities measured at $ADCP_{in}$ and $ADCP_{out}$ indicate a distinct difference in the rip current flow dynamics as it flows from inside to outside the surf zone. The relationship between the VLF pulses measured at $ADCP_{in}$ and $ADCP_{out}$ was examined by performing cross-correlation analysis of u_{VLF} and v_{VLF} individually in the near-surface reference levels for the duration of the experiment using 3-hour record segments. The maximum correlation values, $R_{\max}(\tau)$, between $ADCP_{in}$ and $ADCP_{out}$ are shown in Figure 14 for the cross-shore and alongshore velocity components. The significance level of the correlation values was determined based on N_{pulse} measured at $ADCP_{in}$ and $ADCP_{out}$, where the minimum N_{pulse} measured for each 3HRLT was used to determine the corresponding degrees of freedom ($dof = N_{pulse} - 1$) and correlation value for the 95% significance level, which are shown in Figure 14. The cross-shore and alongshore velocities were not significantly correlated between $ADCP_{in}$ and $ADCP_{out}$ for any of the 3HRLTs, indicating the VLF pulses inside and outside the surf zone were independent.

Previous work showed that the VLF velocity was related to the mean rip current flow, as well as the offshore wave height and tidal conditions (MacMahan et al. 2004b). This was evaluated here by performing linear regression analysis between $U_{rms,VLF}$ and various flow and wave parameters averaged over each 3HRLT, for all thirty 3HRLTs (significance level of $r^2 = 0.35$ at the 95% significance level) (Figure 15). There was no significant correlation between $U_{rms,VLF}$ measured at $ADCP_{out}$ and the offshore wave conditions of H_{rms}, T_{m01}, and θ_{mn} (Figure 15a, b, c), while $U_{rms,VLF}$ measured at $ADCP_{in}$ was only correlated with H_{rms} (Figure 15a). Therefore, the VLF pulses inside the surf zone are dependent upon the incoming wave energy, due to the forcing of the VLF motions by the spatially varying breaking wave groups. However, the VLF pulses outside the surf zone are not dependent upon the offshore wave conditions, supporting the notion that they originate inside the surf zone but travel offshore randomly. The correlation between $U_{rms,VLF}$ and the corresponding $U_{mean,VLF}$ (Figure 15d) shows significant

correlation at $ADCP_{in}$ ($r^2 = 0.73$), but no correlation at $ADCP_{out}$. There was no significant correlation between $U_{rms,VLF}$ and the local water depth (i.e., indicative of tidal elevation) at either ADCP. The highest degree of significant correlation for both ADCPs was $U_{rms,VLF}$ and the local H_{rms}/h ($r^2 = 0.74$ and 0.44 at $ADCP_{in}$ and $ADCP_{out}$). Therefore, the strength of the VLF pulses is dependent upon both the wave energy and water depth. These results further suggest that the VLF pulses at $ADCP_{out}$ are independent of those at $ADCP_{in}$.

The u_{VLF} and v_{VLF} measured throughout the water column at $ADCP_{out}$ was further examined to evaluate the VLF pulses as they move offshore. On yearday 125 (Figure 6), significant u_{VLF} pulses near the surface are apparent, while v_{VLF} was approximately zero (not shown), indicating the rip current pulsation was directed predominantly offshore. For some other 3HRLTs, the magnitude of the u_{VLF} and v_{VLF} pulses was near equal at the same time (not shown), indicating the rip current pulsation was moving offshore at an angle. Both of these cases suggest the rip current flow behaved like a jet, but with the rip current pulses changing direction as they exit the surf zone. However, on yearday 137 (Figure 16) there was a variation in time in the strength of the u_{VLF} and v_{VLF} pulses, where at the beginning of the record on yearday 137 u_{VLF} is dominant and v_{VLF} is basically zero, then briefly u_{VLF} and v_{VLF} are approximately equal, and within minutes, v_{VLF} is dominant and u_{VLF} is basically zero, with this pattern repeating once more. This successive change in magnitude and direction of the rip current VLF pulse suggests the fixed point ADCP is observing the passage of a detached VLF eddy. The range in magnitude and direction of the measured VLF pulses at $ADCP_{out}$ is consistent with field measurements that showed a large range in Lagrangian drifter trajectories exiting the surf zone via a rip current on the same beach, with drifters moving offshore at different angles and travelling varying distances (MacMahan et al. 2010a; Brown et al. 2014, submitted manuscript). The numerical modeling results of Reniers et al. (2010) showed similar virtual drifter trajectories due to the presence of wave-group induced VLF motions temporarily extending the rip current flow beyond the surf zone, resulting in the corresponding VLF eddies becoming subsequently detached.

2. Surface Transport and Vertical Mixing by Rip Currents Outside Surf Zone

The movement of the rip current pulse as it moves at the surface out of the surf zone and offshore is further investigated. It is hypothesized that the rip current moves offshore as a jet at the surface, and its movement over the surfzone break (defined as the abrupt change in depth at the surfzone boundary) as it exits the surf zone results in the surface dominated flow offshore. For 3HRLTs with strong VLF pulses at $ADCP_{in}$, the corresponding 3-hour mean cross-shore velocity profiles at $ADCP_{in}$ and $ADCP_{out}$, as a function of vertical elevation, z, are examined, where $z = 0$ corresponds to MSL and is positive upward (Figure 17a). The cross-shore velocity profiles are shown relative to the mean cross-shore bathymetry profile in the rip channel. At $ADCP_{in}$, the rip current velocity is depth uniform, extending to the sea-bed. At $ADCP_{out}$, the surface-dominated rip current appears to be moving offshore as a jet. From a maximum near the surface, the velocity decreases downward with a large amount of shear to a certain depth, and then appears to decrease less rapidly or remain constant. The depth corresponding to this change in shear in the velocity appears to be the depth of the surfzone break. The jet-like behavior of the seaward flowing rip current measured here supports the observations of Smith and Largier (1995) of well-defined jets of water extending offshore from the surf zone as rip currents.

The vertical mixing of material carried offshore by a rip current jet is further investigated with observations of dye releases that were performed at the same field site at Monterey, California, in June 2010 (Figure 17b-c). Fluorescent Rhodamine dye was released at a point inside of the surf zone and the distribution over time and space was measured. In particular, the vertical structure of the dye plume outside of the surf zone was examined by performing vertical casts from a GPS-equipped vessel with a co-located dye sensor and CTD throughout the deployment and at various locations. The casts extended to the sea-bed, and the measurements from the downcast and upcast were averaged to obtain mean profiles of dye concentration and temperature with depth (Figure 17b-d). The temporal and spatial variation of the dye profiles outside the surf zone was examined to evaluate the material transport of the rip current jet offshore. Note that the

dye profiles measured outside the surf zone were from randomly chosen locations between the surfzone boundary and several surfzone widths offshore, and at variable alongshore locations offshore of rip channels and shoals. Therefore, each profile may not correspond to the same rip current pulse from the same rip channel, so the evolution of one rip current pulses is not being described, rather the evolution of all material that is transported offshore due to rip currents.

In general, the measured profiles revealed that the offshore dye plumes were relatively deep, encompassing greater than half, or all, of the water column. Near the surfzone boundary, and within the first 30 minutes after the dye was released (Figure 17b), the vertical profiles of the dye were surface dominated, within the depth range of the depth at the edge of the surf zone. Later in time (Figure 17c), the vertical profiles taken closer to shore ($200 < x < 275$ m) became more vertically mixed within the depth range of the depth at the edge of the surf zone, while the vertical profiles farther offshore were still nearer to the surface and had not been mixed down yet. After an hour (Figure 17d), the dye was well offshore of the surf zone and encompassed approximately half of the water column. At these cross-shore locations well offshore of the surf zone ($x > 275$ m), the vertical profiles of dye were also observed to be coincident with the thermocline (Figure 17d). More mixing occurs in the upper water column offshore, resulting in warmer water and dye vertically mixed downward. At depths below the thermocline, the dye is no longer mixed down and the water temperature decreases. These results suggest that as the vertically-uniform rip current exits the surf zone, it moves offshore as a surface jet with its vertical extent remaining the same as at the edge of the surf zone. As the water depth increases outside the surf zone, the rip current transport remains near the surface, resulting in a surface dominated rip current flow offshore. The material transported offshore due to rip currents is then mixed down vertically to a depth coincident with the thermocline. The surface material transported by the rip current outside the surf zone, which encompasses a large portion of the water column, spreads laterally and can have a significant effect on the overall 3-D material transport.

F. SUMMARY AND CONCLUSIONS

Field measurements of the vertical structure of a rip current, inside and outside the surf zone, were obtained on a rip-channeled beach at Monterey, California. The observations presented here provide new insight into the temporal and depth variation of a rip current as it moves offshore, and contribute to the previous findings of horizontal rip current circulation dynamics, also obtained at the same field site (MacMahan et al. 2004a,b; MacMahan et al. 2005; Brown et al. 2009; MacMahan et al. 2010a). In these measurements, wave-group induced VLF motions were found to be a significant component of the rip current flow, accounting for 37% to 50% of the total energy inside and outside the surf zone. The counter-rotating SZEs associated with these VLFs, which are coupled to the underlying bathymetry and oscillate in the cross-shore direction, occasionally converge in the rip channels and these VLF pulses cause the rip current to extend outside the surf zone (MacMahan et al. 2004b; Reniers et al. 2009, 2010). The VLF pulses in the near-surface rip current flow, both inside and outside the surf zone, were found to be aperiodic, with the number and amplitude of significant VLF pulses increasing with increasing wave energy. Evaluating the VLF signal in the surface rip current flow during 3-hour time windows centered around low tide, there are times when zero or only one significant VLF pulse was measured, but during larger wave conditions up to 20 significant VLF pulses occurred, where a significant pulse is defined as being greater than $\mu + 2\sigma$, which equated to 0.7 and 0.2 m s^{-1} inside and outside the surfzone. On average, the significant VLF pulses occurred for approximately 10% of the time. The magnitude and vertical structure of the mean rip current flow was controlled by the strength of the surface VLF pulses, where inside the surf zone the VLF pulses were found to add to the strength of the background rip current flow, and outside the surf zone, where there was no background flow, the stronger VLF pulses resulted in stronger rip current flows and more shear in the vertical.

As the rip current moved from inside the surf zone to offshore, the significant VLF rip current pulses at $ADCP_{in}$ and $ADCP_{out}$ did not occur simultaneously, and there was no significant correlation in the cross-shore and alongshore velocity measured at the two locations. There was no significant correlation between the VLF energy measured at

each ADCP and the offshore wave conditions, except for with the local H_{rms}/h ($r^2 = 0.74$ and 0.44 at $ADCP_{in}$ and $ADCP_{out}$), indicating the VLF pulses were dependent upon both the wave energy and water depth, and that the VLF pulses occurring at each ADCP was random and the VLF pulses at $ADCP_{out}$ are independent of those at $ADCP_{in}$.

The VLF pulses outside of the surf zone behave like a surface jet moving directly offshore or at an angle at times, with u_{VLF} either dominating or being equal to v_{VLF} at the surface. Other times the VLF pulse has detached and moved as an eddy passing by the stationary sensor, with u_{VLF} and v_{VLF} at the surface successively being dominant. The lack of correlation between inside and outside the surf zone (Figure 14) also suggests that the VLF pulse detaches from the surf zone and moves offshore. The vertical profiles of dye that were measured outside the surf zone indicate the rip current pulses encompass a significant portion of the water column, and therefore the VLF pulses in the surface rip current flow result in a significant amount of cross-shore exchange. Offshore, the dye profiles were coincident with the thermocline, which thereby limited the depth of the vertical mixing of material in the surface rip current flow. The vertical profiles measured by the ADCPs indicated that inside the surf zone the VLF pulses were depth-uniform with minimal rotation throughout the water column, while outside the surf zone they became surface-dominated as they moved offshore (Figures 5 and 6), and there is more rotation throughout the water column, with the near-bottom flow not correlated with the strong near-surface flow (Figures 12 and 13). These results suggest that as the depth-uniform rip current exits the surf zone and moves over the surfzone break, it behaves like a surface jet with its vertical extent remaining the same depth as the depth at the offshore edge of the surf zone, and remains near the surface controlled by the depth of the thermocline as it continues to be transported and mixed offshore.

THIS PAGE INTENTIONALLY LEFT BLANK

III. DRIFTER MEASUREMENTS OF CROSS-SHORE EXCHANGE ON A RIP-CHANNELED BEACH

A. INTRODUCTION

The cross-shore exchange of material across the surfzone boundary, in both the seaward and shoreward directions, plays an important role in processes ranging from how land-based pollution, which enters the ocean in the surf zone, is carried offshore to the inner shelf, to how harmful algae blooms and offshore operational discharges, such as oil, which originate in the inner shelf, are transported into the surf zone. Understanding the transport and retention of hazardous pollutants and biological matter in the nearshore region is important for reasons ranging from human health factors to sustaining ecosystems.

Studies of cross-shore circulation over the inner shelf, focusing on wave-driven flows (i.e., during weak wind forcing), demonstrate the importance of the onshore Lagrangian Stokes drift, $u_{St}(z)$, associated with shoreward propagating surface gravity waves (Stokes 1847), and the compensating wave-driven offshore Eulerian flow, $u_E(z)$, referred to as undertow. The presence of wave-driven undertow inside the surf zone is widely known and has been measured extensively in the field (Haines and Sallenger 1994; Garcez Faria et al. 2000; Reniers et al. 2004b). Wave-driven undertow has also been found to extend well offshore of the surf zone (Lentz et al. 2008; Kirincich et al. 2009; Ohlmann et al. 2012), and to be the dominant component of the depth-averaged Eulerian cross-shore flow during weak wind conditions. The changes in the distribution of $u_{St}(z)$ and $u_E(z)$ throughout the water column as the water depth decreases from the offshore waters of the inner shelf to the shallower waters near the surfzone boundary was shown to control the net cross-shore transport between the inner shelf and the surf zone (Lentz et al. 2008; Ohlmann et al. 2012). An in-depth description of the theory of Stokes drift and undertow, including typical profiles inside and outside the surf zone, is given in the next Section.

On the inner shelf of Martha's Vineyard, Massachusetts, and Duck, North Carolina, during weak wind conditions and along-shelf uniform flows, Lentz et al. (2008)

found that the onshore Stokes drift opposed the offshore Eulerian undertow flow throughout the water column, resulting in zero net Lagrangian transport at all depths. Expanding upon these findings, Ohlmann et al. (2012) released drifters during weak wind conditions on the inner shelf off the coast of two beaches in Southern California, which are relatively alongshore uniform and typically do not support rip currents, and observed a deceleration of shoreward-moving surface drifters as they approached the surfzone boundary. This was attributed to changes in the relative shapes of the onshore Stokes drift and offshore wave-driven undertow profiles with decreasing water depth near the surfzone boundary, resulting in an imbalance of $u_{St}(z)$ and $u_E(z)$ with a net offshore Lagrangian flow near the water surface. The reason for the initial onshore motion of the drifters could not be discerned by Ohlmann et al. (2012). The results of Ohlmann et al. (2012) suggest that surface waves drive offshore Eulerian flows in the upper water column that may prevent the onshore transport of material into the surf zone from the inner shelf.

These findings of cross-shore transport over the inner shelf on relatively alongshore homogeneous beaches are used as a starting point to investigate cross-shore exchange on rip-channeled beaches, which are known to have different dynamics, including the fate of material transported offshore from the surf zone to the inner shelf, which has never been thoroughly investigated. Rip currents are known to be capable of transporting material offshore, and have even been confused with wave-driven undertow flows (Shepard 1936), so it is conceivable that the interaction of the onshore Stokes drift associated with surface gravity waves and the offshore rip current flows will influence the net cross-shore transport on a rip-channeled beach. The conventional theory of rip current transport and an overview of previous rip current studies are given in the next Section.

In this work, an extensive set of Lagrangian and Eulerian field measurements of surf zone and inner shelf rip current flows is analyzed to evaluate cross-shore exchange on a rip-channeled beach at Monterey, California. The observations are unique in that they not only describe the surf zone circulations, but they also explain flows outside of the surf zone, which have not been extensively measured before on a rip-channeled

beach. The results of these observations are presented, and the contribution to previous work evaluating rip current behavior is discussed. The findings of this study support a new theory of how material is exchanged and conserved within the nearshore region on a rip-channeled beach.

B. THEORY

1. Wave Forcing

As surface gravity waves propagate onshore from the inner shelf to the surf zone, the time-averaged particle velocity in a wave results in a net onshore drift in the direction of wave propagation (Stokes 1847), referred to as Stokes drift. In a Lagrangian (particle following) reference frame, Stokes drift is depth varying (Figure 18a), where

$$u_{St}(z) = \frac{H_s^2 \omega k}{16} \frac{\cosh\left[2k(z+h)\right]}{\sinh^2 kh} \cos\theta_w, \tag{2}$$

where z is vertical elevation defined as positive upward relative to mean sea level (MSL), H_s is significant wave height, ω is wave frequency, k is the dominant wave number, h is local water depth, and θ_w is the mean wave direction (Stokes 1847). In a Eulerian (fixed in space) reference frame, the onshore volume Stokes transport occurs between the wave trough and crest (Figure 18a), because at a fixed point there is either no water above the wave trough or an onshore wave-averaged Stokes drift above the wave trough. In both reference frames, the onshore volume Stokes transport, Q_{St}, is the theoretical depth-integrated $u_{St}(z)$, and is given by

$$Q_{St} = \frac{gH_s^2}{16c} \cos\theta_w, \tag{3}$$

where g is gravitational acceleration, and $c = \omega/k$ is the wave phase speed (Stokes 1847). In wave environments, a compensating Eulerian offshore flow, $u_E(z)$, exists below the wave trough, referred to as undertow (Haines and Sallenger 1994; Garcez Faria et al. 2000; Reniers et al. 2004b). The distribution of $u_E(z)$ throughout the water column is a function of the local water depth, h. The summation of $u_E(z)$ and $u_{St}(z)$, at a given location, results in a wave-averaged Lagrangian velocity, $u_L(z)$, distributed throughout the water column, and is given by

$$u_L(z) = u_E(z) + u_{St}(z). \tag{4}$$

Material transport between the inner shelf and the surf zone is described in terms of the Lagrangian transport, Q_L, which equals the depth-integrated $u_L(z)$ and is defined as

$$Q_L = Q_E + Q_{St}, \tag{5}$$

where Q_E is the offshore Eulerian volume transport, equal to the depth-integrated $u_E(z)$, and estimates of the depth-averaged velocity, $\overline{u}_E$ or $\overline{u}_{St}$ are found by dividing Q_E or Q_{St} by the local water depth h.

On the inner shelf, in a Lagrangian reference frame, the Stokes drift is largest at the water surface and decays exponentially with depth (Figure 18b). During weak wind conditions and alongshore-uniform flows, the compensating wave-driven undertow is distributed as predicted by Hasselmann with a maximum offshore flow at the surface and decreasing toward the bottom (Figure 18b) (Hasselmann 1970; Lentz et al. 2008; Fewings et al. 2008). The wave-driven Eulerian undertow profile cancels the Lagrangian Stokes drift, which results in a vertical balance between $u_E(z)$ and $u_{St}(z)$, so $u_L(z)$ is zero at all depths and there is a zero net Lagrangian transport Q_L (Hasselmann 1970; Xu and Bowen 1994; Smith 2006; Monismith et al. 2007; Lentz et al. 2008; Hendrickson and MacMahan 2009).

Inside the surf zone, current dynamics are predominantly driven by breaking surface gravity waves and are largely dependent on the surf zone bathymetry. As the water depth decreases, the Lagrangian Stokes drift profile becomes more vertically uniform, and is constant throughout the water column shoreward of wave breaking (Figure 18c). In a surf zone characterized by an alongshore-homogeneous morphology, the onshore Stokes transport is balanced by an undertow flow with a parabolic velocity profile (Figure 18c) with maximum offshore velocity at mid-depth or near bottom (Svendsen 1984; Putrevu and Svendsen 1993; Haines and Sallenger 1994; Garcez Faria et al. 2000; Reniers et al. 2004b). Based on Equation (4), this results in a vertical imbalance between $u_E(z)$ and $u_{St}(z)$ and a net onshore Lagrangian transport near the surface and offshore Lagrangian transport below the wave trough. In decreasing water depths from offshore to the surfzone boundary, changes in the relative shapes of the onshore

Lagrangian Stokes drift and offshore wave-driven Eulerian undertow profiles predicted by Ohlmann et al. (2012), resulted in an imbalance between $u_E(z)$ and $u_{St}(z)$ throughout the water column, and an offshore Lagrangian flow near the water surface, consistent with the decelerating shoreward-moving drifters on the inner shelf as they approached the surfzone boundary.

2. Rip Currents

Rip currents are strong, seaward-directed flows that originate near the shoreline and are generally coupled to the underlying beach bathymetry, characterized by deeper, incised channels in shallower, shore-connected shoals or alongshore bars. Rip currents have long been believed to extend far offshore, well beyond the surf zone and wave breaking, and thereby be a means of continuously transporting material offshore (Shepard et al. 1941; Inman and Brush 1973). On a rip-channeled beach, conventional theory suggests that seaward flowing rip currents are the compensating return flow, $Q_{E,rip}$, that balance the continuous transport of water shoreward and into the surf zone by Stokes drift (Figure 18d). Therefore, at the surfzone boundary, a balance exists where the onshore Stokes transport Q_{St} integrated over the rip channel spacing, λ_{rip}, would equal the offshore Eulerian rip current transport exiting through the rip channel, defined as

$$Q_{St}\lambda_{rip} = Q_{E,rip}b_{rip}, \tag{6}$$

where b_{rip} is the width of the rip current. Rip currents commonly occur in some variation on most sandy beaches, and have been observed in nature and studied extensively for many years (e.g. Shepard 1936; Shepard et al. 1941; Bowen 1969; Smith and Largier 1995; Brander and Short 2001; MacMahan et al. 2005; MacMahan et al. 2010a). However, it still remains largely unknown how rip currents act as a transport mechanism, both temporally and spatially, between the surf zone and the inner shelf. Most rip current studies focused on surfzone measurements, and very few field observations of exchange across the surfzone boundary have been obtained.

Recently, MacMahan et al. (2010a) deployed a fleet of position-tracking surface drifters in different open coast beach rip current systems and obtained spatially synoptic estimates of rip current flow patterns, which revealed semi-enclosed, large-scale vortices

that were contained within the surf zone and largely retained drifters (only 17% drifter exits per hour). Rip current surfzone retention and exchange evaluated with a three-dimensional (3-D) numerical model demonstrated the importance of including Stokes drift and very low frequency (VLF) motions to accurately describe the behavior of rip current exits (Reniers et al. 2009; Reniers et al. 2010), where excluding Stokes drift or VLF motions resulted in an over or under estimation, respectively, of drifter exits (Reniers et al. 2009). Smith and Largier (1995) observed rip currents that episodically transported water offshore with a sector-scanning Doppler sonar in La Jolla, California, and concluded that rip currents could cause significant exchange between the surf zone and offshore, capable of flushing the surf zone in roughly three hours.

These studies did not investigate the fate of the material (drifters) that was transported outside the surf zone by the rip currents. Talbot and Bate (1987) obtained qualitative aerial observations of dye released in rip currents and examined "exchange" rips that discharged dye offshore of the breaker line, which either traveled a short distance past the breaker line and was recycled back into the surf zone within seconds, or moved up to 2 km beyond the breaker line and then moved alongshore and sometimes re-entered the surf zone. Rip current flows outside the surf zone were investigated by Reniers et al. (2010) using a numerical model and unveiling Lagrangian Coherent Structures (LCSs) within the pulsating rip current surface velocity field. LCSs represent transport barriers hidden in the flow that control the motion of passively advected particles in unsteady flows. Numerical drifters released in the model demonstrated narrow streaks of floating material observed outside the surf zone on rip-channeled beaches. The model results showed that the LCSs were elongated in the cross-shore at the locations of rip currents, allowing the transport of drifters offshore until they reached the offshore extent of the LCS. Then they could move only alongshore and were shown to gradually re-enter the surf zone. Occasionally, the LCSs became detached from the nearshore rip current circulation cell at the outer surf zone due to VLF eddy motions.

C. FIELD EXPERIMENT

1. Field Site

The exchange of material between the surf zone and the inner shelf was examined during an extensive field experiment on a rip-channeled beach in southern Monterey Bay, California, in May 2009. Bathymetry, offshore waves, wind, tidal elevation and currents were measured throughout the field experiment. At the field site in Sand City, CA, the beach is composed of a relatively steep foreshore (1/10 slope) with straight and parallel contours, flattening out inshore (1/100 slope), with quasi-periodic, O(125m), incised rip channels and continuing with a 1/20 offshore slope and straight and parallel contours seaward of the breaker zone (Figure 19). Feeder channels were present near the shoreline and converged with the incised rip channels. Regular bathymetric surveys were conducted throughout the experiment using a kinematic global positioning system (GPS) device mounted to a sonar-equipped personal watercraft (MacMahan 2001) to measure the inner shelf and outer surf zone, and a walking person to measure the shallow surf zone and dry beach. The local coordinate system used in this work is defined as positive offshore and to the south.

2. Wave, Wind, Tide and Current Measurements

Offshore waves were measured in 13 m water depth with an acoustic Doppler current profiler (ADCP) (Figure 20). There were gaps in the offshore ADCP wave data due to instrument fouling, therefore during those times wave parameters measured by National Data Buoy Center (NDBC) buoy 46240, located in 18.5 m water depth and just south of the field site, were shoaled to 13 m using linear wave theory (Dean and Dalrymple 1984) and hourly-averaged (Figure 20, gray lines). Wind speed and direction were recorded atop a 10 m tower onshore of the field site and rotated to the local coordinate system, and wind stress was calculated using the method by Large and Pond (1981) (Figure 20). Tidal elevation was obtained from the nearby National Ocean Service (NOS) tidal station 9413450 (Figure 20).

Five ADCPs were deployed to obtain in-situ Eulerian current and pressure measurements for 17 days in an alongshore array at the approximate offshore edge of the

surf zone (Figure 19). ADCPs 1 to 4 had a sample period of dt = 2 s with a measurement bin size of 0.11 m, and ADCP 5 sampled at dt = 3 s with a measurement bin size of 0.25 m. For the last 4 days of the experiment (yeardays 134 to 138), one ADCP was moved offshore (labeled ADCP 6), in line with a rip channel in the surf zone, to measure inner shelf flows, and three ADCPs remained in the alongshore array (Figure 19). During this time, ADCPs 1, 3 and 6 had a sample period of dt = 1 s with a measurement bin size of 0.10 m, and ADCP5 sampled at dt = 3 s with a measurement bin size of 0.25 m. The hourly-mean, depth-averaged cross-shore and alongshore velocities measured by the ADCP in the primary rip channel (ADCP 3: x = 140 m, y = 100 m) are shown in Figure 20, and the depth-averaged cross-shore velocity averaged over the duration of each drifter deployment is given in Table 1.

In order to estimate the surfzone-width, L_x, the mean wave conditions in 13 m water depth (measured by the offshore ADCP when data were available or by NDBC buoy 46240) were shoaled to the shoreline using a mean cross-shore beach profile, adjusted for the tidal elevation, with a depth-limited wave-breaking criterion of $H_s/h \geq 0.4$ (Thornton and Guza 1982). The cross-shore location of the surfzone boundary, X_{sz}, is defined as the cross-shore location of the maximum significant wave height H_s, and the cross-shore location of the shoreline, X_{sh}, is defined as the cross-shore location where h = 0 m, with the surfzone-width $L_x = X_{sz} - X_{sh}$. Throughout this work distances are given in terms of the number of surfzone-widths from the shoreline, where one L_x represents the edge of the surf zone.

3. Drifter Deployments

A fleet of Lagrangian surfzone drifters equipped with GPS devices was deployed to measure surface current patterns outside the surf zone. See MacMahan et al. (2009) for a complete description of the drifter design and performance. The drifter positions, sampled every 2 s, were converted to the local coordinate system and filtered to remove erroneous points. Velocity estimates were computed using a forward-differencing scheme. Nine drifter deployments were conducted during varying wave and tidal conditions, each lasting approximately 3 hours with between 28 to 45 drifters being

released. In an attempt to capture the spatial variation of rip-current flows that exit the surf zone, drifters were released using three approaches: 1) by swimmers in a cluster at the offshore edge of a rip channel, just outside of the surf zone, 2) by a boat in an alongshore line just outside of the surf zone, spanning four to five rip-channel/shoal systems, and 3) by a boat in a cross-shore line spanning from the edge of the surf zone and extending up to two surfzone widths offshore, in line with a rip channel (Figure 19). Conditions during the drifter deployments consisted of offshore waves with significant wave heights H_s of 0.43 to 1.31 m, peak wave periods T_p of 6.7 to 12.6 s, total wind stress magnitude $|\tau_s| < 0.04$ N/m^2, and L_x of 78 to 123 m (Table 1). All drifter deployments occurred during low tides (tidal elevation < MSL), to ensure rip current flows would be induced by the rip-channeled morphology, and during weak wind conditions, defined as $|\tau_s|<0.05$ N/m^2 by Ohlmann et al. (2012), allowing for the wave-driven transport to be examined separately.

D. LAGRANGIAN OBSERVATIONS

1. Qualitative Drifter Patterns

In general, the drifters released outside the surf zone initially moved seaward due to rip currents and eventually returned shoreward in an arcing pattern, at times re-entering the surf zone over shoals, with no drifters being permanently removed from the nearshore region. The qualitative drifter observations support the numerical modeling results of Reniers et al. (2010), which showed LCSs in the rip current flows had offshore limits prohibiting farther cross-shore transport and resulting in the shoreward return of drifters. Results from each individual drifter deployment are shown in Figures 21 and 22, where the track of every drifter that was released during the deployment is plotted, and the color of the drifter track represents the speed of the drifter. The drifters typically moved one to two L_x seaward of the surf zone before returning shoreward, with a maximum cross-shore extent of about six L_x. Two distinguishable drifter patterns were observed: 1) the drifters moved seaward and returned sharply back shoreward a short alongshore distance from where they exited, resulting in cross-shore exchange that was locally contained (Figure 21), and 2) the drifters moved seaward and travelled farther in the alongshore direction as

they gradually moved shoreward, resulting in cross-shore and alongshore exchange (Figure 22). During two of the drifter deployments (yeardays 135 and 136), the majority of the drifters moved into and remained inside the surf zone and no distinguishable offshore pattern was observed (not shown), therefore the results from these days will not be further discussed qualitatively.

a. Locally Contained Cross-Shore Exchange

Locally contained cross-shore exchange pattern occurred on yeardays 122, 129, and 132, when the rip currents were stronger during low tides and the alongshore currents outside the surf zone were weak (indicated by small mean alongshore drifter velocities outside the surf zone, as shown in Table 1). On yearday 122 (Figure 21), drifters released at the edge of the surf zone, offshore of a rip-channel, tended to move seaward and to the south, moving back shoreward and re-entering the surf zone over shoals less than 350 m down the beach. A cluster of drifters released about 2.5 L_x offshore in line with the rip channel were also pushed slightly seaward and south by the rip current pulse, then returned shoreward. The maximum extent of all drifters, whether released at the edge of the surf zone or farther offshore, was approximately the same and was 3.6 L_x. At different times during the deployment, drifters were observed to move shoreward and seaward at approximately the same location offshore of a rip channel (y = 250 m, x = 200 m), depending on if the rip current was pulsing or not at that time.

On yearday 129 (Figure 21), the first drifter release occurred just after low tide, with a total of 27 drifters being released in an alongshore line approximately 1.5 L_x offshore, spanning the width of two rip channels and two shoals. In general, drifters that were released to the south of the primary rip channel moved directly shoreward and entered the surf zone over a shoal. Drifters that were released offshore of the primary rip channel and to the north initially moved seaward, then turned either north or south and moved back shoreward. The drifters that moved north travelled about 200 m farther seaward, reaching a maximum distance of 3.8 L_x offshore, before arcing sharply and moving back shoreward. These drifters returned shoreward within 200 m or less in the alongshore direction from where they initially moved seaward. Two hours after the initial

drifter release, another alongshore line of drifters was released at the approximate same cross-shore location spanning two shoals and a rip channel. All of these drifters moved shoreward, most likely due to the rising tide and the weakening of the rip current.

Similar results were seen on yearday 132 (Figure 21), where drifters released offshore of shoals moved directly shoreward, entering the surfzone over the shoal. Drifters released offshore of the primary rip channel moved seaward and to the north, and returned shoreward within 300 m in the alongshore of their release location. Interestingly, all of these drifters were pushed back offshore when they reached y = -100 to -200 m (offshore of a rip channel), due to a neighboring pulsing rip current. The drifters again moved seaward and north, then returned shoreward within 200 m or less in the alongshore. The maximum offshore extent of the drifters on this day was 3.7 L_x.

b. Cross-Shore and Alongshore Exchange

Cross-shore and alongshore exchange pattern occurred on yeardays 125, 126, 130, and 137, when the rip currents were weak during high tides and the alongshore current outside the surf zone was stronger (Table 1). On yearday 125 (Figure 22), the first drifter release consisted of 29 drifters being released in an alongshore line, approximately 20 m apart, spanning an alongshore distance of about 600 m and five shoals and four rip channels. The surf zone was relatively wide (L_x = 122 m) this day, so the alongshore line was actually inside of the surf zone. Drifters released to the south of the primary rip channel (y > 100 m) meandered alongshore to the north inside the surf zone, following the underlying bathymetry contours. A number of these drifters ended up on the beach, and others were pushed seaward due to the rip current at y = 100 m. The drifters released near the primary rip channel and to the north, moved seaward and to the north. Once the drifters were outside of the surf zone they continued to move seaward and to the north, and then gradually moved back shoreward, with some even being pushed back offshore due to rip currents to the north. These drifters were picked up before they could re-enter the surf zone, which was 500 to 700 m alongshore to the north from the primary rip current where they exited the surf zone. The cross-shore extent of the drifters on this day was within 2 L_x. Additional drifter releases on this day consisted of clusters of drifters

being released in the primary rip channel near the offshore edge of the surf zone, and these all moved in a similar pattern seaward and to the north. A similar drifter pattern was observed on yearday 126 (Figure 22). Again, an alongshore line of drifters was released, this time just outside of the surf zone, and the drifters either moved into the surf zone or alongshore and were eventually pushed seaward and to the north. The cross-shore extent was about 2.8 L_x, and again the drifters were picked-up greater than 600 m to the north from where they were pushed seaward as they were beginning to gradually move shoreward.

On yearday 130 (Figure 22), in general, drifters that were released outside of the surf zone and offshore of the primary rip channel or to the north, were pushed seaward as they moved alongshore to the south, and then began moving shoreward once they were about 300 m to the south of the rip channel (y = 400 m). Drifters that were released outside of the surf zone and to the south of the primary rip channel moved predominantly alongshore with little to no seaward movement and gradually shoreward. The cross-shore extent of the rip current was demonstrated by a release of drifters in a cross-shore array offshore of the primary rip channel, approximately 1.5 to 2.5 L_x offshore, where all of the drifters moved south and seaward and seemed to converge at a cross-shore extent of about 3.3 L_x, where they then began moving shoreward. Drifters that were released at the surfzone boundary and inshore were immediately pulled into the surf zone over a shoal. As the tide rose during the deployment, the rip current weakened and no drifters moved seaward, and the drifters inside of the surf zone exhibited a meandering current pattern. Throughout the deployment, all drifters that moved seaward and alongshore outside of the surf zone were picked-up 300 to 500 m south of the primary rip channel, before they had a chance to re-enter the surf zone, indicating a significant amount of alongshore exchange was occurring.

The drifter deployment on yearday 137 (Figure 22) occurred during low tide with relatively small wave conditions, resulting in a narrow surf zone (L_x = 81 m). Drifters were released in a cross-shore array in line with the primary rip channel between 1 to 2 L_x. The rip current pulse pushed the drifters seaward and to the south, with a maximum cross-shore extent of about 2.5 L_x. All of the drifters gradually returned shoreward, and

approached the surf zone boundary greater than 500 m from the primary rip channel where they were released, with a majority of the drifters then being pushed back offshore and to the south exhibiting a meandering alongshore current pattern outside of the surf zone within 2 L_x. Shear in the alongshore current outside of the surf zone can be seen in the drifter results, with the alongshore current magnitude decreasing near the surfzone boundary.

2. Drifter One-Particle Diffusivity Statistics on the Inner Shelf

The movements of the drifters outside the surf zone were evaluated using one-particle statistics, which describe the average drifter evolution from a common release point. The trajectories of the drifters are represented as the collection of relative position displacements, $\boldsymbol{r}(t') = \boldsymbol{x}(t'_0 + t') - \boldsymbol{x}(t'_0)$, for a relative time step t', computed as the difference between the drifter position, $\boldsymbol{x} = (x, y)$, at an earlier time t'_0 from the position a time t' later. Each recorded drifter position is considered a possible starting position, $\boldsymbol{x}(t'_0)$, therefore a drifter time series with N total position measurements yields $(N - 1)$ values for $\boldsymbol{r}(t' = 2\text{ s})$, where the drifter positions were sampled at $dt = 2$ s. Assuming a spatially homogeneous and temporally stationary flow field, all drifters released during a given deployment can be viewed as originating from a common release point, and the random motions represented by the drifter trajectories can be described in the same manner as the bulk molecular diffusion (Taylor 1922). The one-particle absolute diffusivity, κ_{ij}, is related to the change in drifter displacement variance, σ^2_{ij}, with time

$$\kappa_{ij}(t') = \frac{1}{2}\frac{d}{dt'}\sigma^2_{ij}(t'), \tag{7}$$

where $i, j = x, y$ and σ^2_{ij} is the second moment of displacements

$$\sigma^2_{ij}(t') = \iint r'_i r'_j P\left(r'_x r'_y; t'\right) dr'_i dr'_j, \tag{8}$$

and $P(r_x', r_y'; t')$ is the probability distribution function (pdf) of the anomalous relative particle displacements $\boldsymbol{r'}=(r_x', r_y')$. The anomalous relative position displacements were calculated for each drifter as $\boldsymbol{r'}(t') = \boldsymbol{r}(t') - \boldsymbol{R}(t')$, where $\boldsymbol{R}(t')$ is the mean spatial displacement of all drifters for the time step t' and all arbitrary t'_0 (Spydell et al. 2007; Brown et al. 2009). The pdf of the anomalous relative position displacements $P(r_x', r_y'; t')$

represents the ensemble average evolution of the drifters from a common initial point source.

In order to evaluate the fate of material outside the surf zone, only drifter positions recorded outside the surf zone ($x > L_x$) for durations of at least one minute were evaluated. The probability distributions of the anomalous displacements for $t' = 2$ s, $P(r_x', r_y'; t' = 2$ s), were relatively centered about zero in the cross-shore direction, indicating an equal amount of drifters moved seaward and shoreward (Figure 23). Examining just the cross-shore anomalous relative displacements, the distributions were similar for all drifter deployments regardless of drifter pattern observed (Figure 23), and were slightly negatively skewed (skewness of -0.24 to -0.05), and had kurtosis values ranging from 2.8 to 4.9, suggesting that the distributions were basically Gaussian (kurtosis = 3). Therefore, there was a relatively equal chance that a drifter outside of the surf zone would move seaward or shoreward, which supports the qualitative observations that the drifters did not leave the nearshore system (Figure 21 and 22).

The cross-shore absolute diffusivities κ_{xx} (Equation 7) outside the surf zone showed similar behavior for all current patterns, with κ_{xx} rising to a peak then decreasing to an asymptotic value (Figure 24). The time to reach the peak κ_{xx} was generally 15 to 19 minutes, with the exception of yearday 129 which occurred at 36 minutes. The values of κ_{xx} were greater during observations of locally-contained cross-shore exchange, with peak values of κ_{xx} of 1.11 to 2.41 $m^2\ s^{-1}$ and asymptotic values of κ^{∞}_{xx} of 0.36 to 1.74 $m^2\ s^{-1}$. During observations of alongshore and cross-shore exchange, the difference in the peak and asymptotic values of κ_{xx} were relatively small, with peak values of κ_{xx} of 0.28 to 1.00 $m^2\ s^{-1}$ and asymptotic values of κ^{∞}_{xx} of 0.27 to 0.73 $m^2\ s^{-1}$. The alongshore absolute diffusivities κ_{yy} outside the surf zone increased approximately monotonically to an asymptotic level for all drifter releases (Figure 24).

During observations of locally-contained cross-shore exchange, κ^{∞}_{xx} was greater than κ^{∞}_{yy} (1.25 to 1.83) due to the predominant movement and spreading of the drifters in the cross-shore direction while remaining within a relatively narrow alongshore region. However, during observations of cross-shore and alongshore exchange, values of κ^{∞}_{yy} (0.36 to 5.01 $m^2\ s^{-1}$) were generally greater than κ^{∞}_{xx} due to the drifters spreading more in

the alongshore direction and remaining within a smaller cross-shore extent. For these reasons, κ^{∞}_{xx} was largest when there was more cross-shore exchange, and κ^{∞}_{yy} was largest when there was more alongshore exchange (Figure 24).

The asymptotic values of diffusivity obtained outside the surf zone (κ^{∞}_{xx} = 0.27 to 1.74 m^2 s^{-1}, κ^{∞}_{yy} = 0.36 to 5.01 m^2 s^{-1}) were smaller than those measured in previous experiments inside the surf zone (κ^{∞}_{xx} = 0.10 to 2.50 m^2 s^{-1}, κ^{∞}_{yy} = 2.00 to 12.60 m^2 s^{-1}) (Spydell et al. 2007; Brown et al. 2009), regardless of the measured current pattern (i.e. rip current circulation versus alongshore current). Additionally, κ_{xx} and κ_{yy} rise more rapidly inside the surf zone, and the time to approach κ^{∞}_{xx} and κ^{∞}_{yy} is longer outside the surf zone, similar to the limited inner shelf observations of drifter diffusivity obtained by Spydell et al. (2007) and Brown et al. (2009). For all drifter deployments, the absolute diffusivities lacked oscillations, indicating a lack of rotational structures outside the surf zone (Brown et al. 2009), and that different eddy processes with different spatial and time scales are responsible for mixing material on the inner shelf.

3. Cross-Shore Variation in Drifter Cross-Shore Velocity Magnitude

The behavior of the drifters moving seaward ($u_{drift,off}$) and shoreward ($u_{drift,on}$) was evaluated by examining the drifter cross-shore velocity magnitude $\left|u_{drift,off/on}\right|$ as a function of cross-shore location L_x. The study area was divided into 25 m bins in the cross-shore direction, and the seaward ($u_{drift} \geq 0$ m/s) and shoreward ($u_{drift} < 0$ m/s) moving drifters in each cross-shore bin were averaged separately over the entire alongshore distance (Figure 25). Outside the surf zone, the magnitude of the seaward and shoreward moving drifters were relatively equal, $\left|u_{drift,on}\right| \approx \left|u_{drift,off}\right|$, indicating the total alongshore-averaged cross-shore drifter velocity was approximately zero, as a function of cross-shore distance. At the edge of the surf zone, the shoreward drifter velocities were greater than the seaward component, possibly due to the surfing of the shoreward moving drifters in the breaking waves. Inside the surf zone, the shoreward drifter velocities over the shoals were larger than the seaward drifter velocities in the rip channel, due to continuity and differences in water depth (MacMahan et al. 2004a). The $\left|u_{drift,off/on}\right|$ were

similar for all drifter deployments, that is the drifter velocities measured for the locally contained cross-shore exchange drifter pattern were not necessarily greater or less than those measured for the cross-shore and alongshore exchange drifter pattern.

The drifter cross-shore velocity magnitude $\left|u_{drift,off/on}\right|$ tended to decrease over the distance of one surfzone-width offshore of the surf zone (i.e., from $x = 1L_x$ to $x = 2L_x$), and $\left|u_{drift,off/on}\right|$ was relatively constant offshore of $x > 2L_x$, for all drifter deployments (Figure 25). The average change in $\left|u_{drift,off/on}\right|$ offshore of the surf zone was $\Delta\left|u_{drift,off/on}\right| = \left|u_{drift,off/on}\left(L_x\right)\right| - \left|u_{drift,off/on}\left(2L_x\right)\right| \approx 0.12$ m/s, including seaward and shoreward drifter velocities. The drifters exiting the surf zone due to rip current pulses and moving seaward had large velocities at the edge of the surf zone, which subsequently decreased as they continued to move seaward, resulting in a deceleration of the drifters as they exited the surf zone. The drifters outside the surf zone moving shoreward demonstrated an increase in velocity magnitude as they approached the edge of the surf zone. Therefore the shoreward moving drifters were actually accelerating as they re-entered the surf zone over shoals. These results differ from those of Ohlmann et al. (2012), who observed a tendency for drifters released on the inner shelf to decelerate as they moved shoreward, due to a net offshore Lagrangian surface velocity, on beaches that do not typically support rip currents.

The $\left|u_{drift,off/on}\right|$ measurements outside the surf zone were compared to theoretical estimates of the Stokes drift, u_{St}. The cross-shore variation of $u_{St}(z)$ was computed using wave parameters measured in 13 m water depth and shoaled to the shoreline using the mean cross-shore beach profile adjusted for tides. The $u_{St}(z)$ was averaged over the upper 0.5 m of the water column corresponding to the depth of the surface drifters, indicated as u_{St}(0.5 m). In all cases, $\left|u_{drift,off/on}\right|$ was greater than the u_{St}(0.5 m) estimates as a function of cross-shore location (Figure 25). Therefore, the return of the drifters shoreward was not solely due to the net onshore Stokes drift due to waves.

E. EULERIAN OBSERVATIONS

1. 3-D Variations of the Rip Current Flow

The Eulerian measurements made by the array of ADCPs show differences in the magnitude and vertical structure of the cross-shore flows between the ADCPs on the shoals (ADCPs 1 and 5) and the ADCPs in the rip channel (ADCPs 2, 3, 4, and 6). To examine these differences, the cross-shore velocities measured during low tides, when rip current flows are known to be strongest (MacMahan et al. 2006), were evaluated. For each ADCP, the vertical current profiles were interpolated to a depth-relative reference frame z/h, where $z/h = 0$ is at the sea-bed and $z/h = 1$ is at MSL, and a 3-hour mean centered about low tide was computed. These mean current profiles were then sorted by local H_s/h and bin-averaged, as shown in Figure 26.

In general, at a given ADCP location, the magnitude of the cross-shore velocity was greater for larger H_s/h, representative of larger waves and/or lower tides. These Eulerian measurements support the Lagrangian drifter observations of decreasing $\left|u_{drift,off/on}\right|$ with increasing distance offshore, where smaller H_s/h are indicative of measurements farther outside of wave breaking. Additionally, for a given H_s/h range, the magnitude of the seaward cross-shore velocities were greatest in the center of the rip channel near the edge of the surf zone at ADCP 3, and were smallest over the shoals at ADCPs 1 and 5 (Figure 26).

The measured Eulerian cross-shore velocity profiles revealed more shear over the vertical, particularly near the surface, within the rip channel, and depth-uniform currents below the wave trough over the shoals. In the center of the rip channel near the surfzone boundary at ADCP 3, the measured mean rip current velocity profile was surface dominated and had more vertical structure for smaller H_s/h, and was more depth-uniform for larger H_s/h representative of times when it was near the onset of wave-breaking and just outside the surf zone (Figure 26). Well offshore of the surf zone, at ADCP 6, the measured seaward rip current flow was also surface dominated, demonstrating the cross-shore extent of the rip current flows that exit the surf zone. These results support the laboratory measurements of Haas and Svendsen (2002), and reveal that the vertical

profile of the rip current velocity is strongest and depth-uniform as it exits the surf zone, then becomes surface dominated and decays in magnitude with distance offshore. The cross-shore velocity profiles measured by ADCPs 1 and 5 over the shoals were vertically uniform below the wave trough for all values of H_s/h, and were even onshore at times for $H_s/h > 0.4$ when they were inside the surf zone.

2. Volumetric Transport Estimates

The volumetric transport on the rip-channeled beach is evaluated using the Eulerian current measurements, and is compared to conventional theory. If the conventional theory of rip current transport (Figure 18e) is valid, a volumetric balance across the surfzone boundary on a rip-channeled beach would exist where the continuous deposition of water into the surf zone via the Stokes transport over the shoals ($Q_{St}\ \lambda_{rip}$) would be balanced by the steady compensating offshore Eulerian rip current transport through the rip-channels ($Q_{E,rip}\ b_{rip}$). Therefore, the depth-averaged offshore Eulerian rip current flow $\overline{u}_{E,rip}$ would equal

$$\overline{u}_{E,rip} = \frac{\overline{u}_{St}\lambda_{rip}}{b_{rip}}, \tag{9}$$

according to Equation (6), where the depth-averaged Stokes drift $\overline{u}_{St}$ associated with the surface gravity waves is

$$\overline{u}_{St} = -\frac{Q_{St}}{h} = -\frac{gh}{16c}\left(\frac{H_s}{h}\right)^2 \cos\theta_w . \tag{10}$$

Observed hourly-mean cross-shore velocity profiles measured by each ADCP were used to estimate the depth-averaged Eulerian flows below the wave trough, $\overline{u}_E$. The velocity was assumed uniform between the lowest measurement (generally 0.5 m above the sea-bed) and the sea-bed (Lentz et al. 2008), and $\overline{u}_E$ was estimated using trapezoidal integration and averaging over the depth of the wave trough. The measured $\overline{u}_E$ was normalized by ($16c/gh$), represented as $\overline{u}_{N,E}$, and were bin-averaged as a function of H_s/h, and are shown in Figure 27. Theoretical estimates of $\overline{u}_{E,rip}$ were computed using Equation (9), where the rip-channel spacing λ_{rip} =125 m and width b_{rip} = 40 m were based on the

measured bathymetry, and also normalized by ($16c/gh$), represented as $\overline{u}_{N,E,rip}$, and are shown in Figure 27 (dashed black line). Additionally, the theoretical normalized $\overline{u}_{N,St}$ based on Equation (10), as a function of H_s/h, is shown in Figure 27 (solid black line), which represents the balance between $u_E(z)$ and $u_{St}(z)$ found on the inner shelf by Lentz et al. (2008). The location of the onset of wave breaking is defined as $H_s/h > 0.4$ and is shown in Figure 27 to describe the observations as being inside or outside of the surf zone.

In general, field observations of $\overline{u}_{N,E}$ increased with increasing H_s/h, associated with increasing wave heights and/or lower tides. For small waves and/or higher tides ($H_s/h < 0.2$), measured $\overline{u}_{N,E}$ was between the two theoretical volumetric balances (Equations (9) and (10)), and was generally equal to $\overline{u}_{N,St}$ (Figure 27, solid black line). This is consistent with observations on the inner shelf by Lentz et al. (2008), and indicates zero net Lagrangian cross-shore transport well outside of the surf zone. A transition in $\overline{u}_{N,E}$ exists approaching the surfzone boundary ($0.2 < H_s/h < 0.4$), where for a given range of H_s/h, the magnitude of $\overline{u}_{N,E}$ was dependent upon the alongshore location of the ADCP (i.e., within the rip channel). The $\overline{u}_{N,E}$ measured by ADCP 1 (Figure 27, blue) and ADCP 5 (Figure 27, yellow) remained consistent with Equation (10) and Lentz et al. (2008). This is attributed to ADCPs 1 and 5 being located at the borderline of the rip current width, yet not over the shoals, and therefore the measured velocities were typically small and not representative of strong rip current nor onshore flows. However, $\overline{u}_{N,E}$ measured within the rip channel by ADCPs 2, 3, and 4 (Figure 27, green, magenta, and cyan) tended to exceed the theoretical Stokes drift transport $\overline{u}_{N,St}$ (Equation (10)) and the conventional rip current volumetric transport $\overline{u}_{N,E,rip}$ (Equation (9)). The fact that the measured $\overline{u}_{N,E}$ in the rip current was greater than $\overline{u}_{N,E,rip}$ near the edge of the surf zone indicates an imbalance in the volume transport across the surfzone boundary on the rip-channeled beach, with more offshore transport exiting the surf zone through the rip channels than the onshore Stokes transport entering the surf zone over the shoals. Additionally, there is a greater imbalance (larger offshore transport) at the surfzone

boundary that decreases with distance offshore (decreasing H_s/h), consistent with the drifter observations. The consistency in the measurements by ADCPs 2, 3, and 4 demonstrates that each ADCP was measuring seaward rip current flows, and the alongshore spacing of the ADCPs verifies the narrow rip current width, b_{rip} = 40 m, used in Equation (9). Inside of the surf zone ($H_s/h > 0.4$), $\overline{u}_{N,E}$ measured on the shoals was less than the theoretical $\overline{u}_{N,E,rip}$ (Equation (9)), but unfortunately no measurements of $\overline{u}_{N,E}$ in the rip currents were obtained shoreward of wave breaking.

F. DISCUSSION

1. Mass Balance Controlling Cross-Shore Exchange on a Rip-Channeled Beach

The extensive data set presented here, incorporating measurements of Eulerian rip current flows and transport inside and outside the surf zone, as well as Lagrangian drifter observations on the inner shelf, combined with previous surf zone drifter observations (MacMahan et al. 2010a), is contrary to the conventional paradigm of rip current transport. Based on the conventional theory (Equation (6)), if onshore Stokes transport was continuously depositing water into the surf zone over the shoals ($Q_{St}\ \lambda_{rip}$), a steady compensating offshore transport through the rip channels would exist ($Q_{E,rip}\ b_{rip}$). However, the measured $\overline{u}_{N,E}$ in the rip channel was greater than $\overline{u}_{N,E,rip}$ suggested by theory (Figure 27), indicating a greater amount of offshore transport by the rip current across the surfzone boundary than the filling of the surfzone by Stokes transport over the shoals. Also, the drifter observations show that $\left|u_{drift,off/on}\right| > u_{St}$(0.5 m), indicating that Stokes transport associated with short waves does not seem to transport mass shoreward in the nearshore and across the surfzone boundary on the rip-channeled beach. The excess $\overline{u}_{N,E}$ measured above $\overline{u}_{N,E,rip}$ does not indicate a net offshore transport, however, because the drifter observations on the inner shelf show that no drifters completely left the nearshore system. The seaward and shoreward drifter velocity magnitudes were relatively equal outside the surf zone (Figure 25), implying there was no net Lagrangian transport, consistent with Lentz et al. (2008). These results suggest that a recirculation exists across the surfzone boundary. Additionally, based on the high retention of drifters within the

surf zone observed on this same beach by MacMahan et al. (2010a), the offshore flow via the rip current $\overline{u}_{N,E}$ could not be constant. This is consistent with the findings of Reniers et al. (2009, 2010), who found rip current exchange is driven by VLF rip current pulsations forced by wave groups for a rip-channeled beach with O(10 minute) timescales. Therefore, as material is transported offshore by rip current pulsations, some factor besides Stokes transport must be responsible for pulling material shoreward on the inner shelf and into the surf zone. This also explains why the drifters did not decelerate as they approached the surfzone boundary, as observed by Ohlmann et al. (2012) on the inner shelf where there were no rip channels or surfzone rip current circulations present.

It is hypothesized that a mass balance exists on the rip-channeled beach, where the surfzone rip current circulations both eject material offshore in the rip channels as VLF pulses, as well as pull material back into the surfzone over shoals (Figure 18e). This is investigated by further examining the Lagrangian and Eulerian measurements during the time of the drifter deployment on yearday 132, when locally-contained cross-shore exchange was observed. The mean cross-shore velocity observations of the drifters from the entire deployment on this day were re-evaluated by spatially binning and averaging the observations into 10 m by 10 m bins, with the mean cross-shore movement of the drifters at each bin represented as a percentage of time that the drifters were moving seaward, i.e. always (100% of the time, red) or never (0% of the time, blue), as shown in Figure 28. It is evident that the drifters moved out of the surf zone and seaward through the rip channel, and returned shoreward and re-entered the surf zone over the shoals. Figure 28 also shows that for this particular drifter deployment, out of the ADCPs that were within the rip channel, only ADCPs 2 and 3 were located where drifters were exiting the surf zone, with ADCPs 4 and 5 being located where drifters were moving both seaward and shoreward, and ADCP 1 being located where a slightly higher percentage of drifters were moving shoreward. This demonstrates the narrow width of the rip current, and highlights the asymmetry in the re-circulation of the flow. Therefore, the values of $\overline{u}_{N,E}$ shown in Figure 27 measured by the ADCPs in the rip channel (ADCPs 2, 3, and 4) are assumed to describe the seaward rip current transport, and support the observations of the seaward moving drifters. However, ADCPs 1 and 5 were on the edge of the rip

current flow and did not necessarily measured the strong onshore flows occurring over the shoals, which is why the values of $\overline{u}_{N,E}$ measured by ADCPs 1 and 5 do not match the observations of the shoreward moving drifters.

The vertical structure of the cross-shore flows measured by the ADCPs during the drifter deployment on yearday 132 (excluding ADCP 2, which was inoperative this day) is shown in Figure 29 (top row). The profiles show offshore flows, which were surface dominated, measured inside the rip channel (ADCPs 3 and 4), and onshore flows, which were vertically uniform below the wave trough, measured by ADCPs 1 and 5, where the measured onshore flows were a fraction of the measured offshore rip current flows. The presence of VLF pulses in the measured rip current surface flow was examined by low-pass filtering (f < 0.004 Hz) the near-surface cross-shore velocity measured by the ADCPs (Figure 29, bottom row). Oscillations were present in the low-passed filtered offshore surface rip current velocity (ADCP3 and 4) at the VLF timescale with relatively large amplitudes (0.5 to 1.0 m s^{-1}) that represent the VLF rip current pulsations responsible for the rip current exits. Additionally, similar VLF oscillations of smaller magnitude (0.1 to 0.2 m s^{-1}) were present in the onshore surface velocities over the shoals. These results demonstrate the VLF pulsating nature of the seaward rip current flows as well as the shoreward flows re-entering the surf zone.

A new paradigm of rip current behavior is presented (Figure 18e). It is proposed that the onshore Stokes transport associated with short waves does not transport mass into the surf zone on a rip-channeled beach, but rather deposits momentum at the wave group timescale that drives the cross-shore exchange and forces episodic, VLF rip current pulsations. To balance the mass transported offshore by the rip current exits, the surfzone rip current circulations over the shoals pull material back into the surf zone at the same VLF time scale. Ultimately little or no material is completely removed from the nearshore system.

G. SUMMARY AND CONCLUSIONS

Cross-shore exchange on a rip-channeled beach at Monterey, California, was examined using an extensive set of Lagrangian and Eulerian field measurements of surf

zone and inner shelf rip current flows. The results revealed differences in cross-shore transport from that measured on the inner shelf of alongshore homogeneous beaches, and is contrary to the conventional theory of mass transport due to rip currents. Position-tracking drifters released on the inner shelf were observed to move seaward due to rip current pulses, then return shoreward in an arcing pattern, re-entering the surf zone over shoals. Two drifter patterns were observed: 1) locally-contained cross-shore exchange, where the drifters moved seaward and returned sharply back shoreward a short alongshore distance from where they exited (Figure 21), and 2) cross-shore and alongshore exchange, where the drifters moved seaward and traveled farther in the alongshore direction as they gradually moved shoreward (Figure 22). The cross-shore extent of the drifters was typically one to two surfzone-widths L_x beyond the surfzone boundary. The qualitative drifter observations were similar to the numerical model results of Reniers et al. (2010), which showed that at the locations of rip currents LCSs constrained the offshore extent of drifter transport in the cross-shore where they then moved alongshore and re-entered the surf zone. Additional LCS model simulations with drifters seeded on the inner shelf would help to further explain the fate of the detached LCSs and cross-shore exchange of material on the inner shelf.

On the inner shelf of the rip-channeled beach, the rate of spreading and mixing (κ^{∞}_{xx} = 0.27 to 1.74 m^2 s^{-1}, κ^{∞}_{yy} = 0.36 to 5.01 m^2 s^{-1}) was slower than that measured inside the surf zone during previous studies (Brown et al. 2009), suggesting there is less shear in the flow field outside the surf zone. The probability distributions of the drifter cross-shore anomalous relative displacements outside the surf zone were basically Gaussian, indicating there was a relatively equal chance that a drifter anywhere on the inner shelf would move seaward or shoreward, consistent with the qualitative observations that no drifters left the nearshore system. The seaward and shoreward moving cross-shore drifter velocities were approximately equal in magnitude as a function of cross-shore location, resulting in a total Lagrangian velocity of approximately zero The seaward moving drifters were observed to decelerate after exiting the surf zone through rip channels, while the shoreward moving drifters were observed to accelerate as they re-entered the surf zone over shoals. Near the surfzone boundary, the depth-averaged

Eulerian flows $\overline{u}_{N,E}$ measured in the rip channel were largest near the edge of the surf zone, consistent with the drifter observations, and were greater than the offshore rip current transport $\overline{u}_{N,E,rip}$ suggested by conventional theory to balance the filling of the surfzone by Stokes transport over the shoals. The magnitude of the shoreward moving drifters outside the surf zone was greater than the near-surface theoretical Stokes drift, therefore Stokes drift was not responsible for moving the drifters shoreward and back into the surf zone, and Stokes transport does not provide a continuous, wave mass flux into the surf zone across the surfzone boundary that would induce a continuous, compensating mass flux out of the surf zone via rip currents on a rip-channeled beach, as conventionally thought. The results support a new theory of how material is exchanged and conserved within the nearshore region on a rip-channeled beach: 1) short waves deposit momentum into the surf zone at the wave group timescale, then 2) spatial variations in the wave groups force VLF motions and rip current circulations inside the surf zone that episodically expel material offshore through the rip channels, and 3) the surfzone rip current circulations act to pull the material back onshore into the surf zone over shoals to satisfy a mass balance, with ultimately little or no material being completely removed from the nearshore system on the rip-channeled beach.

IV. MIXING AND TRANSPORT ON A STEEP BEACH

A. INTRODUCTION

The mixing and transport of material in the nearshore, including suspended sediment, pollutants, biological matter, and nutrients, influences beach composition, water quality, and ecosystem stability. There have been few field studies on mass transport and cross-shore exchange across the surfzone boundary, and most have occurred on wide, dissipative beaches in Southern California (Inman et al. 1971; Boehm 2003; Grant et al. 2005; Clark et al. 2010). These beaches support communities with large human populations, and an understanding of the mixing and transport of pollutants on dissipative beaches has both health and economic relevance (Grant et al. 2005; Given et al. 2006; amongst others). In contrast, steep beaches typically do not support a lot of recreational activities, owing to their hazardous shore break. However, steep reflective beaches are important because they are common and are typically situated between rocky outcrops where there are often dense and diverse communities of organisms. Therefore, steep beaches can be studied to understand exchange processes that are important for those communities, such as biological recruitment. In general, a better understanding of how material is dispersed on beaches with varying topography and wave and current conditions is needed.

Mixing and transport in the surf zone results from several physical processes with distinctive temporal and spatial scales, which can be separated into two dominant mechanisms that act to disperse material horizontally: 1) advection, which describes the bodily transport of material due to wave-driven surfzone currents, and 2) diffusion, which describes the spreading of material due to turbulent motions. These processes can be described by the two-dimensional (2-D), depth-averaged, advection-diffusion equation

$$\frac{\partial(hC)}{\partial t}+\left\{\frac{\partial(uhC)}{\partial x}+\frac{\partial(vhC)}{\partial y}\right\}=\left\{\frac{\partial}{\partial x}\left[\kappa_x\frac{\partial(hC)}{\partial x}\right]+\frac{\partial}{\partial y}\left[\kappa_y\frac{\partial(hC)}{\partial y}\right]\right\}+S \qquad (11)$$

where C is the depth-averaged tracer concentration, h is the total water depth, u and v are the cross-shore (x) and alongshore (y) components of the time- and depth-averaged

velocity, κ_x and κ_y are the eddy diffusion coefficients, and S is a source/sink term (Fischer et al. 1979). Solving Equation (11) for an instantaneous point source of dye mass M_0 input at $x = 0$, $y = 0$, $t = 0$ ($S = M_0\delta(x,y,t)$), with a no-flux boundary condition applied at the shoreline ($x = 0$) using the method of images (Fischer et al. 1979), and assuming constant diffusion coefficients, results in the solution (Rutherford 1994)

$$C(x,y,t) = \frac{1}{\bar{h}} \frac{M_0}{4\pi t\sqrt{\kappa_x \kappa_y}} \left[2\exp\left(-\frac{\left(x-\bar{U}t\right)^2}{4\kappa_x t} \right) \exp\left(-\frac{\left(y-\bar{V}t\right)}{4\kappa_y t} \right)^2 \right] \tag{12}$$

where $C(x,y,t)$ is in ppb, $\bar{h}$ = 0.5 m is the mean surfzone water depth, and $\bar{U}$ and $\bar{V}$ are the surfzone averaged cross-shore and alongshore currents.

Previous studies used fluorescent dye as a tracer to examine surfzone mixing and transport on wide, dissipative beaches, focusing on either alongshore dispersion (Harris et al. 1963; Inman et al. 1971; Boehm 2003; Grant et al. 2005; Clarke et al. 2007) or cross-shore dispersion (Clark et al. 2010), but often lacked high resolution, 2-D measurements and utilized simple models to describe the 2-D evolution of the surfzone mixing and transport processes. Lagrangian surface drifters have also been used to study dispersion on alongshore-uniform (Spydell et al. 2007) and rip-channeled (Brown et al. 2009) dissipative beaches, however drifters do not perform well in the energetic, narrow surf zone of a steep beach. Visual observations of dye released in the surf zone reveal rapid vertical mixing (Clark et al. 2010), and initial 2-D horizontal (cross-shore and alongshore) dispersion until the surf zone was saturated (approximately uniform cross-shore concentration) (Harris et al. 1963; Inman et al. 1971; Clarke et al. 2007; Clark et al. 2010). The dye was dispersed by advection and diffusion; however, once the width of the dye patch was of the order of the width of the surf zone (100 m to over 1 km alongshore from the dye release location), mixing by diffusion was not important and advection dispersed the dye, becoming one-dimensional (1-D) in the alongshore direction (Harris et al. 1963; Inman et al. 1971; Grant et al. 2005; Clarke et al. 2007; Clark et al. 2010).

A measure of the amount of cross-shore exchange occurring on a beach can be expressed as the ratio of alongshore transport to cross-shore transport (Grant et al. 2005). In the absence of an ambient current, local wave conditions control the wave-driven

currents and influence the exchange ratio $\bar{V}/\bar{U}$. The case where $\bar{V}/\bar{U} \approx 0$ indicates complete cross-shore exchange, which occurs when waves break shore-normally and $\bar{V}/\bar{U}$ increases with increased alongshore advection and decreased cross-shore exchange, which occurs when waves approach the shore obliquely. On a wide (50 m surf zone width), dissipative (1/50 beach slope), relatively alongshore uniform beach, that spanned O(km) in the alongshore, at Huntington Beach, California, Grant et al. (2005) found the cross-shore flux was 50 to 300 times smaller than the alongshore flux. The resulting ratio of $\bar{V}/\bar{U} > 50$ indicates that alongshore advection dominates, and therefore suggests that most of the material remains within the surf zone and travels alongshore between the shoreline and active wave breaking with only a small amount of cross-shore exchange occurring continuously across the surfzone boundary. Field measurements of alongshore mass transport on dissipative beaches indicate an exponential decay of tracer as a function of distance along the shoreline from the release point (Inman et al. 1971; Boehm 2003; Grant et al. 2005), consistent with a conceptual model where alongshore advection dominates both alongshore mixing and cross-shore mixing (Boehm 2003; Grant et al. 2005).

Previous studies estimated surfzone diffusivities by fitting tracer measurements to a Fickian diffusion model (Inman et al. 1971; Clarke et al. 2007; Clark et al. 2010). Using discrete tracer samples at the shoreline, and assuming constant alongshore currents and depth, and prescribing no-flux boundaries at the shoreline and wave-breaker line, Inman et al. (1971) and Clarke et al. (2007) found that in general $\kappa_x >> \kappa_y$, however these estimates were not statistically reliable. Clark et al. (2010) estimated surfzone cross-shore diffusivities on a wide, dissipative beach at Huntington Beach, California, using ensemble-averaged cross-shore profiles of tracer concentration and a Fickian diffusion model with a no-flux boundary at the shoreline. They observed shoreline-attached cross-shore tracer concentration profiles, with κ_x = 0.5 to 2.0 $m^2\ s^{-1}$, and decreased tracer concentrations downstream of the source and seaward of the surf zone, consistent with lower diffusivity outside the surf zone (Harris et al. 1963; Inman et al. 1971; Clark et al. 2010). Surfzone diffusivities on dissipative beaches have also been estimated using surface drifters, with asymptotic (long time) κ_x = 0.7 to 1.5 $m^2\ s^{-1}$ and κ_y = 2.0 to 4.5 $m^2\ s^{-}$

[1] found for an alongshore uniform, dissipative beach (Spydell et al. 2007), and asymptotic κ_x = 0.9 to 2.2 $m^2 s^{-1}$ and κ_y = 2.8 to 3.9 $m^2 s^{-1}$ found on a rip-channeled beach (Brown et al. 2009).

In this work, field observations of the mixing and transport processes that occur on a sandy steep, reflective beach are investigated and compared to the findings on dissipative beaches. Dye was released in the narrow surf zone and the temporal and spatial evolution was measured, resulting in simultaneous alongshore and cross-shore dye concentration profiles, and estimates of alongshore and cross-shore transport of dye and diffusion coefficients were obtained.

B. FIELD EXPERIMENT

1. Field Site, and Wave and Current Measurements

Field observations were obtained during an experiment in June and July 2011 on a sandy, steep, reflective beach at Carmel River State Beach (CRSB), California. Bathymetry was surveyed multiple times throughout the experiment using a kinematic global positioning system (GPS) mounted to an electric kayak equipped with an echosounder to measure the offshore profile and to a backpack carried by a walking person to measure the dry beach, and the beach step was measured by a person swimming cross-shore transects with a survey rod affixed with a GPS atop at numerous alongshore locations. The survey data were combined and interpolated to a spatial grid, resulting in a single bathymetry. The alongshore-averaged, cross-shore beach profile was composed of a 1/7.6 subaerial beach slope, a steep 1/3 subaqueous beach step, and a 1/19 subaqueous offshore profile (Figure 30). Due to the steepness of the beach, depth-limited wave breaking occurred very close to the shore, resulting in a narrow surf zone that was intermittent in width at the frequency of the sea-swell waves. The plunging/surging breakers were effectively the run-up associated with the swash zone that alternately wets and dries the beach. Therefore, the surf zone on this beach is considered to be more of a large swash zone rather than a typical surf zone.

Offshore waves and currents (Figure 31) were measured with a cross-shore array of four bottom-mounted, upward-looking acoustic Doppler current profilers (ADCPs) and

pressure sensors (Figure 30), sampled at 1 Hz, throughout the experiment. Additionally, a vertical array of six Electromagnetic current meters (EMCMs) spaced at 0.2 m intervals was deployed in 0.4 m water depth relative to mean sea level (MSL) and sampled at 16 Hz for 5 days (yeardays 169 to 173) to observe the vertical structure of the cross-shore and alongshore currents associated with the steep beach surf zone. Hourly, depth-averaged currents (u_{avg}, v_{avg}) were computed from the ADCPs and EMCM array measurements to evaluate the mean currents inside and outside the surf zone (Figure 31c,d). The tidal elevation with respect to MSL during the experiment was approximately ± 1 m (Figure 31e), so the EMCMs were located inside and outside the region of active wave breaking as a function of tidal elevation and wave energy. A local wave breaking criterion of $H_{rms}/h \geq 0.42$ (Thornton and Guza 1982) was used to determine when the EMCMs were inside the surf zone, which was typically during low tides. Throughout the experiment, waves approached the field site obliquely from the northwest, resulting in a predominant alongshore current to the south (Figure 31d). In this work, a local coordinate system is used where positive is offshore and to the south (Figure 30).

2. Dye Experiments

Dye was released on five different days over the course of a 10-day window during varying wave and alongshore-current conditions (Figure 31d), resulting in 15 successful dye releases. An initial volume of 200 mL of fluorescent Rhodamine dye (20% weight per volume) was released as a slug in the surf zone (Figure 32a) at mid-depth in the shallow water at the shoreline. Rhodamine dye was chosen since its decay rate is minimal and it is relatively stable in ambient light (Smart and Laidlaw 1977; Grant et al. 2005). The dye sensors used to measure dye concentration were 1 Hz internal logging WET Labs fluorometers with a 0 to 230 ppb range. Clark et al. (2009) found that the instantaneous 1 Hz concentration errors were ~1 ppb in a bubbly, sediment suspended surf zone with medium-grained quartz sand and minimal fine sediments. Similar measurement errors are assumed at CRSB, which had coarse sand with minimal fines.

The temporal and spatial distribution of the dye was evaluated with an alongshore array of eight dye sensors (Figure 30) mounted on vertical poles jetted into the sea-bed on

the upper beachface (Figure 32c-e) with an approximate alongshore spacing of 25 m. The dye sensors were mounted vertically with their optical sensors faced downward approximately 10 cm off of the sea-bed, such that they were submerged for the longest duration in the surfzone waves. Additionally, during some of the dye releases, swimmers each equipped with a dye sensor and a Global Positioning System (GPS) device performed repeated cross-shore transects at specified alongshore locations, which is described in more detail in Section 4.3. Owing to the fixed location of the stationary dye sensor array, the individual dye studies were performed at approximately the same tidal elevation, about 0.5 m above MSL, such that the dye sensors were located in the active surf zone. The dye was generally released between poles toward the northern end or in the middle of the array owing to the predominant southerly surfzone alongshore current.

The location of the alongshore array in the active surf/swash zone resulted in the dye sensors being alternately submerged and not submerged within the sea-swell water level range, which varied due to tidal elevation and minimal infragravity motions (Figure 32c-e), resulting in dropouts in measurements of dye concentration. Including these dropouts would bias the measurements toward low concentrations; therefore to account for this in the measured dye concentration time series, an envelope was fitted to the maxima of concentration peaks associated with the sea-swell waves (Figure 33) to describe the actual concentration of dye in the surf/swash zone as a function of time. No procedure allowed for 100% automation, so the envelope was manually selected after some initial automation, which also removed erroneous values.

C. EULERIAN CURRENT MEASUREMENTS

1. Steep Beach Surf/Swash Zone Characteristics

The surf zone on the steep beach at CRSB has been described as being a large swash zone. When the EMCM array was inside of the surf/swash zone, the sensors became alternately submerged and not submerged, depending on their location in the water column, with the frequency of the incident waves. A one-minute time series of cross-shore velocity measured by each sensor in the EMCM array when it was inside of the surf zone is shown in Figure 34 (top). At times just prior to and during wave breaking

(e.g., t = 0 s), there were strong onshore (negative) velocities measured by all sensors in the vertical array. As the flow switched direction, the sensors nearest to the water surface (≥ 0.63 m above the sea-bed) immediately became dry and did not measure backwash (positive) velocities, while the sensor 0.43 m above the sea-bed (red line in Figure 34) measured part of the backwash then became dry, resulting in a velocity measurement of zero, and only the bottom-most sensors (0.03 and 0.23 m above the sea-bed, blue and green lines in Figure 34) measured offshore velocities throughout the entire backwash (Figure 34, top). Although the EMCM array was in a mean water depth of 0.7 m during this example time series, the measured velocities still exhibit swash zone velocity characteristics. When the EMCM array was outside of the surf/swash zone, all of the sensors in the vertical array were submerged and measured velocities at all times (Figure 34, bottom).

2. Undertow Inside and Outside Surf Zone

The vertical structure of the cross-shore flow inside and outside of the surf zone was evaluated using half-hour averaged EMCM and ADCP1 velocity measurements (Figure 35). When the EMCM array was inside the surf zone, an undertow profile was observed, with the characteristic parabolic shape and maximum offshore velocity at mid-depth, which is typically observed within the surf zone on alongshore-homogeneous dissipative beaches (Garcez Faria et al. 2000; Reniers et al. 2004a). The undertow velocity changed from a small offshore velocity throughout the water column when the EMCM array was outside of the surf zone (Figure 35b, solid circle, square, and triangle symbols) to a strong offshore flow at mid-depth as the EMCM array transitioned to being inside of the surf zone (Figure 35b, solid star and diamond symbols). This demonstrates that the undertow within the surf zone on this steep, reflective beach was not destroyed by standing waves, which are common on steep, reflective beaches (Wright 1982). The mean measured alongshore velocity was also greatest when the EMCM array was inside the surf zone (Figure 35c, solid star and diamond symbols).

Outside of the surf zone at ADCP1, located in 3 m water depth approximately 35 m from the shoreline, an undertow profile was also observed, which had maximum

offshore flow near the surface and decreased with depth (Figure 35b, open symbols), consistent with undertow profiles measured on the inner shelf by Lentz et al. (2008). The magnitude of the undertow profile at ADCP1 was similar to that measured with the EMCM array when it was outside the surf zone for corresponding times; the magnitude of the alongshore velocity at ADCP1 was less than that measured by the EMCM array for corresponding times (Figure 35c). These results indicate that outside of the surf zone there was a decrease in velocity with increasing water depth.

D. DYE MEASUREMENTS

1. Qualitative Dye Observations

The dye was visually observed to mix rapidly throughout the water column and in the cross-shore immediately after the release, apparently saturating the surf zone within a few incident waves (Figure 32b), and began seeping offshore of the surf zone shortly thereafter. The predominant pattern observed during the experiment consisted of the dye moving alongshore to the south, while also slowly being transported offshore. For times when the alongshore current was weak, the offshore movement of the dye was more visually noticeable because it stayed in approximately the same alongshore location, however it was found to move offshore at the same slow rate as when the alongshore current was strong. A summary of the visual dye patterns is given in Table 2.

The movement of the dye was also examined with the dye concentration time series, $C(t)$, measured at each alongshore sensor (Figure 36). Unfortunately, there were times when the dye concentration was greater than the maximum limit of a dye sensor and the data were clipped, or some sensors were lost or removed when dye was still in the study area, so a complete dye mass balance could not be performed and observations from these dye releases are not discussed. Repeated cross-shore transects performed by swimmers during some of the dye releases also provide a measure of the offshore movement of the dye plume. The dye sensors in the alongshore array and/or the swimmers that were used to compute mass transport estimates during each dye release are given in Table 2.

The dye releases on yeardays 162, 169 and 172 occurred during relatively small offshore wave conditions (H_{rms} < 0.5 m at ADCP1), which forced relatively weak alongshore currents (v_{avg} < 0.1 m s^{-1} at ADCP1) so the dye appeared to move primarily offshore. During the dye releases on these yeardays, two distinct peaks in $C(t)$ were measured by the dye sensor nearest to the dye release, indicating a separation in the dye. The $C(t)$ measured by the alongshore array of dye sensors during dye release 162a is shown in Figure 36 (top) as an example of the weak alongshore current case. The dye initially reached the dye sensor nearest to the dye release location and moved offshore, seen by a narrow peak and sharp decrease in $C(t)$. Then the remaining dye reached the sensor and gradually moved offshore, seen by a second, broader peak in $C(t)$ measured by the same dye sensor. The $C(t)$ measured by the subsequent dye sensors to the south in the alongshore array show broader profiles with smaller peak concentrations, indicating that the dye continued to spread alongshore and travel downstream, which can also be seen in the time evolution of $C(y)$ (Figure 36), which was consistent with visual observations. Due to the weak alongshore current and reduced number of stationary dye sensors that measured concentration time series, quantitative estimates using the alongshore array of stationary sensors were limited. However, cross-shore profiles of dye concentration measured by the swimmers on yeardays 169 and 172 were used to quantify the cross-shore movement of the dye (Table 2).

The dye releases on yeardays 165 and 166 occurred during relatively larger offshore wave conditions (H_{rms} > 0.5 m at ADCP1), which forced relatively strong alongshore currents (v_{avg} > 0.1 m s^{-1} at ADCP1) so the dye was released at the northern end of the array and appeared to move quickly alongshore to the south inside the surf zone with slight cross-shore movement. The $C(t)$ measured by the alongshore array of dye sensors during dye release 166c is shown in Figure 36 (bottom) as an example of the strong alongshore current case. $C(t)$ measured at the sensor nearest to the dye release showed a sharp rise followed by a rapid decay resulting in a relatively narrow concentration peak. As the dye reached the subsequent downstream alongshore sensors, the rise in concentration was less steep and it decayed more slowly, resulting in a broader concentration peak. The measured peak concentration moved quickly alongshore, and

also decreased with alongshore distance from the dye release, as seen in the time evolution of $C(y)$ (Figure 36, bottom). There were no traces of dye measured by the sensors after 35 minutes during these releases. Swimmer data could not be used to quantify the cross-shore movement of dye during these releases because the dye moved too quickly past the locations of the swimmer transects and was not adequately captured.

2. Alongshore Mixing and Transport Inside Surf Zone

a. Surfzone Averaged Alongshore Current

In-situ surfzone velocity measurements were not obtained during most of the dye releases. Therefore, a Eulerian measure of the alongshore current inside the surf zone was estimated as the alongshore velocity that the dye was advected past each dye sensor, using the dye concentration time series measured with the alongshore array of stationary dye sensors, which are assumed to represent the surfzone-averaged and depth-averaged concentration. The surfzone averaged alongshore current, $V(y)$, at each alongshore instrument location, y, was determined by interpolating the alongshore velocity between sensors to the entire length of the alongshore array as a function of distance from the dye release location at $y = 0$. The alongshore velocity was computed by a forward-differencing scheme, defined as

$$V = \frac{\Delta y}{\Delta t_{m01}(y)} \tag{13}$$

where Δy is the linear distance between sensors and $\Delta t_{m01}(y)$ is the difference in time associated with the first moment of the dye concentration time series (e.g. Figure 36), defined as

$$t_{m01}(y) = \frac{\int_0^T tC(y,t)\,dt}{\int_0^T C(y,t)\,dt} \tag{14}$$

where $C(y,t)$ is the dye concentration as a function of alongshore distance, y, and time, t, from the dye release ($y = 0$, $t = 0$) and T is the duration of the dye measurements. Due to separations in the dye patch as it moved alongshore, it was found using t_{m01}, which represents the mean time associated with the dye concentration profile, provided a better

estimate of $V(y)$ rather than using the time associated with the leading edge of the dye plume, the time associated with peak dye concentration, or the time associated with the trailing 10% of the peak dye concentration. The effect of alongshore diffusion on the estimates of t_{m01} are assumed negligible in the $V(y)$ calculations. Estimates of $V(y)$ tended to decrease slightly with distance alongshore (Figure 37a), with estimates of the alongshore-averaged surfzone averaged alongshore current, $\overline{V}$, ranging from 0.1 to 0.3 m/s for all dye releases (Table 2). The decrease in $V(y)$ with distance alongshore to the south could be due to the dynamics associated with the curvature of CRSB and is investigated more in the Discussion.

The estimates of $\overline{V}$ from the dye inside the surf zone were compared with the depth-averaged Eulerian velocities measured by the EMCM array and ADCP1 (Figure 31d, red). Estimates of $\overline{V}$ from the dye were consistent with the alongshore velocities measured by the EMCM array when it was inside of the surf zone, (Figure 31d, green) which typically occurred during low tides. The dye estimates of $\overline{V}$ inside the surf zone were faster than the depth-averaged alongshore velocities measured outside the surf zone by ADCP1 (Figure 31d, blue) and by the EMCM array when it was outside the surf zone (Figure 31d, green), which typically occurred during high tides.

b. Alongshore Mass Transport

Comparisons of the mass of dye measured at each subsequent alongshore sensor during a dye release describe the alongshore advection and dispersion of the dye, and any loss of dye between alongshore sensors is attributed to cross-shore exchange. Assuming the dye is well-mixed (throughout the water column and in the cross-shore) and is moving with $\overline{V}$, the total mass of dye advected past each alongshore dye sensor, $M_{meas}(y)$, measured in grams, where 1 ppb = 10^{-3} g m^{-3}, was estimated by

$$M_{meas}(y) = \int_0^T A_c \overline{V} C(y,t)\, dt \qquad (15)$$

where A_c is the cross-sectional area of the surf zone, which was considered to be a wedge, and was computed as $A_c = 0.5 h_b x_w$, where h_b = 1 m and is the water depth at the offshore edge of the surf zone, and x_w = 10 m and is the approximate surfzone width. The initial

amount of dye released in the surf zone, M_{meas}(y = 0), was M_0 = 46 g. The mass transport measured as a function of alongshore distance from the dye release was computed using estimates of $\overline{V}$ and is shown in Figure 37b. The $M_{meas}(y)$ decreased by a value of 1/e within 10 to 50 m from the dye release location, with a more gradual decrease in dye mass measured with increasing distance alongshore thereafter.

The statistical significance of the alongshore decay of $M_{meas}(y)$ was examined by evaluating the mean dye concentration, $\overline{C}$, measured at each dye sensor in the alongshore array for each dye release. The dependence of $M_{meas}(y)$ on $\int_0^T C(y,t)dt$, can be written in terms of $\overline{C}$, where $\overline{C} = \frac{1}{N}\sum_{n=1}^{N} C_n = \frac{dt}{T}\sum_{n=1}^{N} C_n$, and N is the number of discrete concentration measurements made in time, such that $T = Ndt$. Given $\int_0^T C(t)dt = \sum_{n=1}^{N} C_n dt$ then $\int_0^T C(t)dt = T\overline{C}$ and $M_{meas}(y) = A_c \overline{V} T \overline{C} \cdot 10^{-3} \frac{g}{m^3}$, and the statistics associated with $\overline{C}$ can be applied to $M_{meas}(y)$. Confidence intervals were estimated for $\overline{C}$, and the decay with distance alongshore was found to be statistically significant at the 95% confidence level (not shown), which is used to demonstrate the statistical significance in the decay of dye mass $M_{meas}(y)$ with distance alongshore.

c. Alongshore Diffusivity

The rate of spreading, referred to as diffusivity (κ_i), of the dye in the direction i = x, y is estimated by

$$\kappa_i(t) = \frac{1}{2}\frac{d\sigma_i^2}{dt} \tag{16}$$

where σ_i^2 is the second moment of the concentration profile,

$$\sigma_i^2 = \frac{\int [x_i - \mu_i]^2 C(x_i,t)dx_i}{\int C(x_i,t)dx_i} \tag{17}$$

and μ_i is the dye center of mass given by the first moment of each dye concentration profile,

$$\mu_i(t) = \frac{\int x_i C(x_i,t)\,dx_i}{\int C(x_i,t)\,dx_i} \tag{18}$$

where $C(x_i,t)$ is the dye concentration profile in the i-direction (Clark et al. 2010). The alongshore spreading of the dye inside the surf zone from a narrow peak to a broad profile over a short alongshore distance (< 100 m) as a function of time (Figure 36) is described by the alongshore diffusivity, κ_y. Equations (16), (17) and (18) are evaluated for $i = y$, using $C(y,t)$ measured by the alongshore array and integrating over the length of the alongshore array. The most dye releases occurred on yearday 166, with the fewest instances of data being clipped, so these results were ensemble averaged and used to characterize the alongshore diffusivity at CRSB. Linear regression of σ_y^2 versus t_{m01} (Figure 38) is used to fit a line to the data from all dye releases on yearday 166 ($r^2 = 0.44$, significant in the 95% confidence interval), where half of the slope of the line represents κ_y (Equation (18)). Values of κ_y varied for the individual deployments. The mean κ_y inside of the surf zone was found to be 0.5 $m^2\ s^{-1}$. The alongshore diffusion inside the surf zone at CRSB is attributed to shear in the alongshore surfzone current. The distribution of the alongshore current from zero at the shoreline to a maximum velocity at a cross-shore location within the narrow surf zone (< 10 m) results in a considerable amount of shear in the alongshore current, which is a known mechanism for generating alongshore spreading and diffusion (Clarke et al. 2007).

3. Cross-Shore Mixing and Transport across Surfzone Boundary

The cross-shore movement of the dye was estimated using cross-shore dye concentration profiles measured by swimmers on yeardays 169b and 172a,b. People equipped with a dye sensor and GPS swam repeated, shore-normal, cross-shore transects from the shoreline to beyond the offshore edge of the dye plume and back in approximately the same alongshore location for the duration of the dye deployment (Figure 39, upper panels), resulting in a measure of the dye concentration as a function of cross-shore distance and time, $C(x,t)$. Each swimmer performed 11 to 20 cross-shore transects (out and back) at a given alongshore location during a given dye release, resulting in 22 to 40 measurements of $C(x,t)$ per swimmer per dye release. As the dye

spread offshore, the swimmers had to travel farther offshore, swimming between 5 to 45 m offshore in a transect, taking on average 2 minutes to complete a transect. To summarize the offshore movement of dye, the large number of swimmer concentration profiles was averaged over 5-minute time windows to obtain mean concentration profiles as a function of cross-shore distance (Figure 39, lower panels). The cross-shore location of the dye plume, $\mu_x(t)$, was found at each alongshore swimmer transect location for each 5-minute mean $C(x,t)$ measured by the swimmer using Equation (18) with $i = x$, where the limits of integration were from the shoreline to beyond the offshore extent of the dye plume (x = 80 m).

The cross-shore dye concentration profiles at each alongshore location show the dye was initially shoreline-attached and saturated the surf zone in less than 5 minutes. The measured dye concentration decreased with time, and μ_x moved offshore as the dye concentration profile spread in the cross-shore. The μ_x moved outside the surf zone after 10 minutes, but remained within 20 m (2 surfzone widths) of the edge of the surf zone, indicating a decrease in the cross-shore dispersion of the dye outside the surf zone. Due to the presence of the shoreline, μ_x is expected to move offshore as the dye disperses in the cross-shore, however this could be due to seaward advection and/or plume widening by cross-shore diffusion (Clark et al. 2010; Spydell and Feddersen 2012). Unlike the shoreline-attached cross-shore concentration profiles and offshore μ_x movement with increasing alongshore distance from the dye source observed by Clark et al. (2010), which was attributed to cross-shore plume widening, the cross-shore concentration profiles observed at CRSB showed the peak concentration moving offshore as well as μ_x, indicating the dye was being advected offshore as well as being spread by cross-shore diffusion.

a. Cross-Shore Diffusivity Inside Surf Zone

Unfortunately, the swimmer transects were performed a considerable distance (> 50 m) downstream of the dye release, and due to the steepness of the beach and the narrowness of the surf zone, the dye plume had already spread across the surf zone and moved offshore. Thus, the cross-shore spreading of the dye within the surf zone was not

accurately captured with the swimmer transects. Due to the visual observations of rapid cross-shore mixing in the shallow surf/swash zone during the dye releases, the cross-shore diffusivity inside of the surf zone is attributed to breaking wave-induced turbulence generated within the surf zone by the intense breaking of plunging/surging waves near the shoreline on this steep beach (Feddersen 2007). The cross-shore turbulent eddy diffusion coefficient, κ_x, inside of the surf zone is estimated by the depth-averaged, breaking wave-induced turbulent eddy viscosity, ν_t, using the Reynolds analogy which states that turbulent eddies transport momentum as well as mass, therefore momentum and tracer mass are assumed to mix identically ($\kappa_x \approx \nu_t$) (Rutherford 1994; Brown et al. 2009; Clark et al. 2011). Battjes (1975) found that ν_t associated with cross-shore mixing is related to the surfzone-averaged wave energy dissipation, ε_b, by

$$\nu_t = cH_s\left(\frac{\varepsilon_b}{\rho}\right)^{1/3} \tag{19}$$

where H_s is the significant wave height, which represents the turbulent mixing length, ρ is the density of seawater, and c is a calibration factor (c = 0.7 (Brown et al. 2009)). The dissipation of incident wave energy by breaking waves within the surf zone, ε_b, is obtained using the wave energy balance, assuming straight and parallel contours, and integrating over the width of the surf zone,

$$-\varepsilon_b = \frac{1}{x_w}\int_{x_w}^{0}\frac{d\left(Ec_{gx}\right)}{dx}dx = \frac{\left(Ec_{gx}\right)_{x=0} - \left(Ec_{gx}\right)_{x=x_w}}{x_w} \tag{20}$$

where $E = \frac{1}{16}\rho g H_s^2$ is the wave energy and c_{gx} is the wave group velocity in the cross-shore direction determined using linear wave theory (Battjes 1975). Outside of the surf zone the incident wave energy flux is constant, so measurements made by ADCP1 in 3 m water depth are used to describe the wave energy flux at $x = x_w$, and the wave energy flux at the shoreline, x = 0, is assumed equal to zero. To account for the reflective nature of the steep beach, the incident wave energy flux is multiplied by a factor of $(1 - R^2)$, where R^2 is the reflection coefficient. Hence, the surfzone-averaged wave energy dissipation is found by

$$\varepsilon_b = \frac{\left(Ec_{gx}\right)_{ADCP1}\left(1-R^2\right)}{x_w} \tag{21}$$

where $R^2 = 0.4$ is the reflection coefficient for CRSB computed using the energy flux method by Sheremet et al. (2002). Estimates of ε_b from Equation (21) were used to solve for ν_t using Equation (19), where $\kappa_x \approx \nu_t$.

Recently, Feddersen (2012) derived a surf zone turbulent dissipation rate scaling assuming weak mean currents and a vertically uniform length-scale, resulting in a non-dimensional surf zone eddy diffusivity coefficient, K. The scaling is also based on a balance between vertical turbulent diffusion and energy dissipation, analogous to Battjes (1975), however a vertically-uniform length-scale equal to a fraction, γ, of the mean water depth, h, is used ($l = \gamma h$). The non-dimensional eddy diffusivity K as a function of height about the sea-bed, z, is

$$\frac{K(z)}{h\left(\frac{dF}{dx}\Big/\rho\right)^{1/3}} = \gamma^{4/3}A^{1/3}\exp\left(\frac{\alpha}{3}\frac{z}{h}\right) \tag{22}$$

where $dF/dx = d\left(Ec_{gx}\right)\Big/dx = \varepsilon_b$ from Equation (21), $A = \varepsilon/\exp(\alpha)$, where $\alpha = (3/2)^{1/2} C_\mu/\gamma$ and $C_\mu = 0.57$ (Feddersen 2012). This parameterization allows the surf zone turbulence to be scaled to a fraction of the water depth that is representative of the small-scale turbulent eddies, whereas the calibration factor c used in Equation (19) was based on a best-fit to drifter diffusivity observations, which are due to horizontal motions at scales greater than the water depth. Due to the surf zone at CRSB effectively being a large swash zone, the mean water depth h used in Equation (22) was set equal to the wave height H_s measured at ADCP1, and the turbulent length-scale was assumed equal to the entire water column ($\gamma = 1$). Values of the depth-averaged $K(z)$ are assumed equal to the cross-shore turbulent eddy diffusivity κ_x inside of the surf zone. Nearly identical results were obtained using Equation (19) and Equation (22) to estimate κ_x, with κ_x ranging from 0.2 to 0.5 $m^2\ s^{-1}$ for the times of the dye releases. Estimates of κ_x inside of the surf zone are the same order of magnitude as κ_y found inside of the surf zone, and are similar to asymptotic surfzone κ_x measured on dissipative beaches using drifters (Spydell et al. 2007; Brown et al. 2009) and dye (Clark et al. 2010).

b. Surfzone Averaged Cross-Shore Current

The cross-shore concentration profiles measured by the swimmers indicate that as the dye was spreading in the cross-shore due to turbulent diffusion, it was also being advected offshore with a mean cross-shore current. In order to compute the surfzone averaged cross-shore current at each alongshore instrument location $U(y)$ for each dye release, an initial guess of U = 0.2 m s^{-1} was used in Equation (12), using values representative of the cross-shore averaged surfzone ($x = x_w/2$ = 5 m, $\overline{h}$ = 0.5 m, $A_c = 0.5h_bx_w$ = 5 m^2), to estimate of $C(y,t)$, which was used to compute the mass transport, $M_{comp}(y)$, using Equation (15), and the error between $M_{meas}(y)$ and $M_{comp}(y)$ was computed. Values of U were adjusted incrementally until the error between $M_{meas}(y)$ and $M_{comp}(y)$ at the given alongshore instrument location was less than 0.25 g. This method was applied using the computed $\overline{V}$ from the given dye release, and estimated surfzone diffusivities of κ_x = 0.5 m^2 s^{-1} and κ_y = 0.5 m^2 s^{-1}. This resulted in a measure of the cross-shore advection as a function of alongshore distance y from the dye source, $U(y)$, which was largest closest to the dye release point and decreased by approximately half within 50 m (Figure 37c) due to the initial rapid cross-shore mixing, then effectively leveled off to an asymptotic value $\overline{U}$ = 0.05 to 0.09 m s^{-1} (Table 2). The net values of $\overline{U}$ are similar to u_{avg} measured by the EMCM array when it was inside the surf zone, and are greater than the depth-averaged u_{avg} measured outside the surf zone by ADCP1 (Figure 31). The alongshore variation in $U(y)$ is examined in the Discussion.

c. Cross-Shore Diffusivity Outside Surf Zone

The spreading of the dye outside the surf zone is expected to be slower than the initial rapid cross-shore mixing inside the surf zone due to the lack of turbulence (Harris et al. 1963; Inman et al. 1971; Clark et al. 2010). The dye outside the surf zone is assumed to be well mixed over the vertical and behave independently from the processes inside the surf zone. In order to examine the spreading of the dye outside the surf zone using the swimmer transects during dye releases 169b, 172a, and 172b, the total area under $C(x,t)$ was calculated (C_{tot}), as well as the area under $C(x_{out},t)$ corresponding to the portion of the dye concentration profile outside the surf zone, $x_{out} > x_w$ (C_{out}). A ratio of

C_{out}/C_{tot} > 85% was used to conservatively determine when swimmer transects were predominantly outside the surf zone. The cross-shore diffusivity, κ_x, seaward of the surf zone was calculated using Equations (16), (17) and (18) for $i = x$, and integrating $C(x,t)$ from the shoreline to the seaward limit of the transects for the seaward transects and vice versa for the shoreward transects. Estimates of cross-shore diffusivity outside the surf zone were found using linear regression of σ_x^2 versus t_{m01} (Figure 40), where half of the slope of the line represents κ_x (Equation (18)). The correlation coefficients, r, were computed and those that were significant at the 95% confidence level were used. The mean κ_x outside of the surf zone was found to be 0.01 $m^2\ s^{-1}$, indicating that seaward of the surf zone the dye is spreading slowly. Estimates of κ_x outside of the surf zone are 20 to 50 times smaller than that inside of the surf zone.

The relative importance of the cross-shore diffusivity versus the cross-shore advection outside the surf zone is evaluated by examining the cross-shore advective and diffusive terms in Equation (11). The cross-shore advection at the edge of the surf zone is estimated as uhC = 0.7 ppb $m^2\ s^{-1}$, using the net $\bar{U}$ = 0.07 m s^{-1}, h_b = 1 m, and a maximum C = 10 ppb measured outside the surf zone. The cross-shore diffusivity outside the surf zone is estimated as $\kappa_x \frac{\partial(hC)}{\partial x} = \kappa_x h \frac{\partial C}{\partial x} + \kappa_x C \frac{\partial h}{\partial x}$ = 0.02 ppb $m^2\ s^{-1}$, using the same values for h_b and maximum C outside the surf zone, and $\partial C/\partial x \approx 1$ ppb m^{-1} (where C decays from a maximum of 10 ppb to 0 ppb over a distance of 10 m), and an offshore slope $\partial h/\partial x = 1/10$. This estimate indicates that outside the surf zone the cross-shore transport by advection is thirty-five times greater than the transport by diffusion. These results are consistent with the findings of Clark et al. (2010) for a dissipative beach, and suggest that the processes outside of the surf zone are disconnected from the surfzone dispersion processes, and that once the dye exits the surf zone it moves offshore as a constant patch.

E. DISCUSSION

1. Stages of Mixing and Transport Inside Surf Zone on a Steep Beach

Based on the qualitative and quantitative observations obtained with the alongshore array of dye sensors, two separate stages of mixing and transport are apparent inside the surf zone on the steep beach at CRSB (Figure 41). The results show differences in the decay of dye mass and cross-shore transport between the region within approximately 10 to 50 m of the dye release location and the region farther downstream alongshore (Figure 37). These differing stages of mixing and transport within the surf zone are analogous to the stages of mixing that occur in rivers, which occurs in three stages (Fischer et al. 1979). A tracer discharged into a river channel initially mixes in three dimensions until it becomes vertically well mixed. The tracer then continues to mix across and along the channel primarily by turbulence as it is advected downstream by the mean current. The region between the point of discharge and the downstream location where the tracer is fully mixed vertically and across the channel is considered the near-field. Downstream of this region is considered the far-field where longitudinal shear flow dispersion is the dominant mixing process. The stages of mixing in a surf zone can be compared to those in a river, where the surf zone is considered a channel with the boundaries being the shoreline and the offshore edge of the surf zone.

The near-field stage of mixing and transport in the surf zone on the steep beach at CRSB is defined as the region between the point of the dye release and the location downstream alongshore where the dye was completely mixed vertically and in the cross-shore within the narrow surf zone. The extent of the near-field region is determined using results from dye release 172a when measurements of dye concentration are available both in the alongshore (by the alongshore array of stationary sensors) and in the cross-shore (by swimmers equipped with sensors). The dye appears completely mixed across the surf zone after 5 minutes after the release (Figure 39). At this time the dye is assumed to be completely mixed vertically as well because the surf zone is approximately 10 times wider than it is deep. The time of 5 minutes associated with the near-field stage of mixing corresponds to an alongshore distance of approximately 25 m from the dye release location, using the alongshore surfzone velocity of 0.08 m s^{-1} measured during dye

release 172a. This alongshore location corresponds with the location where $M_{meas}(y)$ decreased by a value of 1/e, which is used to define the near-field region on this steep beach for the different dye releases. Therefore, the near-field region is considered to be conservatively 50 m downstream of the point of the dye release ($0 < y < 50$ m), and the far-field region is considered to be beyond 50 m downstream from the point of the dye release ($y > 50$ m).

a. Near-Field Mixing and Transport

In the near-field region, the dye was rapidly mixed throughout the water column immediately after the dye release, and experienced 2-D horizontal mixing and transport until the surf zone was saturated for $y < 50$ m (Figure 41). The dye was mixed in the cross-shore (κ_x) by turbulence due to breaking waves, and spread in the alongshore (κ_y) due to shear in the alongshore current. The dye was advected alongshore with the surfzone averaged alongshore velocity $\overline{V}$, while also being transported offshore by the surfzone averaged cross-shore velocity $U(y)$, which was found to be relatively large (Figure 37c). $M_{meas}(y)$ was observed to decrease by a value of 1/e within $y < 50$ m. The strong decay in $M_{meas}(y)$ suggests that cross-shore diffusion, as well as cross-shore transport, is an important processes controlling the initial 2-D mixing and transport on this steep beach. Therefore, the surfzone mass transport in the near-field region is due to alongshore and cross-shore advection, as well as longitudinal dispersion and cross-shore diffusion, as summarized in Figure 41.

b. Far-Field Mixing and Transport

In the far-field region, the dye in the surf zone was completely mixed, and the transport was predominantly due to an advection balance (Figure 41). $M_{meas}(y)$ decayed in the alongshore more gradually, as the dye was observed to be advected alongshore with $\overline{V}$, and the cross-shore transport leveled off to a relatively small constant value $\overline{U}$ (Figure 37). Additionally, the dye continued to be dispersed alongshore in the far-field (Figure 36). The decrease in cross-shore transport in the far-field region is due to the dye being completely well mixed, and therefore represents the steady-state cross-shore exchange that occurs between the surf zone and inner shelf on the steep beach. These

findings of mass transport being due to an advection balance in the far-field on the steep beach at CRSB is consistent with the findings of Grant et al. (2005) for the advectively dominated transport conditions observed at the dissipative beaches in southern California.

The exchange ratio $\overline{V}/\overline{U}$ for CRSB was found to range from 1.14 to 3.50 (Table 2), and is much smaller than that found by Grant et al. (2005) ($\overline{V}/\overline{U} > 50$). This indicates there was a greater amount of cross-shore exchange in the far-field on the steep beach at CRSB than measured at dissipative, alongshore current dominated beaches. The net offshore transport of dye at CRSB is consistent with the undertow velocity measurements obtained inside and outside of the surf zone during the field experiment.

2. Offshore Pulses of Dye

It was visually observed that the dye moved offshore in episodic pulses (not captured in quantitative dye measurements). To examine the possible transport associated with different frequency ranges, the cross-shore excursion length is estimated from the frequency-band-passed cross-shore velocities at ADCP1 (Figure 42). Even though the velocities are largest for sea-swell (SS) waves (0.04 Hz < f < 0.2 Hz) and infragravity (IG) waves (0.004 Hz < f < 0.04 Hz) (Figure 42, top), their duration is relatively short and their excursion is small (< 2 m) compared with very low frequency (VLF) motions (0.0005 Hz < f < 0.004 Hz) (Figure 42, bottom). The excursions of the VLFs can be three times larger than SS and IG waves, and owing to their longer duration, O(15 minutes), therefore the VLFs can be the mechanism for the episodic cross-shore exchange. This suggests that the dye pulses on a timescale of about 5 to 15 minutes due to VLF motions as it slowly moves offshore with the mean flow. Clark et al. (2010) similarly found that inside of the surf zone low-frequency horizontal rotational velocities with a length scale of the width of the surf zone (surfzone eddies) played an important role in cross-shore surfzone tracer mixing.

It is hypothesized that the episodic offshore pulses of dye observed at CRSB are due to VLF surfzone eddies (SZEs). VLF SZEs are generated due to alongshore variations in wave breaking, which can occur as a result of several mechanisms: 1) alongshore variations in the underlying bathymetry (Bowen 1969; MacMahan et al.

2004), 2) short-crested wave breaking (Peregrine 1998; Clark et al. 2012), and 3) the interaction of temporally and spatially varying wave groups (Johnson and Pattiaratchi 2004b; Reniers et al. 2004b; Long and Ozkan-Haller 2009).

Spatial variability in the underlying surfzone bathymetry can result in alongshore variations in the breaking waves that force offshore flows, typically in the form of rip currents (Bowen 1969; MacMahan et al. 2004b). However, this is not believed to explain the offshore pulses observed at CRSB because the bathymetry contours are straight and parallel and no alongshore variability was measured. The development of vortices in the surf zone due to short-crested wave breaking and alongshore gradients in wave height has been investigated theoretically (Peregrine 1998) and observed in the field (Clark et al. 2012). Adjacent regions of breaking and non-breaking along individual wave crests results in non-uniform forcing that generates rotational eddies at the end of the breaking wave crest, which can have positive or negative vorticity, and is a mechanism for dispersion near the shoreline (Clark et al. 2012). Alongshore gradients in the breaking short-crested waves was observed at CRSB, however Clark et al. (2012) found that the vorticity generated by short-crested wave breaking decayed over 20 to 60 s, which is a shorter time-scale than the offshore pulses of dye that was observed.

VLF SZEs can also develop as a function of wave-group forcing associated with directionally-spread short waves, which force intermittent circulation cells that persist on O(15 minutes) and have the ability to transport material outside the surf zone (MacMahan et al. 2010b). On an alongshore uniform beach, numerical model results show that alongshore variations in wave breaking can result from an incident wave spectrum that includes a range of wave frequencies and directions, where the interaction of the individual wave components creates temporally and spatially varying wave heights (wave groups) (Reniers et al. 2004b; Long and Ozkan-Haller 2009). Long and Ozkan-Haller (2009) found that vortices were generated for oblique wave groups on an alongshore uniform beach, and the resulting vortices were advected by the mean surfzone current. Field observations under directionally-spread waves found vortex pairs manifest as transient rip currents (Johnson and Pattiaratchi 2004b). These model and field results show vorticity motions at time scales O(5 min), similar to the time scale of the pulses

observed at CRSB. The formation of these VLF SZEs is not steady state, and it is hypothesized that the constructive and deconstructive interaction of these VLF SZEs are the mechanism for the episodic cross-shore exchange observed at CRSB.

3. Effect of Local Bathymetry on Alongshore Surfzone Transport and Cross-shore Exchange

The observed decrease in $\overline{V}$ with distance alongshore to the south (Figure 37a) could be explained by the decrease in wave angle relative to the shoreline with distance alongshore to the south due to the curvature of the bay. Waves coming from the north and driving the alongshore current to the south actually tend to be more shore-normal at the southern end of the experiment area and therefore force weaker alongshore currents. In numerical model simulations investigating biological transport during the CRSB experiment under the same conditions discussed here, Fujimura et al. (2013) found that the alongshore current is to the south and follows the contours of the embayed beach until approximately y = 100 m, where there is a decrease in the alongshore velocity and the current moves predominantly offshore. The southern end of the alongshore array of dye sensors is located where this change in current from alongshore to offshore occurs, which explains the decrease in $V(y)$ with distance alongshore.

4. Effect of Local Wave Conditions on Cross-shore Exchange

It has been noted that mixing and mass transport on natural beaches is likely sensitive to local wave conditions (Boehm et al. 2003; Grant et al. 2005). On dissipative beaches, waves approaching the shoreline at an angle drive alongshore currents, and as the incident wave angle approaches shore-normal rip currents are formed. During obliquely incident, alongshore-current wave conditions, mass transport is advectively dominated (Grant et al. 2005). Additionally, cross-shore wave-driven mixing across a surf zone with alongshore current shear enhances the alongshore spreading of dye (Clarke et al. 2007). During shore-normal wave conditions, rip currents form resulting in increased cross-shore advection, and turbulent diffusion due to breaking waves becomes more important. Therefore, on dissipative beaches, the exchange ratio $\overline{V}/\overline{U}$ is largest for

obliquely incident waves during alongshore-current conditions, and decreases as the incident wave angle decreases and a greater amount of cross-shore exchange occurs.

Similarly, on steep beaches, obliquely incident waves drive alongshore currents; however, in the near-field, there is a greater amount of cross-shore exchange, likely due to wave breaking, and therefore, $\bar{U}$ is relatively large. In the far-field, after the dye is mixed across the surf zone, $\bar{U}$ decreases and levels off to a constant, and the mass transport is advectively dominated and is similar to that observed by Grant et al. (2005) on a dissipative beach under alongshore current conditions. In the far-field, the exchange ratio $\bar{V}/\bar{U}$ is generally less than that on a dissipative beach for oblique wave angles, indicating more cross-shore transport occurs on steep beaches under alongshore current conditions.

F. CONCLUSIONS

Nearshore processes of waves and currents and their impact on mass transport and cross-shore exchange were observed for a steep, reflective beach at Carmel River State Beach, California. Owing to the steep slope (1/7) of the beach, plunging/surging waves broke close to the shoreline resulting in an intense shore break and a large swash zone rather than a typical surf zone generally associated with dissipative beaches. Fluorescent Rhodamine dye was released in the surf zone and an alongshore array of stationary dye sensors and repeated cross-shore transects performed by swimmers equipped with dye sensors at multiple alongshore locations were used to measure the temporal and spatial dye concentration evolution and to examine the alongshore and cross-shore mixing and transport associated with the hydrodynamics on the steep, reflective beach.

Visual dye observations indicate that the dye quickly mixed vertically and dispersed in the cross-shore, completely saturating the narrow surf zone after a few incident waves. Dye concentration time series measured by an alongshore array of stationary dye sensors inside the surf zone revealed sharp-rising, narrow spikes of dye concentration that decayed rapidly near the dye release location, which broadened and decayed more slowly and decreased in peak concentration with distance alongshore, downstream from the dye release location. Mixing and transport processes occur in two

states on the steep beach, which are summarized in a conceptual diagram in Figure 41. In the near-field, within approximately 50 m alongshore from the dye release location, dye was mixed in the cross-shore by turbulent diffusion due to breaking waves (κ_x = 0.2 to 0.5 m^2 s^{-1}) that resulted in a relatively large amount of cross-shore exchange ($U(y < 50$ m) = 0.1 to 0.4 m s^{-1}), and was also advected downstream with the mean alongshore surfzone current ($\overline{V}$ = 0.1 to 0.3 m s^{-1}) and spread in the alongshore due to shear in the alongshore current (κ_y = 0.5 m^2 s^{-1}). In the far-field, once the dye was completely mixed vertically and in the cross-shore, the cross-shore transport leveled off to a constant ($\overline{U}$ = 0.05 to 0.09 m s^{-1}). Dye continued to be transported alongshore with the mean alongshore surfzone current and spread in the alongshore, while also being slowly transported offshore. Even though the offshore velocity is small, it represents a continuous loss and a substantial net offshore transport. Outside the surf zone, the cross-shore diffusion coefficient κ_x was 0.01 m^2 s^{-1} indicating the dye was spreading more slowly than it was being transported offshore, and that it was essentially moving offshore as a constant patch. The offshore movement of the dye plume also pulsed on the order of 5 to 15 minutes, attributed to VLF motions.

The mixing and transport processes observed on this steep beach resemble those observed on dissipative beaches; however, some differences do exist. The mass transport measured on several dissipative beaches in Southern California was found to be dominated by advection, and the dye mass was observed to decay exponentially with distance alongshore (Inman et al. 1971; Boehm 2003; Grant et al. 2005). On the steep beach, in the near-field there was a large amount of cross-shore exchange initially and advection and diffusion processes were important. In the far-field, the mass transport was dominated by advection and was similar to that on dissipative beaches under alongshore current conditions; however, the far-field solution on the steep beach was reached in a much shorter alongshore distance than on dissipative beaches. The cross-shore exchange ratio $\overline{V}/\overline{U}$ in the far-field for CRSB ranged from 1 to 4, and was an order of magnitude less than that found by Grant et al. (2005) for a dissipative beach with similar wave and alongshore current conditions. Therefore, a greater amount of cross-shore exchange across the surfzone boundary was observed on the steep, reflective beach.

THIS PAGE INTENTIONALLY LEFT BLANK

V. SUMMARY

Cross-shore exchange on two contrasting natural beaches has been described: 1) a dissipative, alongshore-inhomogeneous, rip-channeled beach, and 2) a reflective, alongshore-homogeneous, steep beach. The morphology, beach slope, wave conditions, and resulting current patterns differ significantly on these beaches, and therefore so do the mixing and transport processes and the subsequent material exchange and retention.

Material transport was investigated on a rip-channeled beach at Monterey, California. The surfzone morphology consisted of transverse bars, which were relatively dissipative with a slope of about 1/100, and quasi-periodic incised rip channels, with straight and parallel contours outside the surf zone and an offshore slope of about 1/20. Rip currents were observed to occur during low tides and normally incident wave conditions, with increased wave energy resulting in stronger rip current flows. During these conditions, the surf zone width was approximately 100 m, on average. A combination of Eulerian and Lagrangian instruments were used to measure the temporal and spatial evolution of the rip current flow inside and outside the surf zone. These observations, in combination with results from previous studies, give a comprehensive description of the 3-D transport and exchange between the surf zone and the inner shelf due to rip currents, which is summarized here.

The rip current circulations inside the surf zone form when incident waves approach the beach shore-normally, and the alongshore perturbations in the bottom topography induce alongshore variations in the depth-limited wave breaking, resulting in alongshore gradients in pressure and momentum driving water from the shoals to the rip channels (Bowen 1969, Haller et al. 2002). The directionally spread incident waves deposit momentum into the surf zone at the wave group time scale (O(10 minutes)), and the spatial variations in the breaking wave groups force VLF motions inside the surf zone (Reniers et al. 2007, Long and Ozkan-Haller 2009). These energetic motions for frequencies less than 0.004 Hz are outside the gravity restoring region in frequency-wavenumber space, indicating they are horizontal vortices. These large-scale vortices, or surf zone eddies (SZEs) are coupled to the underlying bathymetry and are predominantly

contained within the surf zone (MacMahan et al. 2004b). However, as counter-rotating SZEs oscillate in the cross-shore direction inside the surf zone, they occasionally converge at the locations of rip channels, and the presence of the VLF rip current pulses cause the rip current to extend outside the surf zone (Reniers et al. 2009, 2010).

The VLF component of the rip current flow accounted for a significant portion of the total energy inside and outside the surf zone (37% and 50%, respectively), with a reduction in the VLF rip current intensity as it moved offshore, consistent with previous observations (MacMahan et al. 2004b). The VLF pulses in the near-surface rip current flow responsible for the rip current exits were found to be infrequent and aperiodic, both inside and outside the surf zone. Evaluating 3-hour time windows centered around low tide, when rip currents are known to be strongest, significant VLF pulses (greater than $\mu + 2\sigma$) exceeded 0.7 and 0.2 m s^{-1} and occurred one to twenty times inside and outside the surfzone, with the number and amplitude of significant VLF pulses increasing with increasing wave energy. On average, the significant VLF pulses occurred for approximately 10% of the time. This is consistent with observations of relatively high amounts of surface surfzone retention (Castelle et al. 2010, MacMahan et al. 2010b). The strength of the surface VLF rip current pulses was found to control the magnitude and vertical structure of the mean rip current flow. Inside the surf zone the VLF pulses added to the strength of the background rip current flow, and outside the surf zone, where there was no background flow, the stronger VLF pulses resulted in stronger rip current flows and more shear in the vertical.

As the rip current moved seaward, the VLF pulses inside and outside the surf zone did not occur simultaneously and were not correlated. The mean VLF component of the velocity measured inside the surf zone was significantly correlated with the offshore wave height, indicating the VLF pulses inside the surf zone were dependent upon the incoming wave energy, due to the forcing of the VLF motions by the spatially varying breaking wave groups. However, outside the surf zone the mean VLF component of the velocity was not correlated with the offshore wave conditions, supporting the notion that the VLF pulses originate inside the surf zone but travel offshore randomly. Additionally, the mean VLF component of the velocity was significantly correlated with the local wave

height to water depth ratio both inside and outside the surf zone. These results suggest that the VLF pulses outside the surf zone are independent of those inside the surf zone. Outside the surf zone, the VLF rip current pulses moved offshore like a surface jet, either directly offshore or at an angle. However, at times there was evidence that the rip current VLF pulse was moving offshore as a detached eddy, consistent with numerical model results by Reniers et al. (2010).

The rip current flow was depth-uniform inside the surf zone, with minimal rotation throughout the water column. As the rip current exited the surf zone it moved over the surfzone break as a surface jet with its vertical extent remaining the same as at the edge of the surf zone. As the water depth increased outside the surf zone, the rip current transport remained near the surface, resulting in a surface dominated rip current flow offshore. There was rotation over depth in the rip current flow outside the surf zone, with an ~50° difference between surface and bottom, on average. The material transport offshore at the surface by the rip current flow was then mixed vertically downward to a depth corresponding to the thermocline, often times encompassing greater than half of the water column.

Material that exited the surf zone at the surface due to VLF rip current pulses was observed to move seaward and ultimately return shoreward in an arcing pattern, re-entering the surf zone over shoals, with ultimately no material being completely removed from the nearshore system. The surface material either moved seaward and returned sharply back shoreward a short alongshore distance from where it exited, resulting in locally-contained cross-shore exchange, or moved seaward and travelled farther in the alongshore direction as it gradually moved shoreward, resulting cross-shore and alongshore exchange. The cross-shore extent was typically one to two surfzone-widths L_x beyond the surfzone boundary. The rate of spreading and mixing (κ^{∞}_{xx} = 0.27 to 1.74 m^2 s^{-1}, κ^{∞}_{yy} = 0.36 to 5.01 m^2 s^{-1}) outside the surf zone was slower than that measured inside the surf zone during previous studies (Brown et al. 2009), suggesting there is less shear in the flow field outside the surf zone.

The probability distributions of particle movements at the surface outside the surf zone were basically Gaussian, indicating there was a relatively equal chance that a

particle anywhere on the inner shelf would move seaward or shoreward, consistent with the qualitative observations that no drifters left the nearshore system. The cross-shore velocities of seaward and shoreward moving particles at the surface had a maximum at the edge of the surf zone, and were approximately equal in magnitude as a function of cross-shore location, resulting in a total Lagrangian velocity of approximately zero. Surface material moving seaward decelerated after exiting the surf zone through rip channels, while surface material moving shoreward accelerated approaching and re-entering the surf zone over shoals. The magnitude of the shoreward moving material outside the surf zone was greater than the near-surface theoretical Stokes drift; therefore, Stokes drift was not solely responsible for moving material shoreward and back into the surf zone.

These results support a new theory of how material is exchanged and conserved within the nearshore region on a rip-channeled beach.

1) Initially, short waves deposit momentum into the surf zone at the wave group timescale.

2) Then spatial variations in the wave groups force VLF motions and rip current circulations inside the surf zone, where the rip current cells are topographically fixed in the alongshore direction, but oscillate in the cross-shore direction within the surf zone.

3) The episodic convergence of these SZEs causes the rip current to pulse and expel material offshore through the rip channels.

4) Material is transported seaward like a jet at the surface, with the depth-uniform rip current flow inside the surf zone becoming surface dominated as it moves over the surfzone break, remaining between the surface and the depth at the edge of the surf zone.

5) Outside the surf zone, material at the surface spreads laterally slowly, and is also mixed vertically downward to a depth controlled by the thermocline, often encompassing greater than half the water column.

6) Ultimately, the surfzone rip current circulations act to pull the material back onshore into the surf zone over shoals to satisfy a mass balance, with little or no material being completely removed from the nearshore system on the rip-channeled beach.

Material transport was also investigated on a steep beach at Carmel River State Beach, California. The bathymetry was alongshore uniform, and had a cross-shore profile consisting of a linear beach face with a slope of about 1/7, connected to a steep 1/3 subaqueous beach step, and continuing offshore with a slope of about 1/19. Due to the steepness of the beach, plunging/surging waves broke very close to the shoreline, resulting in a narrow surf zone that was approximately 10 m wide. The intense shore break was effectively the run-up that alternately wets and dries the beach; therefore, the surf zone on this steep beach is considered to be more of a large swash zone than a typical surf zone generally associated with dissipative beaches. Lagrangian measurements were obtained to quantify the movement and exchange of material.

Mixing and transport processes occur in two states on the steep beach. 1) In the near-field, within approximately 50 m alongshore from the source, material quickly mixed vertically and dispersed in the cross-shore, completely saturating the narrow surf zone after a few incident waves. The material was mixed in the cross-shore by turbulent diffusion due to breaking waves (κ_x = 0.2 to 0.5 m^2 s^{-1}) that resulted in a relatively large amount of cross-shore exchange ($U(y < 50$ m) = 0.1 to 0.4 m s^{-1}), and was also advected downstream with the mean alongshore surfzone current ($\bar{V}$ = 0.1 to 0.3 m s^{-1}) and spread in the alongshore due to shear in the alongshore current (κ_y = 0.5 m^2 s^{-1}). 2) In the far-field the material was completely mixed vertically and in the cross-shore, and advection processes were dominant. The material continued to be transported alongshore with the mean alongshore surfzone current and spread in the alongshore, while also being slowly transported offshore, with the cross-shore transport leveling off to a constant ($\bar{U}$ = 0.05 to 0.09 m s^{-1}). This resulted in a continuous loss and a substantial net offshore transport. Outside the surf zone, the cross-shore diffusion coefficient κ_x was 0.01 m^2 s^{-1} indicating material was spreading more slowly than it was being transported offshore, and that it was essentially moving offshore as a constant patch.

The natural beaches studied in this work represent two vastly different beach states, which commonly occur in nature. In reality, a given beach can change beach states over time based on the incident waves and resulting currents. Additionally, changes in the incident wave characteristics on a given beach can result in greatly different current patterns and exchange processes. Therefore, measuring mixing and transport for all types of beach states will provide information on how material might be transported as the state of a beach or the current patterns on a beach progresses. For example, rip currents are known to form when waves approach shore-normally on a beach with transverse bars and incised rip channels, however when the waves approach the same beach obliquely, an alongshore sinuous current pattern develops where the flow follows the underlying bathymetry contours (MacMahan et al. 2010b). The mixing and transport associated with these two current patterns are likely to be different. Forthcoming analysis examining field measurements of exchange processes during varying wave and current conditions on the rip-channeled beach will provide further insight into the potentially variable mixing and transport processes.

Ultimately, future work investigating cross-shore exchange on these beaches will require the use of a numerical model, supplemented by the field observations, to quantify temporal and volumetric exchange estimates. While field measurements are crucial for understanding current dynamics, the number of observations points is ultimately limited spatially, therefore a numerical model allows for the transport and mixing processes to be evaluated everywhere in space (3-D), as well as in time. However, the model forcing parameters and subsequent hydrodynamic output must be validated by the field measurements to ensure the transport and mixing processes are accurately implemented (i.e., accurate wave-group forcing on the rip-channeled beach is critical for producing VLFs in the surfzone, which were shown to control the magnitude and amount of rip current transport). Ultimately, numerical models can be used to estimate surfzone flushing times and volumetric transport rates, based on the quantified mixing and transport processes, on all types of natural beaches.

TABLES

Table 1. Summary of conditions observed during the drifter deployments at Monterey, California, grouped by observed drifter pattern. Tidal elevation was obtained from NOS tidal station 9413450; wave parameters and surfzone characteristics were obtained from offshore ADCP in 13 m water depth when data was available, otherwise were obtained from NDBC buoy 46240; wind data was recorded atop a 10 m tower onshore of the field site; depth-averaged cross-shore velocity u_{avg} was measured by ADCP 3, and alongshore velocity v_{avg} was computed from the drifters; cross-shore location of the surfzone boundary X_{sz} and surfzone width L_x were determined by shoaling waves from the ADCP in 13m water depth to the shoreline using linear wave theory.

*sensor was buried

yearday	drifter pattern/ exchange type	tidal elevation (m)	H_s (m)	T_p (s)	$\lvert\tau_s\rvert$ (N/m^2)	u_{avg} (m/s)	v_{avg} (m/s)	X_{sz} (m)	L_x (m)	maximum drifter cross-shore extent (L_x)
122	cross-shore	-0.87	0.43	10.6	0.00	0.01	0.05	147	78	3.6
129	cross-shore	-0.30	1.31	9.5	0.02	0.70	0.00	180	123	3.8
132	cross-shore	-0.51	0.77	7.6	0.04	0.35	-0.04	157	97	3.7
125	cross-shore & alongshore	-0.14	0.97	11.5	0.02	0.03	-0.14	176	122	1.9
126	cross-shore & alongshore	-0.05	1.22	12.6	0.00	0.20	-0.15	174	122	2.8
130	cross-shore & alongshore	-0.02	0.92	9.2	0.04	—*	0.13	162	111	3.3
137	cross-shore & alongshore	-0.54	0.55	8.2	0.01	0.08	0.13	142	81	2.5
135	none	-0.63	0.63	6.7	0.04	0.04	0.02	149	86	3.7
136	none	-0.70	0.86	8.3	0.01	0.07	0.02	169	105	6.2

Table 2. Description of dye releases and observations at Carmel River State Beach, California, and sensors used to estimate mixing and transport. Surfzone averaged alongshore current $\overline{V}$ is equal to the alongshore-mean $V(y)$ computed using Equation (13). Surfzone averaged cross-shore current $\overline{U}$ is for the far-field and is computed iteratively using Equation (12).

Release	Dye Release Location (between poles)	Visual Dye Observations	Sensors Used for Flux Calculations	$\overline{V}$ (m s^{-1})	$\overline{U}$ (m s^{-1})	Exchange Ratio, $\overline{V}/\overline{U}$
162a	3 & 4	predominantly offshore	1-8	0.11	0.06	1.83
165a	3 & 4	predominantly alongshore	1-6, 8	0.12	0.07	1.71
165b	1 & 2	predominantly alongshore	1, 3-6, 8	0.14	0.05	2.80
165c	1 & 2	predominantly alongshore	1, 3-6, 8	0.10	0.05	2.00
165d	1 & 2	predominantly alongshore	1, 3-6	0.13	0.06	2.17
166a	1 & 2	predominantly alongshore	1, 3-6, 8	0.18	0.08	2.25
166b	1 & 2	predominantly alongshore	1, 3-6, 8	0.22	0.07	3.14
166c	1 & 2	predominantly alongshore	1, 3-6, 8	0.28	0.08	3.50
166d	2 & 3	predominantly alongshore	1, 4-6, 8	0.28	0.09	3.11
166e	2 & 3	predominantly alongshore	1, 3-6, 8	0.27	0.08	3.38
166f	2 & 3	predominantly alongshore	1, 3-6, 8	0.18	0.07	2.57
169b	5 & 6	predominantly offshore	3 swimmers			
169c	4 & 5	offshore and alongshore	4-8	0.09	0.05	1.80
172a	4.5 & 5	predominantly offshore	4.5-8, 3 swimmers	0.08	0.07	1.14
172b	4.5 & 5	predominantly offshore	2 swimmers			

FIGURES

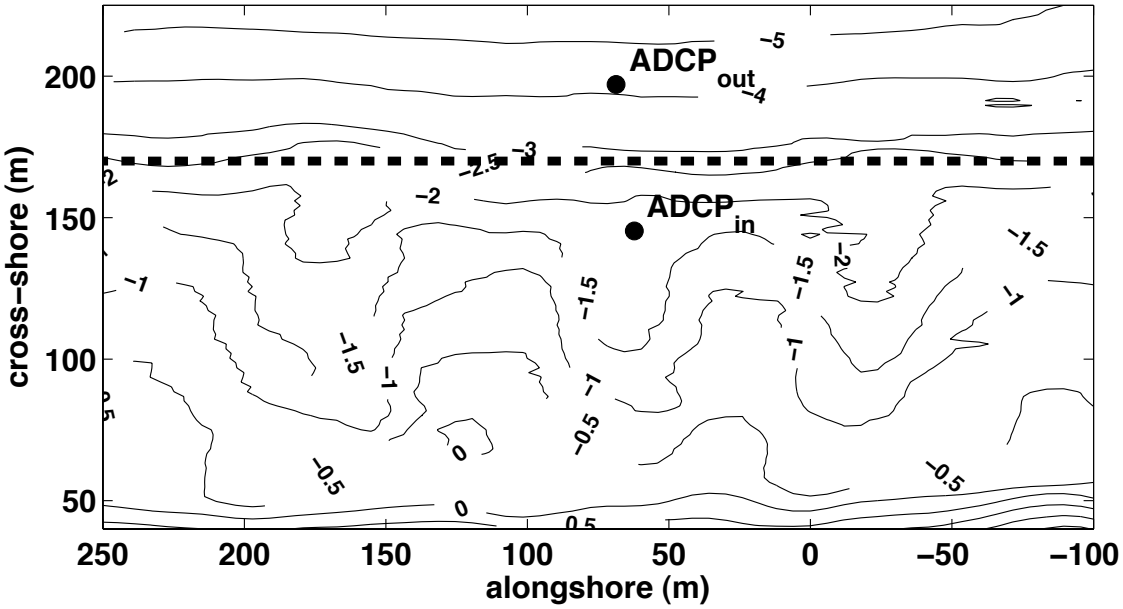

Figure 1. Measured bathymetry in the local coordinate system, where the contours are labeled with the elevation in meters relative to MSL. ADCP locations are shown by the black circles. Dashed black line represents the approximate edge of the surf zone.

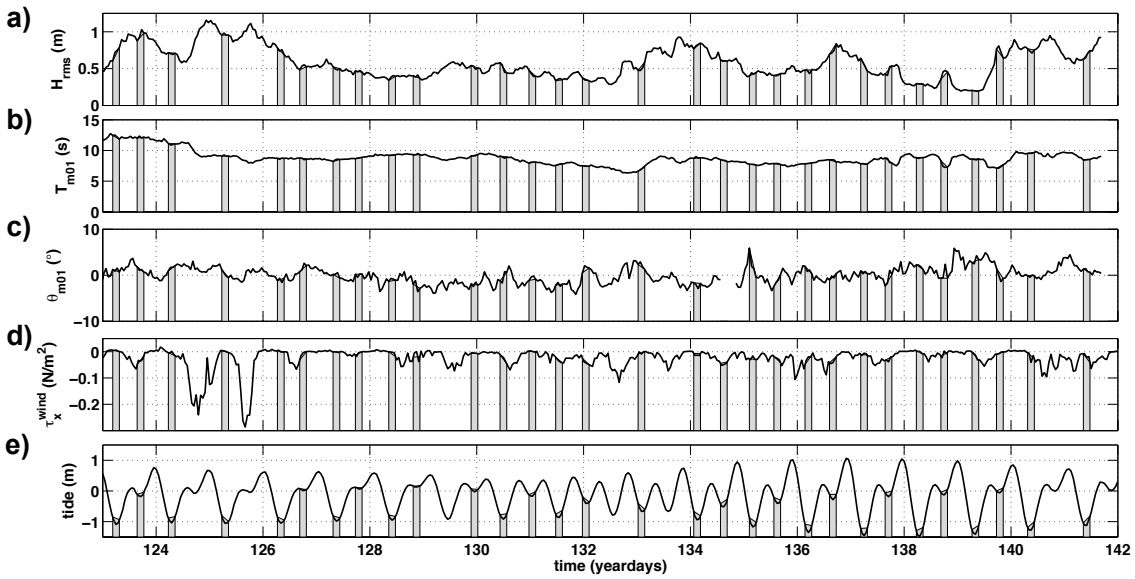

Figure 2. Wave conditions measured by the ADCP in 13 m water depth of (a) root-mean-square wave height H_{rms}, (b) mean wave period T_{m01}, (c) and mean wave direction θ_{m01}, (d) cross-shore wind stress computed for winds measured onshore of the field site, and (e) tidal elevation measured at NOAA/NOS tidal station 9413450 relative to MSL. Gray shaded regions represent 3-hour records, centered around low tide, used in the analysis of the VLF rip current pulses.

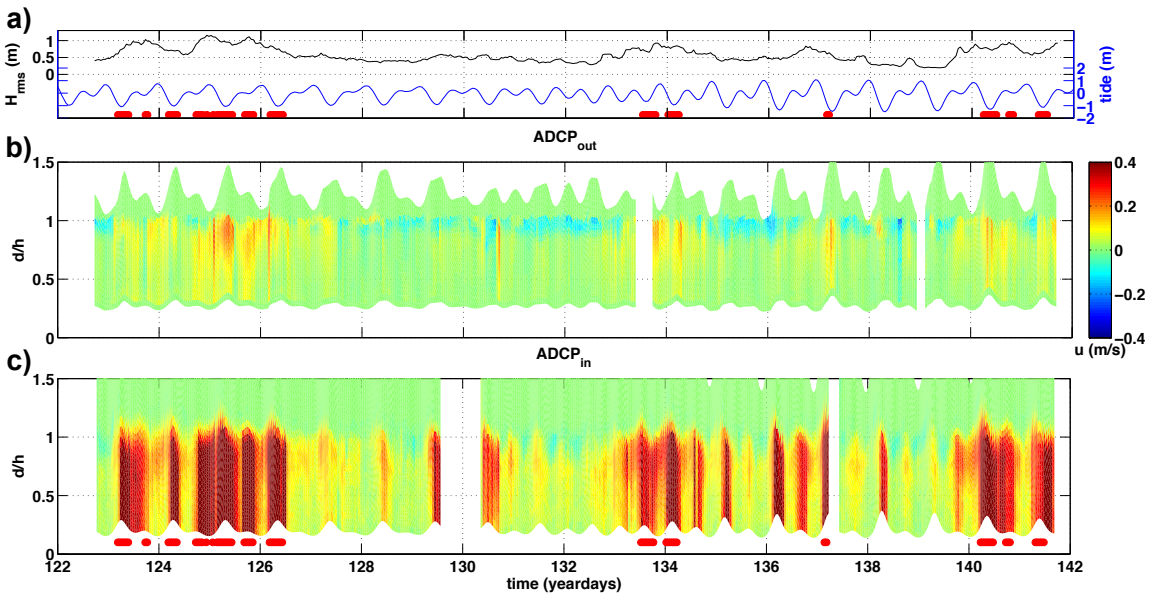

Figure 3. Conditions of (a) offshore root-mean-square wave height H_{rms} (left axis) and tidal elevation (right axis), shown for reference, and the hourly mean cross-shore velocities measured by (b) $ADCP_{out}$ and (c) $ADCP_{in}$, as a function of relative-depth, d/h. Colorbar in (b) represents the cross-shore velocity magnitude for (b) and (c). Red dots at the bottom in (a) and (c) represent times when $ADCP_{in}$ was located inside the surf zone ($H_{rms}/h \geq 0.4$).

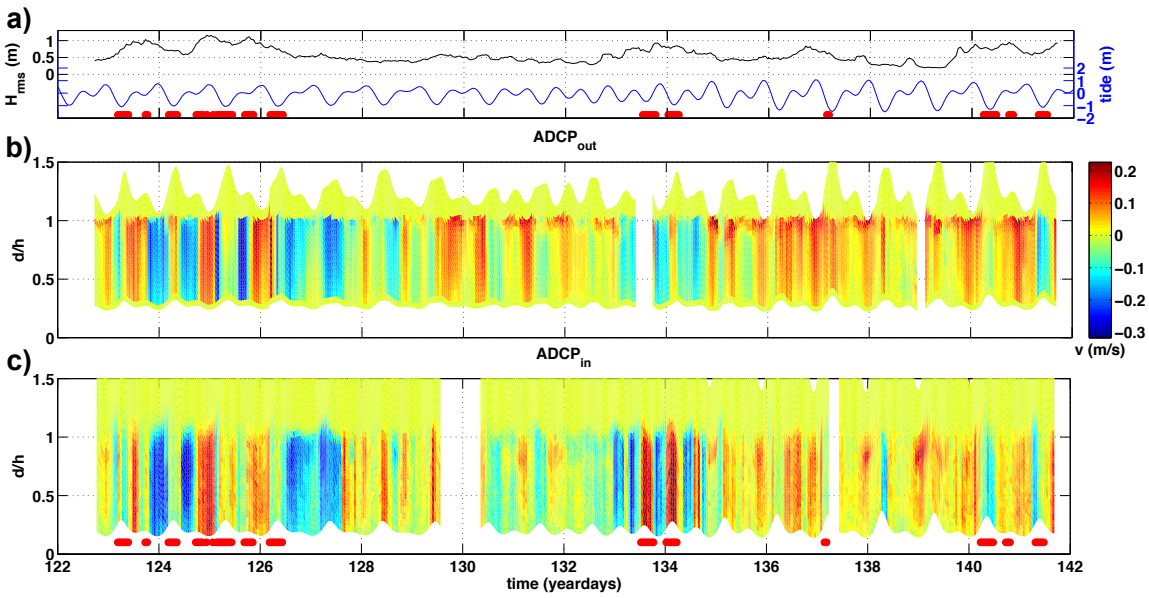

Figure 4. Conditions of (a) offshore root-mean-square wave height H_{rms} (left axis) and tidal elevation (right axis), shown for reference, and the hourly mean alongshore velocities measured by (b) $ADCP_{out}$ and (c) $ADCP_{in}$, as a function of relative-depth, d/h. Colorbar in (b) represents the alongshore velocity magnitude for (b) and (c). Red dots at the bottom in (a) and (c) represent times when $ADCP_{in}$ was located inside the surf zone ($H_{rms}/h \geq 0.4$).

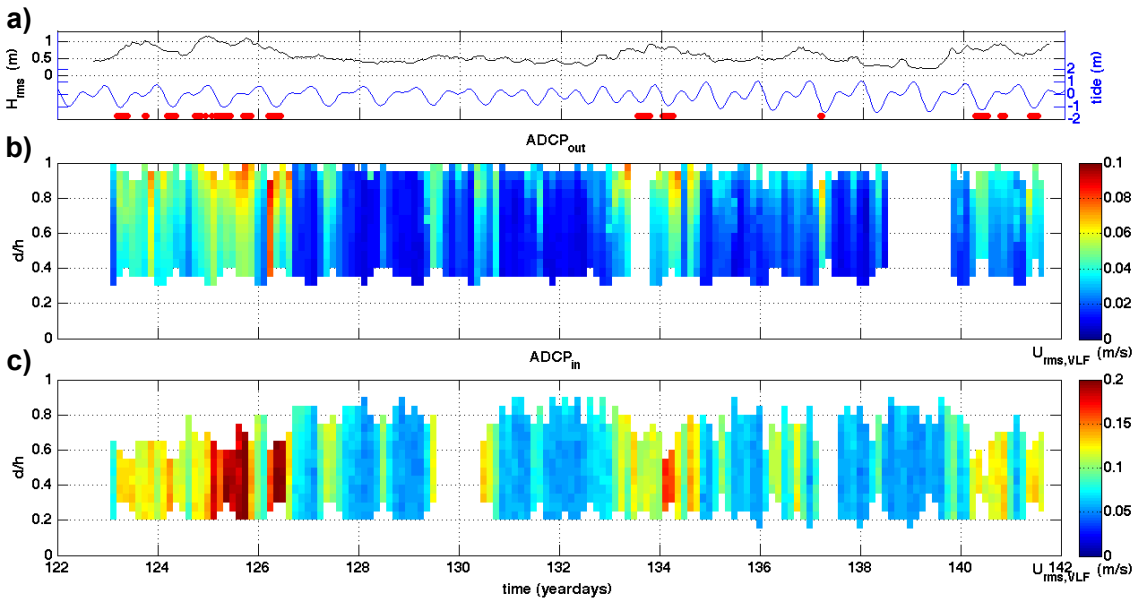

Figure 5. Conditions of (a) offshore root-mean-square wave height H_{rms} (left axis) and tidal elevation (right axis), shown for reference, and the 3-hour averaged root-mean-square VLF total horizontal velocity, $U_{rms,VLF}$, measured by (a) $ADCP_{out}$ and (b) $ADCP_{in}$, as a function of relative-depth, d/h. Colorbar represents the $U_{rms,VLF}$ magnitude, note the different scales. Red dots at the bottom in (a) represent times when $ADCP_{in}$ was located inside the surf zone ($H_{rms}/h \geq 0.4$).

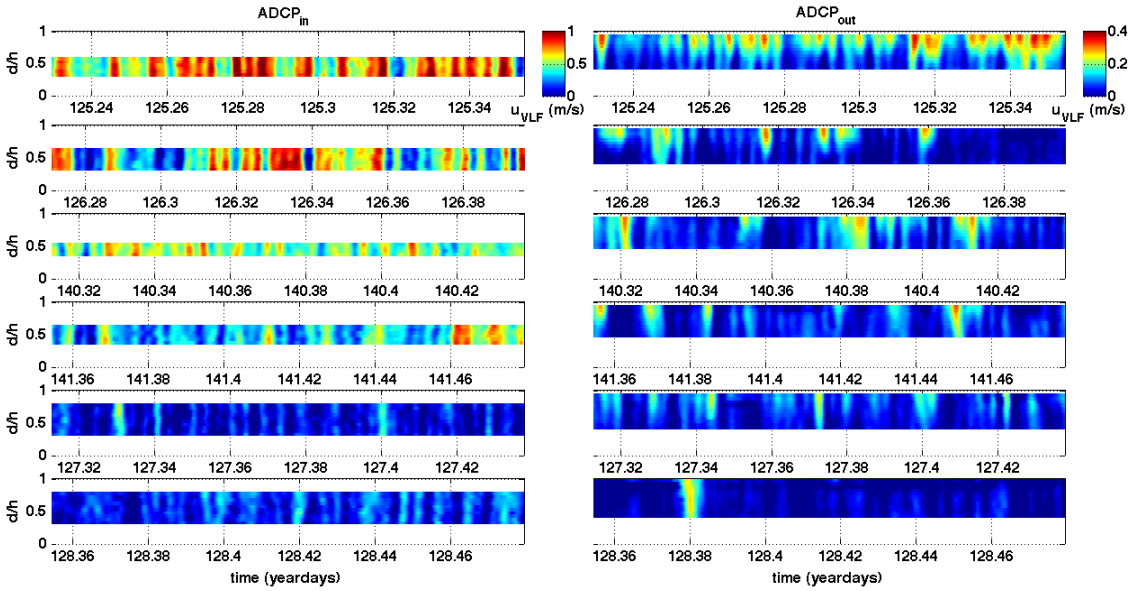

Figure 6. Examples of low-pass filtered cross-shore velocity, u_{VLF}, as a function of relative-depth, d/h, measured at (left column) $ADCP_{in}$ and (right column) $ADCP_{out}$ during 3HRLTs with (row 1 and 2) high, (row 3 and 4) intermediate, and (row 5 and 6) low VLF energy conditions. Colorbars represent u_{VLF} magnitude.

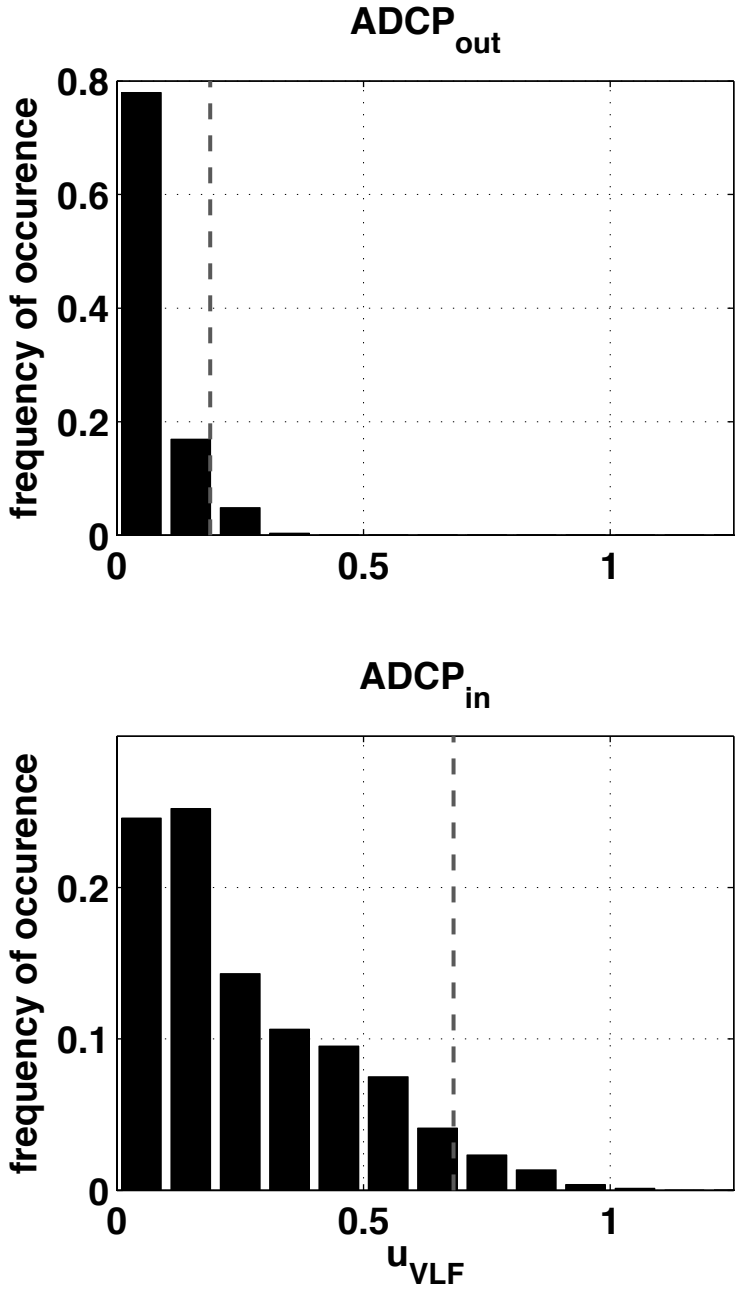

Figure 7. Frequency distribution of u_{VLF} measured during all 3HRLTs at (top) $ADCP_{out}$ and (bottom) $ADCP_{in}$. Vertical gray dashed lines represent the threshold used to determine significant VLF pulses, which was two times the standard deviation above the mean $(\mu + 2\sigma)$.

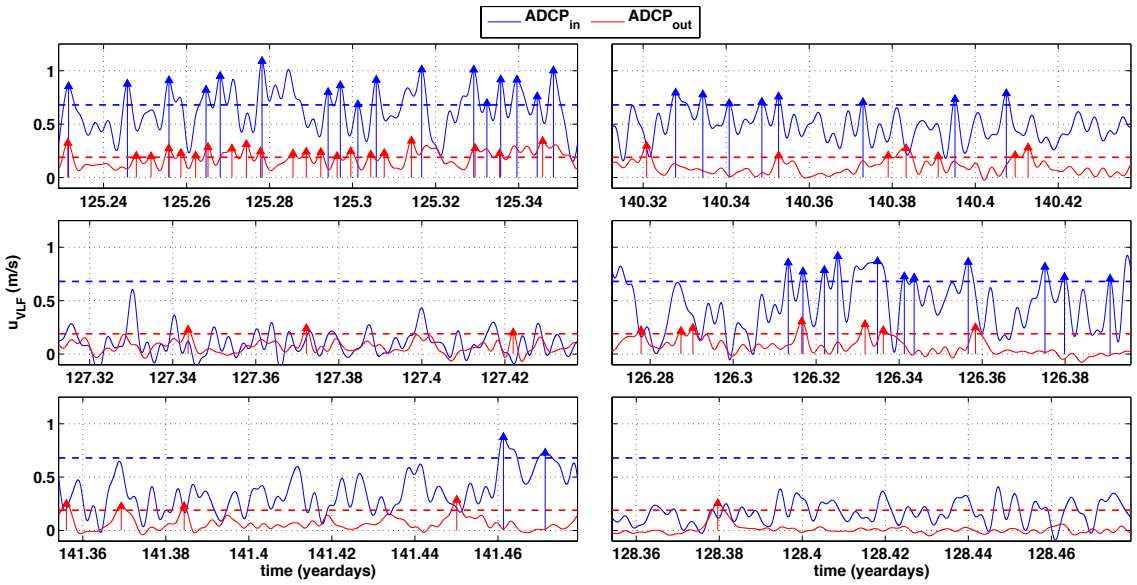

Figure 8. Examples of low-pass filtered cross-shore velocity, u_{VLF}, measured in the reference level at $ADCP_{in}$ (blue) and $ADCP_{out}$ (red) during 3HRLTs with (row 1) high, (row 2) intermediate, and (row 3) low VLF energy conditions. Colored horizontal dashed lines represent the threshold used to determine significant VLF pulses, and colored arrows indicate time and amplitude of the significant pulses.

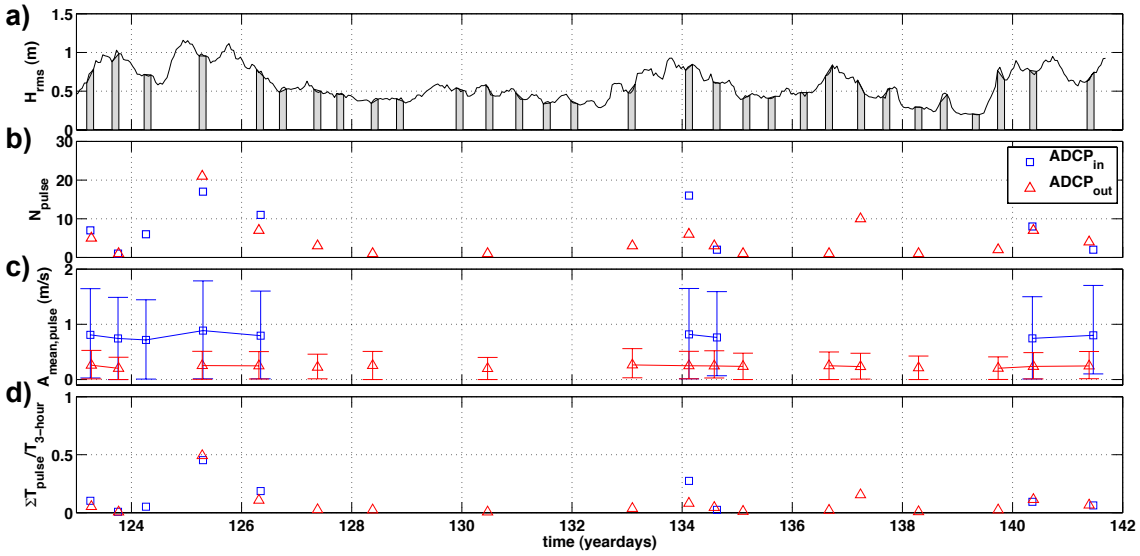

Figure 9. Conditions of (a) offshore root-mean-square wave height H_{rms}, (b) number of significant VLF pulses, N_{pulse}, (c) mean amplitude of significant VLF pulses, $A_{mean,pulse}$, and (d) the fraction of the time that the VLF pulses were occurring, defined as the sum of the individual pulse durations divided by the 3-hour record length, $\sum T_{sig,pulse}/T_{3-hour}$, measured at ADCP$_{in}$ (blue) and ADCP$_{out}$ (red) during the 3HRLTs (indicated by gray shaded regions in (a))

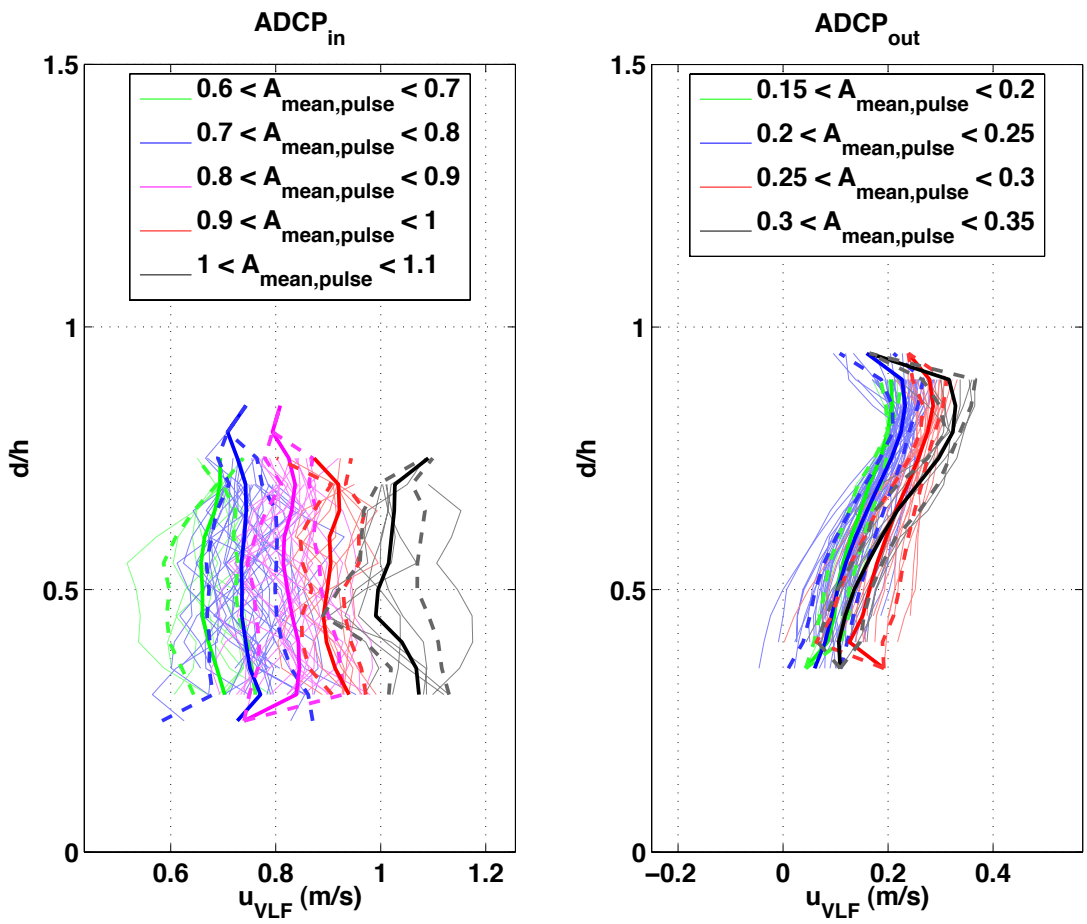

Figure 10. Vertical profiles of the low-passed filtered cross-shore velocity, u_{VLF}, as a function of relative-depth, d/h, measured at (left) $ADCP_{in}$ and (right) $ADCP_{out}$, bin-averaged as a function of the mean amplitude of significant VLF pulses, $A_{mean,pulse}$, measured in the reference level (colored lines, defined in legend).

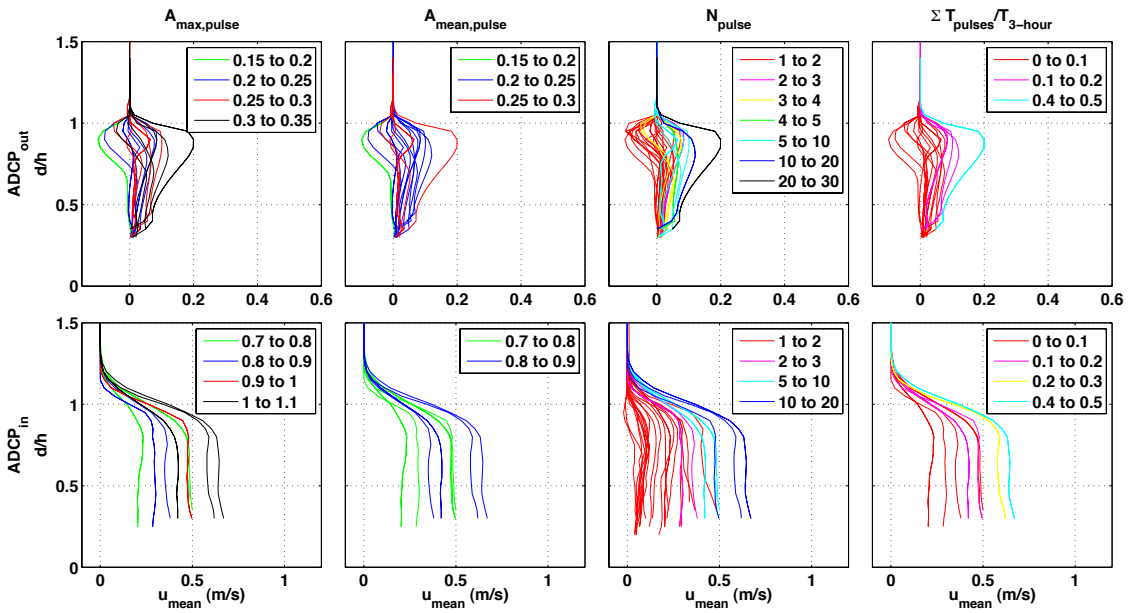

Figure 11. Vertical profiles of the mean cross-shore velocity, u_{mean}, as a function of relative-depth, d/h, measured at (top row) $ADCP_{out}$ and(bottom row) $ADCP_{in}$, bin-averaged as a function of (column 1) the maximum amplitude of significant VLF pulses, $A_{max,pulse}$, (column 2) the mean amplitude of significant VLF pulses, $A_{mean,pulse}$, (column 3) the number of significant VLF pulses, N_{pulse}, and (column 4) the duration of significant VLF pulses, $\sum T_{sig,pulse}/T_{3-hour}$, measured in the reference level (colored lines).

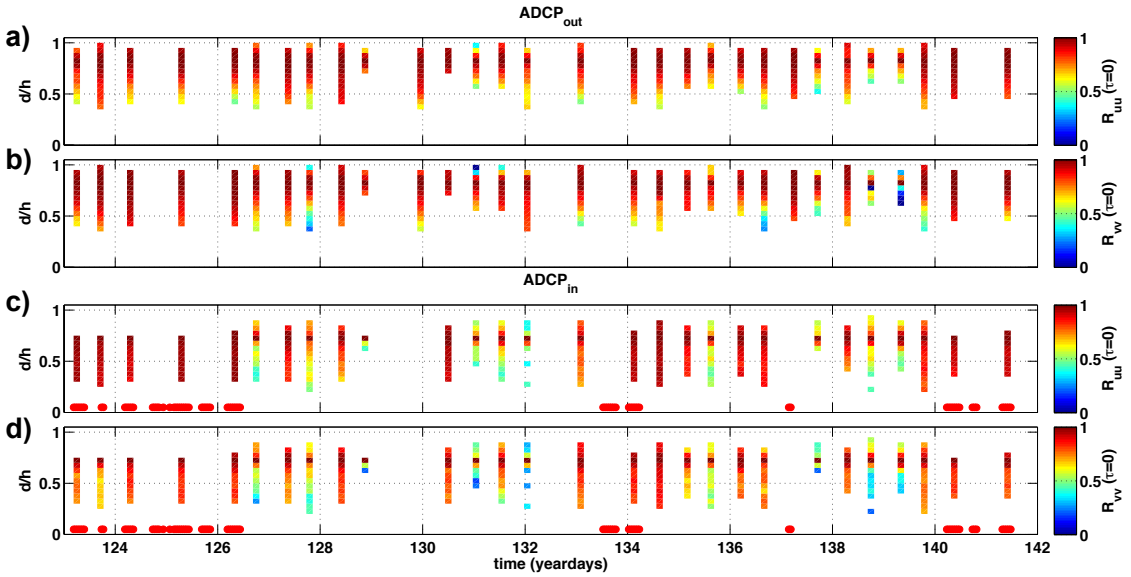

Figure 12. The cross-correlation $R(\tau = 0)$ as a function of relative-depth, *d*/*h*, of the (a, c) cross-shore and (b, d) alongshore velocity measured at each depth with the relative velocity measured in the surface reference level, measured at (a, b) $ADCP_{out}$ and (c, d) $ADCP_{in}$. Colorbars show correlation values.

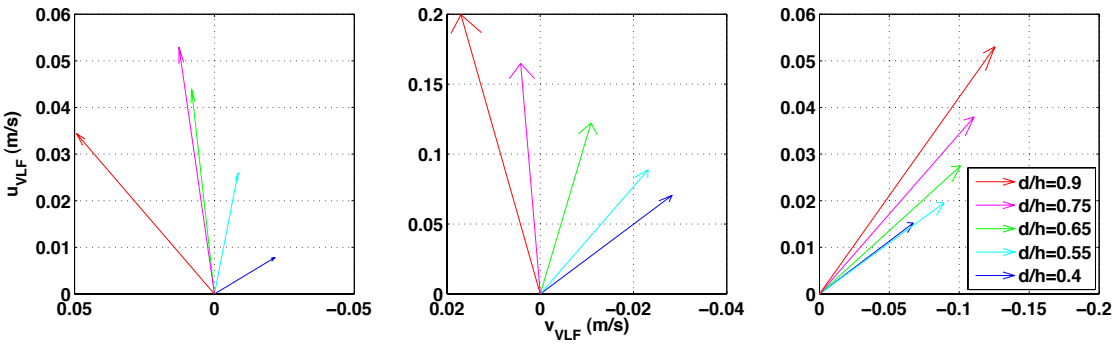

Figure 13. Examples of mean horizontal VLF velocity vectors measured at $ADCP_{out}$ at various relative-depths, d/h (colored lines, defined in legend) during 3HRLTs, showing differences in angle between the surface and sub-surface VLF velocities.

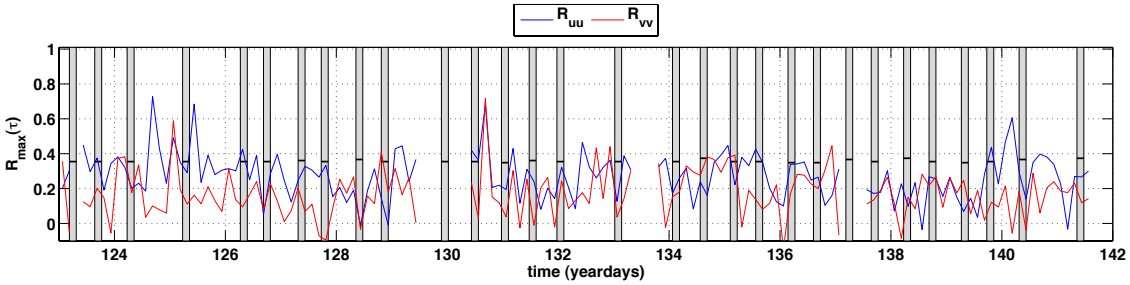

Figure 14. The cross-correlation $R_{\max}(\tau)$ of the cross-shore (blue) and alongshore (red) velocity measured at $ADCP_{out}$ with $ADCP_{in}$. Gray shaded regions represent 3HRLTs and horizontal black lines represent significant correlation values for each 3HRLT.

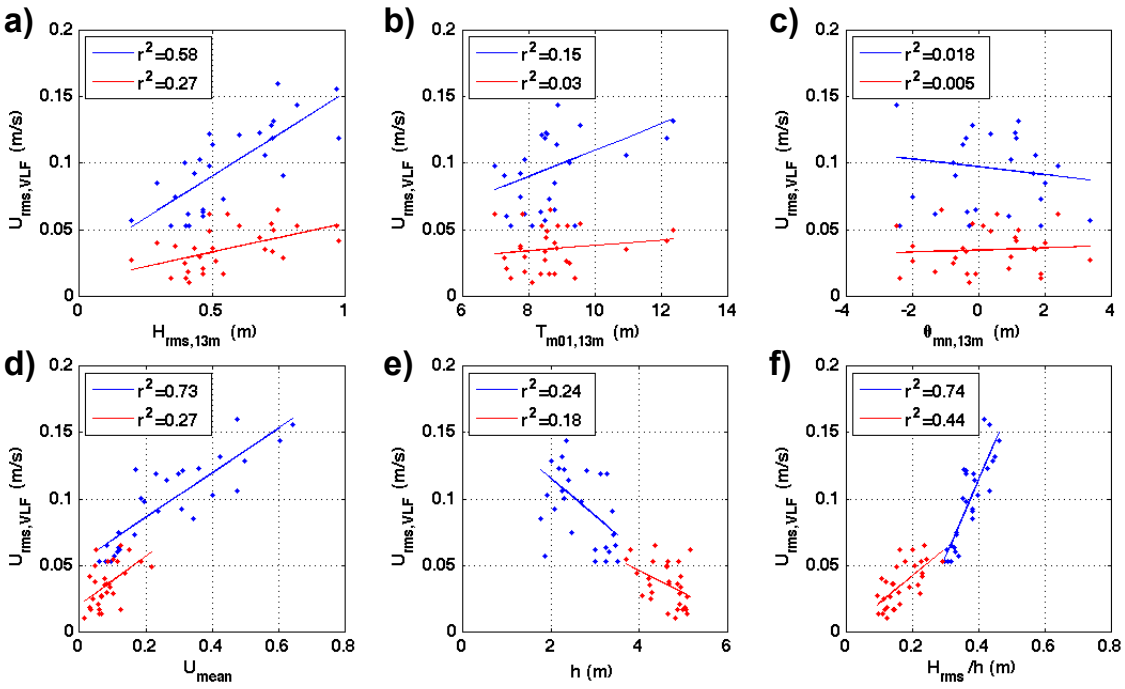

Figure 15. Linear regression of the 3-hour averaged root-mean-square VLF total horizontal velocity, $U_{rms,VLF}$, measured in the reference level and the 3-hour averaged (a) offshore root-mean-square wave height H_{rms}, (b) offshore mean wave period T_{m01}, (c) offshore mean wave direction θ_{m01}, (d) mean total horizontal velocity, U_{mean}, measured in the reference level, (e) local water depth, h, and (f) local root-mean-square wave height normalized by the local water depth, H_{rms}/h, measured by $ADCP_{in}$ (blue) and $ADCP_{out}$ (red) during the 3HRLTs. Colored lines represent bet-fit lines, and correlation coefficients, r^2, given in legends. Significant correlation coefficient is $r^2 = 0.35$ at the 95% significance level for all cases.

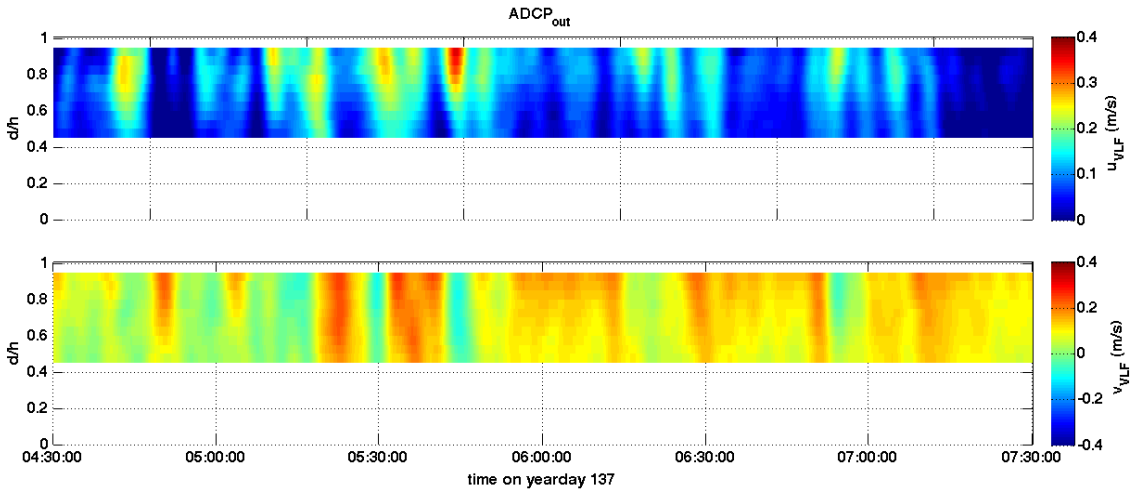

Figure 16. Example of low-pass filtered (top) cross-shore velocity, u_{VLF}, and (bottom) alongshore velocity, v_{VLF}, as a function of relative-depth, d/h, measured at ADCP$_{out}$ during a 3HRLT on yearday 137. Colorbars represent u_{VLF} and v_{VLF} magnitude.

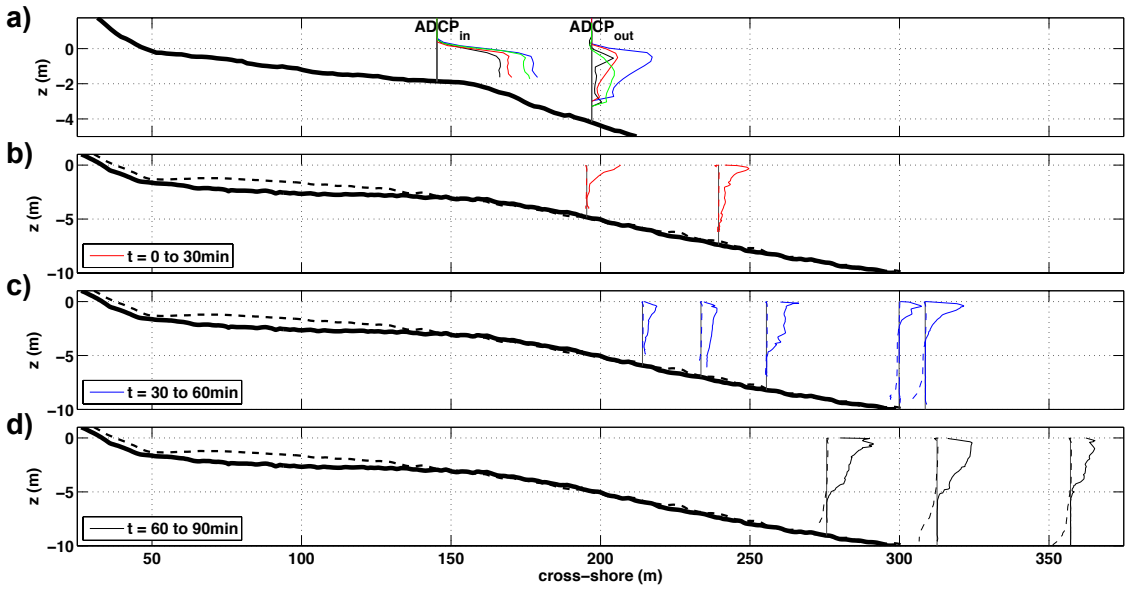

Figure 17. (a) 3-hour mean cross-shore velocity profiles corresponding to times of strong VLF pulses measured at $ADCP_{in}$ and $ADCP_{out}$ showing the rip current moving offshore as a jet. (b-d) Vertical measurements of dye concentration (solid) and de-meaned temperature (dashed) at varying cross-shore locations for time intervals after the dye release of (b) 0 to 30 minutes, (c) 30 to 60 minutes, and (d) 60 to 90 minutes. Mean cross-shore bathymetry profile in a rip channel (solid black line) and on a shoal (dashed black line).

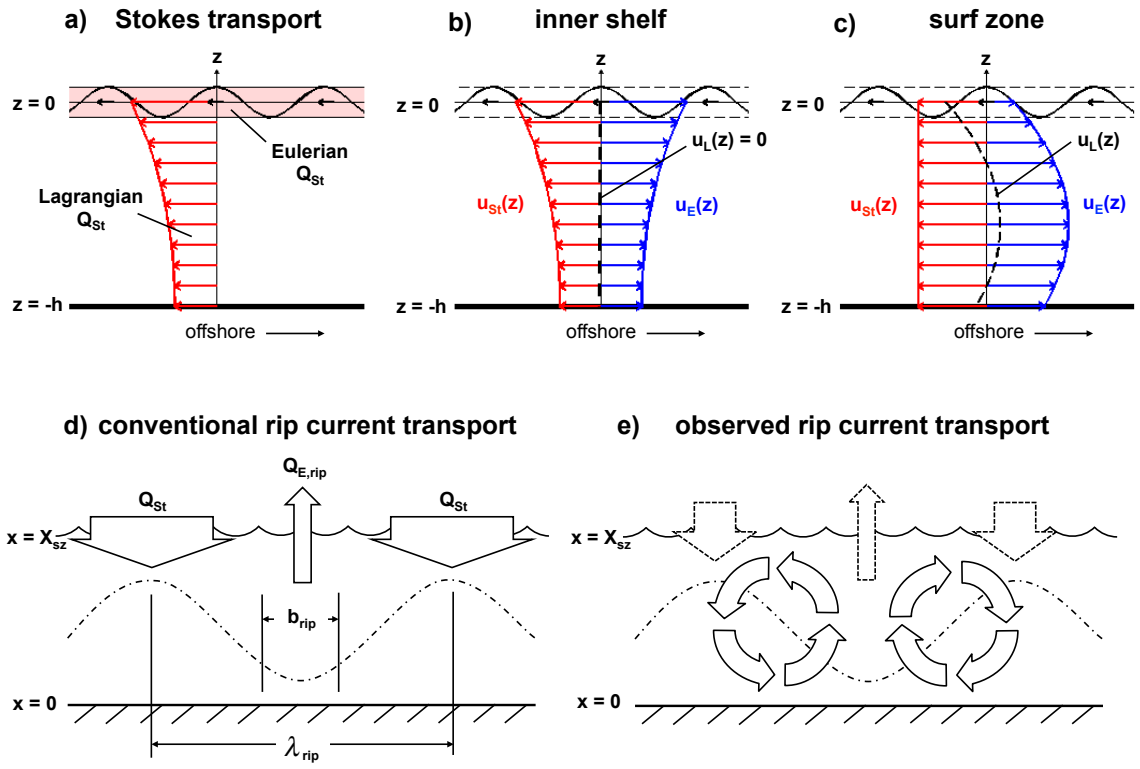

Figure 18. (a) Two-dimensional (x, z) onshore volume Stokes transport Q_{St} in a Lagrangian (particle following, red line) and a Eulerian (fixed in space, red shaded area) reference frame. Two-dimensional (x, z) wave-driven circulation in a Lagrangian reference frame typically observed (b) over the inner shelf, where the onshore Lagrangian Stokes drift $u_{St}(z)$ (red) and the offshore wave-driven Eulerian undertow $u_E(z)$ (blue) cancel resulting in a net Lagrangian velocity $u_L(z) = 0$ (black dashed line) at all depths, and (c) inside the surf zone, where the onshore Lagrangian Stokes drift $u_{St}(z)$ (red) is depth-uniform and the offshore wave-driven Eulerian undertow $u_E(z)$ (blue) is parabolic resulting in a vertical imbalance and $u_L(z) \neq 0$ (black dashed line). Two-dimensional (x, y) conceptual diagrams of (d) the conventional rip current theory, where a continuous onshore Stokes transport over the shoals ($Q_{St}\ \lambda_{rip}$) is balanced by a steady offshore rip current transport through the rip channels ($Q_{E,rip}\ b_{rip}$), and (e) the observed rip current cross-shore exchange, where surfzone rip current circulations (solid line block arrows) largely retain material inside the surf zone, and episodic, VLF rip current exits transport material offshore (offshore block arrow) and surf zone rip current circulations pull material back into the surf zone (onshore block arrow) to satisfy a mass balance, with no material being completely removed from the nearshore system.

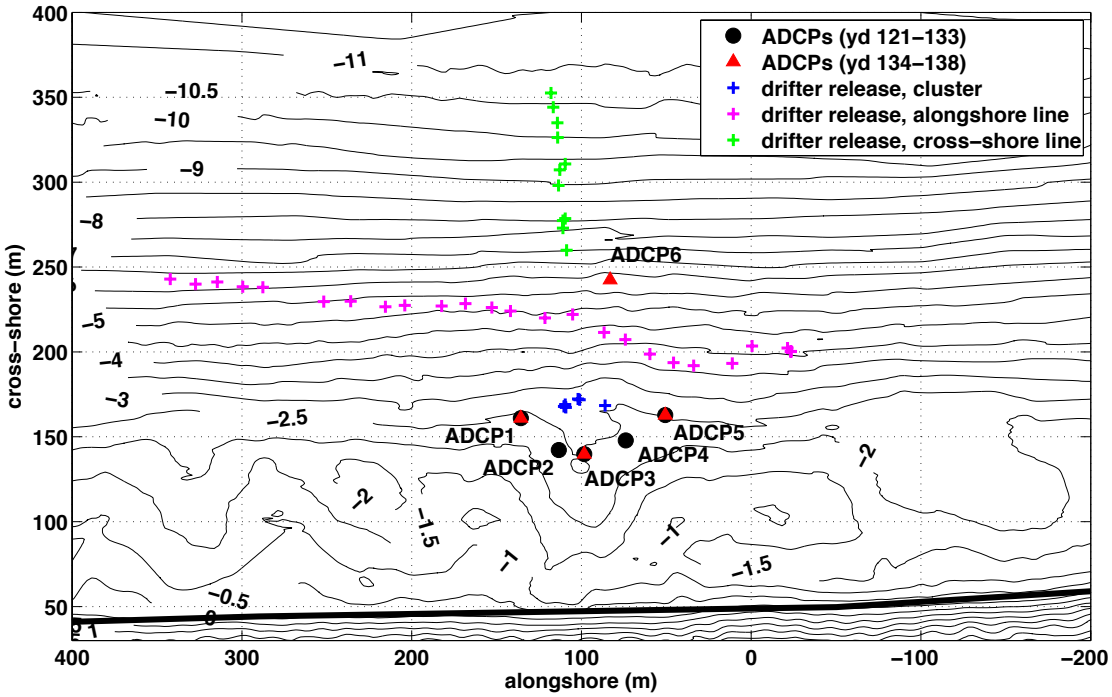

Figure 19. Field experiment site at Monterey, California, in the local coordinate system, where the thin black lines are the bathymetry contours (labeled with the elevation in meters relative to MSL) and the thick black line represents the mean shoreline. In-situ ADCP locations are shown, where black circles are the locations for yeardays 121 to 133 and red triangles are the locations for yeardays 134 to 138. Examples of the three drifter release approaches are shown from yearday 130 as crosses: 1) in a cluster at the offshore edge of a rip channel, just outside the surf zone (blue), 2) in an alongshore line outside the surf zone, spanning multiple shoals and rip channels (magenta), and 3) in a cross-shore line outside the surf zone, in line with a rip channel (green).

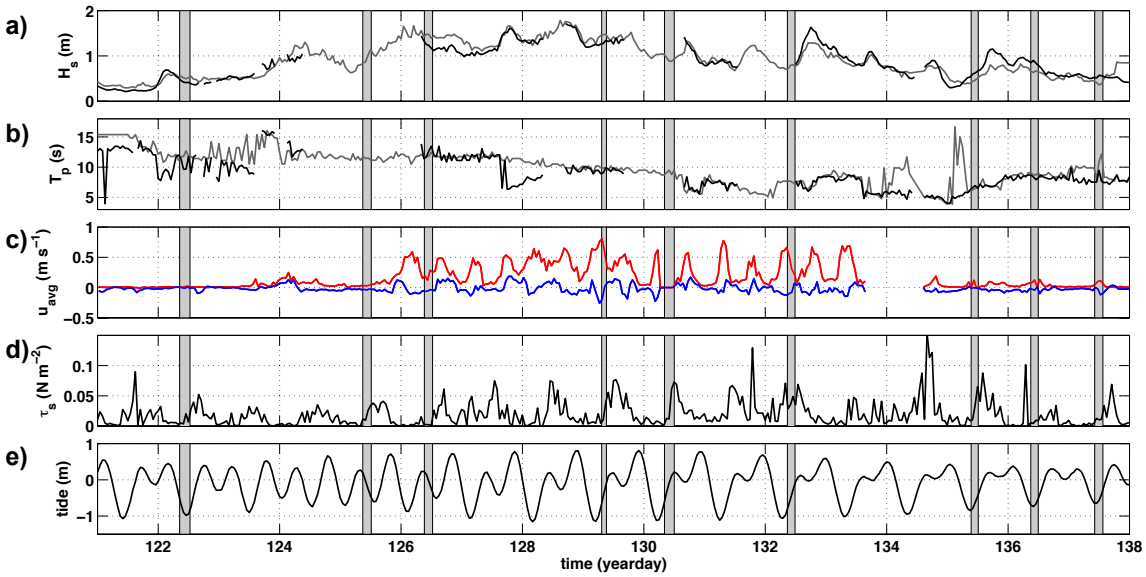

Figure 20. Conditions measured during the field experiment of (a) significant wave height H_s, (b) peak wave period T_p, (c) depth-averaged cross-shore (red) and alongshore (blue) velocities measured by ADCP 3 in the rip channel, (d) total wind stress magnitude, and (e) tidal elevation relative to MSL. In (a) and (b) the black lines are measured by the ADCP in 13 m water depth, and gray lines are measured by NDBC buoy 46240 shoaled to 13 m water depth. Gray shaded regions represent times of drifter deployments.

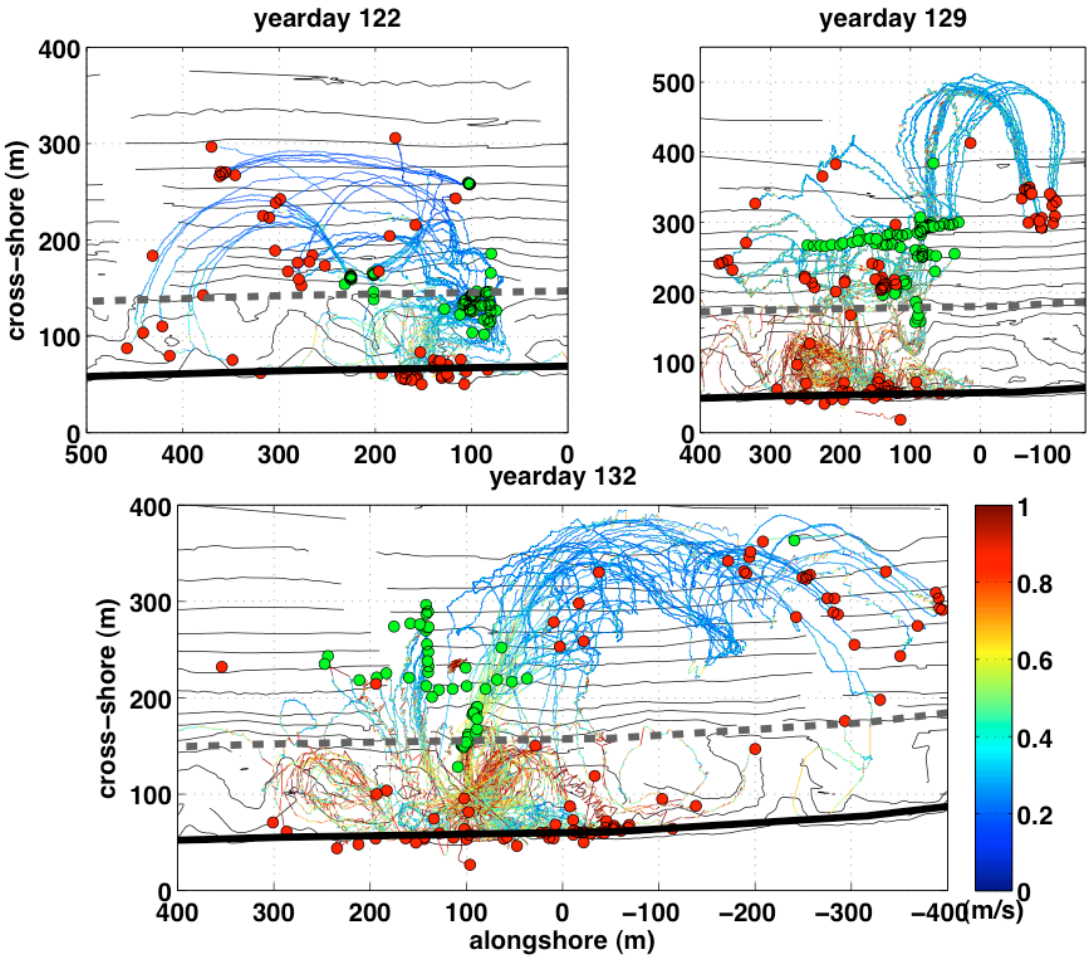

Figure 21. Drifter positions and speed, where the color of the line represents the speed, for drifter deployments exhibiting the locally-contained cross-shore exchange drifter pattern on yeardays 122, 129, and 132. Bathymetry contours are shown in the background in black, the shoreline is shown as the solid black line, and the approximate surfzone boundary is shown as the dashed gray line. Colorbar represents the drifter speed. Green circles show drifter release locations and red circles show drifter retrieval locations. Note there are different cross-shore and alongshore scales between plots.

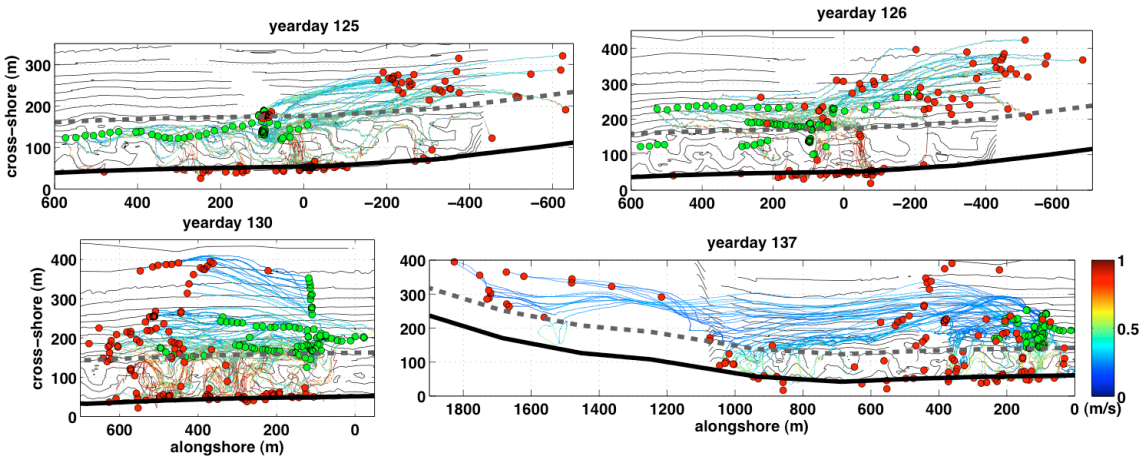

Figure 22. Drifter positions and speed, where the color of the line represents the speed, for drifter deployments exhibiting the cross-shore and alongshore exchange drifter pattern on yeardays 125, 126, 130, and 137. Bathymetry contours are shown in the background in black, the shoreline is shown as the solid black line, and the approximate surfzone boundary is shown as the dashed gray line. Colorbar represents the drifter speed. Green circles show drifter release locations and red circles show drifter retrieval locations. Note there are different cross-shore and alongshore scales between plots.

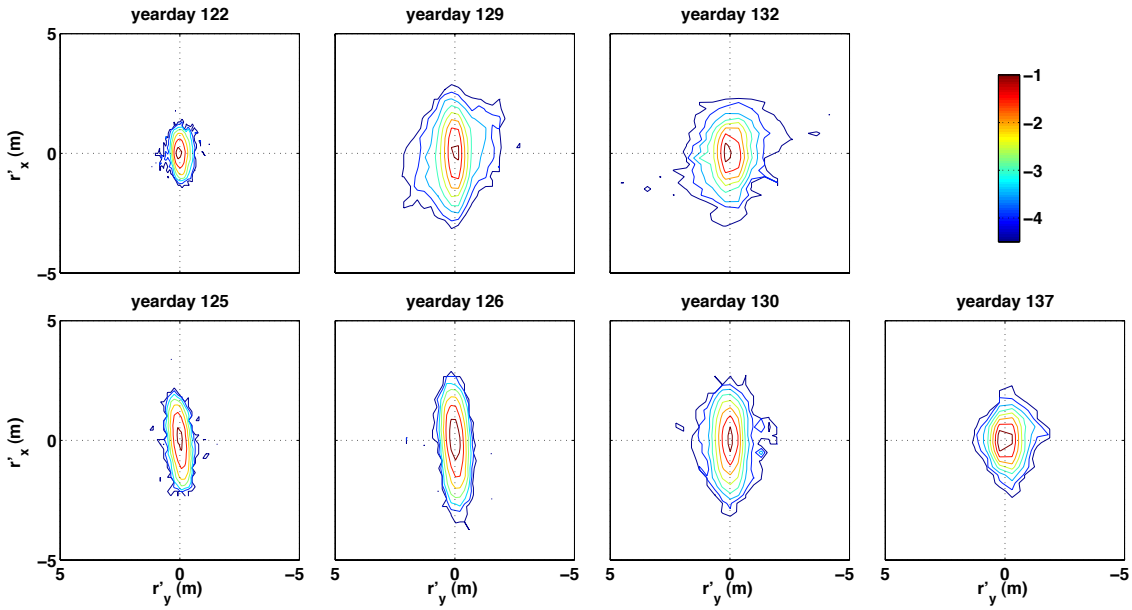

Figure 23. Log-log plots of the probability density function (pdf) of the anomalous relative drifter position displacements outside the surf zone for a relative time step of $t' = 2$ s for (top row) drifter deployments exhibiting the locally-contained cross-shore exchange drifter pattern on yeardays 122, 129, and 132, and (bottom row) drifter deployments exhibiting the cross-shore and alongshore exchange drifter pattern on yeardays 125, 126, 130, and 137. Contours are $\log_{10}[P(r_x', r_y'; t' = 2 \text{ s})] = -4.5, -4, -3.5, \ldots 1, 1.5$.

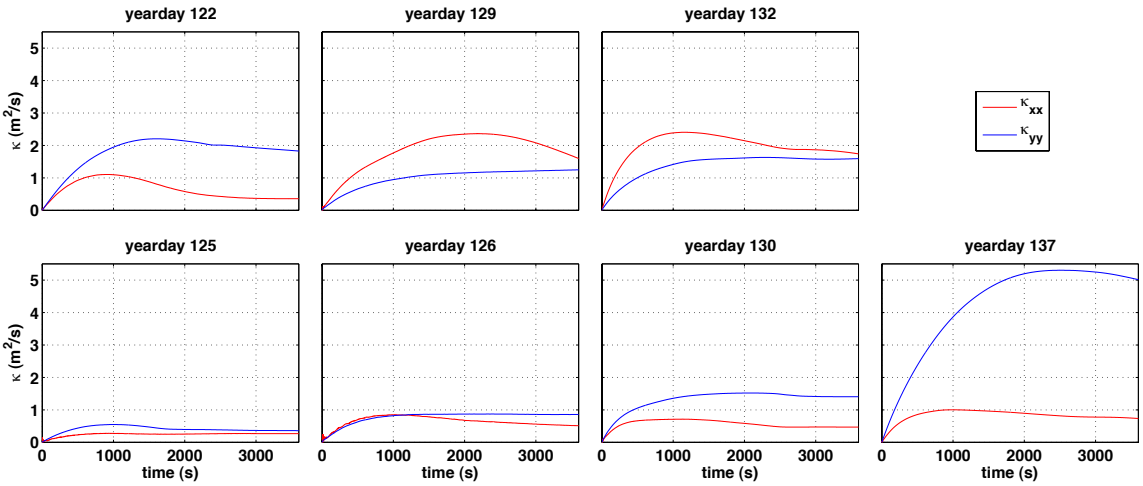

Figure 24. Absolute diffusivity (one-particle) statistics for the cross-shore (κ_{xx}, red) and alongshore (κ_{yy}, blue) for drifter positions recorded outside the surf zone for (top row) drifter deployments exhibiting the locally-contained cross-shore exchange drifter pattern on yeardays 122, 129, and 132, and (bottom row) drifter deployments exhibiting the cross-shore and alongshore exchange drifter pattern on yeardays 125, 126, 130, and 137.

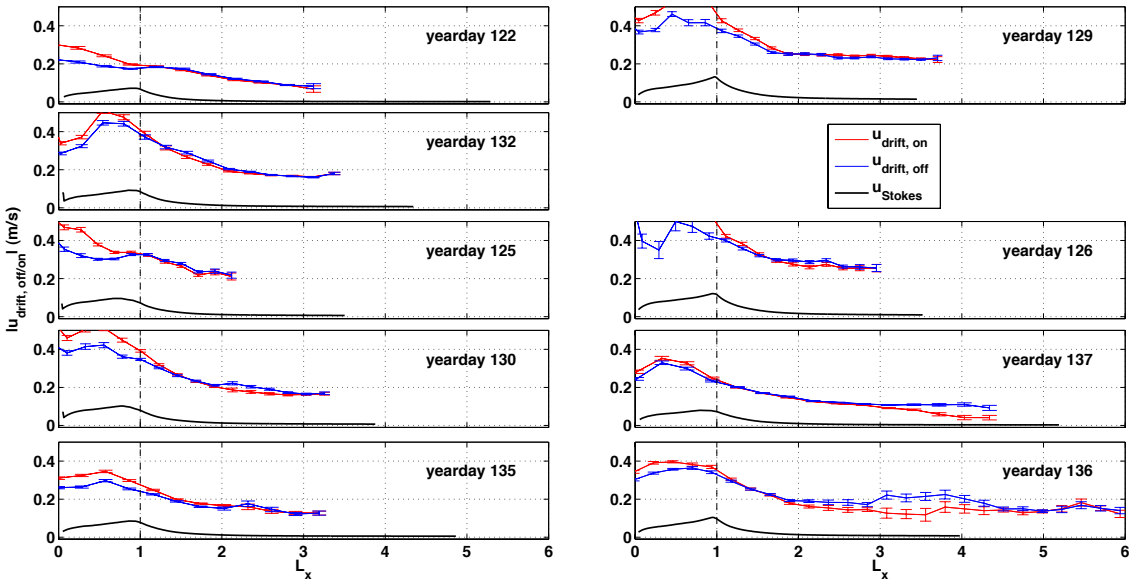

Figure 25. Drifter cross-shore velocity magnitude $\left|u_{drift,off/on}\right|$ as a function of cross-shore distance, measured in surfzone-widths L_x, for each drifter deployment, where onshore velocities $\left|u_{drift,on}\right|$ are shown in red and offshore velocities $\left|u_{drift,off}\right|$ are shown in blue, and error bars are shown. Black line represents the theoretical estimate of the Stokes drift averaged over the upper 0.5 m of the water column, u_{St}(0.5 m), which correspond to the depth of the surface drifters. Rows 1 and 2 show drifter deployments exhibiting the locally-contained cross-shore exchange drifter pattern on yeardays 122, 129, and 132, rows 3 and 4 show drifter deployments exhibiting the cross-shore and alongshore exchange drifter pattern on yeardays 125, 126, 130, and 137, and row 5 shows drifter deployments with no distinguishable exchange pattern on yeardays 135 and 136.

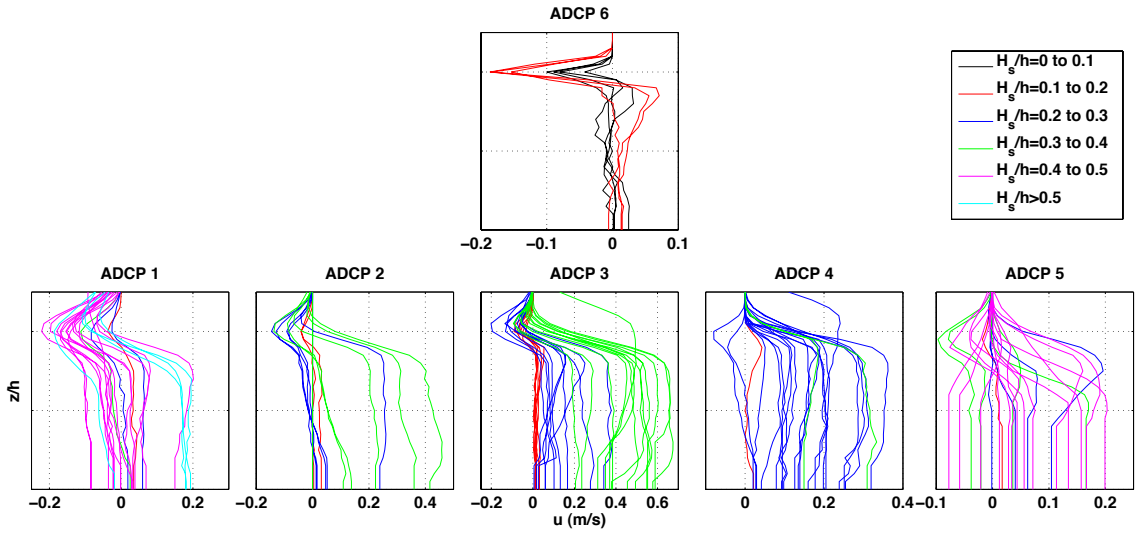

Figure 26. 3-hour mean vertical profiles, centered around low tide, of cross-shore currents measured at each ADCP, sorted by H_s/h and bin-averaged for H_s/h ranges given in the legend, where ADCPs 2, 3 and 4 were located at the surfzone boundary inside the rip channel, ADCPs 1 and 5 were located at the surfzone boundary over shoals, and ADCP 6 was located outside the surf zone offshore of the rip channel. Note the variable velocity scales.

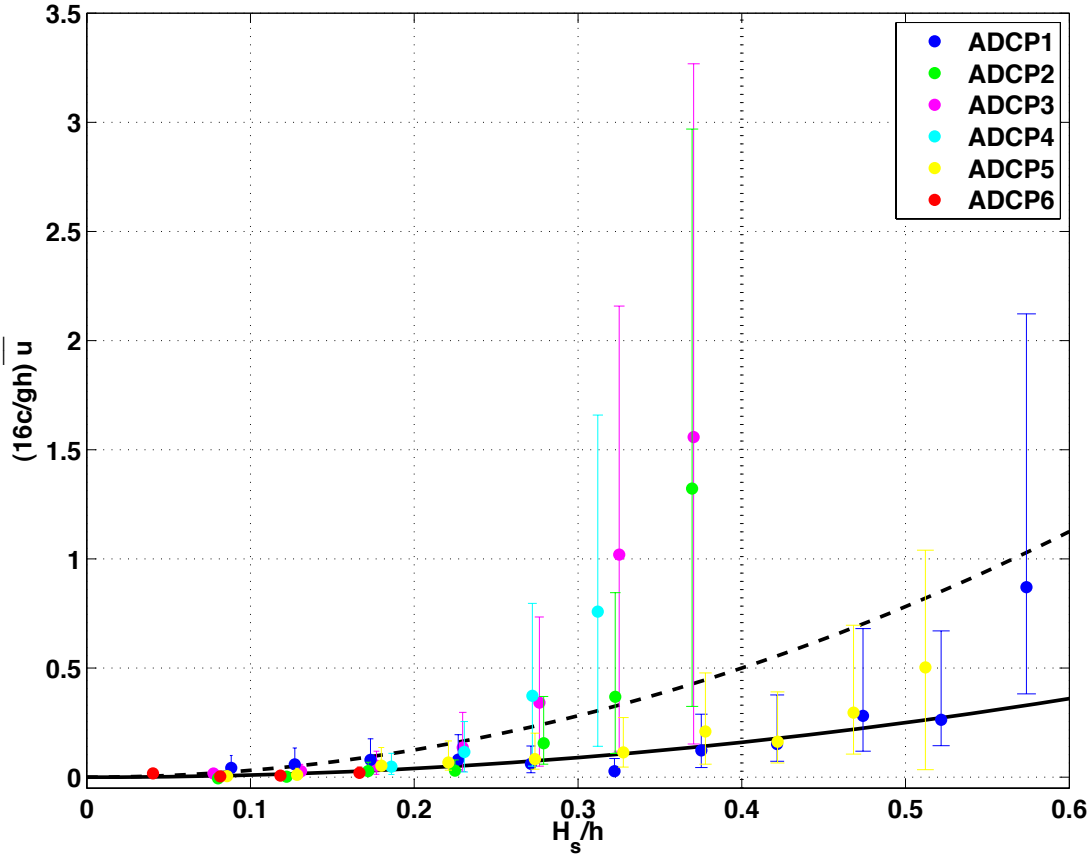

Figure 27. Normalized depth-averaged cross-shore Eulerian currents $\overline{u}_{N,E}$ measured at each ADCP and bin-averaged by H_s/h, where ADCPs 2, 3 and 4 were located at the surfzone boundary inside the rip channel, ADCPs 1 and 5 were located at the surfzone boundary over shoals, and ADCP 6 was located outside the surf zone offshore of the rip channel. Solid black line represents theoretical Stokes drift $\overline{u}_{N,St}$ that balances $\overline{u}_{N,E}$ according to Lentz et al. (2008), and the dashed black line represents theoretical $\overline{u}_{N,E,rip}$ through the rip channel that would balance the continuous onshore Stokes transport over the shoals according to the conventional rip current theory.

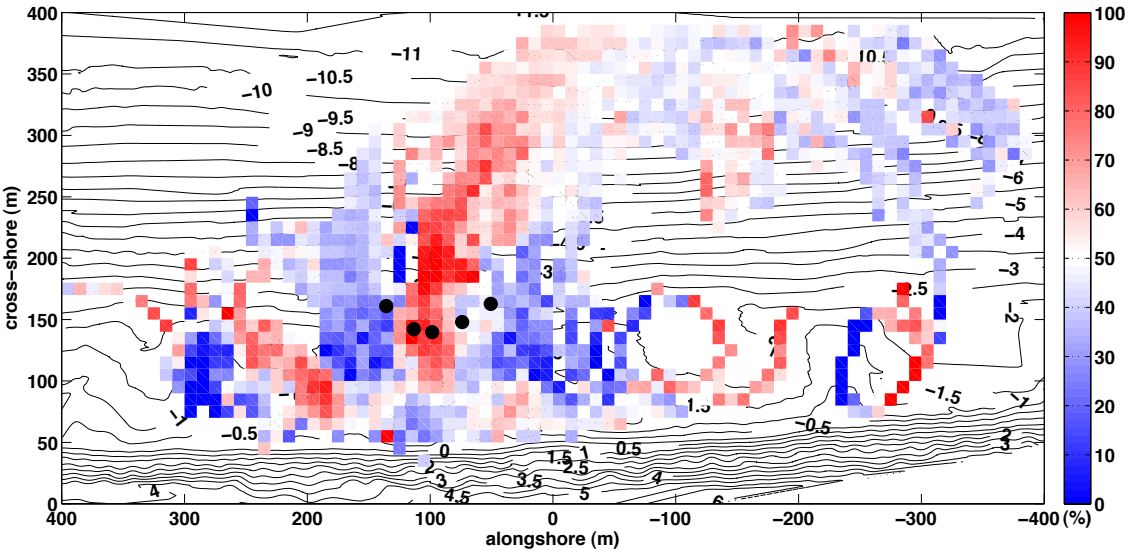

Figure 28. Drifter observations spatially binned into 10 m by 10 m bins and averaged for yearday 132, with the mean cross-shore movement in each bin represented as a percentage of time during the drifter deployment that the drifters were moving seaward. Red indicates drifters moved seaward 100% of the time, blue indicates drifters only moved shoreward (moved seaward 0% of the time), and lighter colors indicate a tendency for drifters to move in both directions. Bathymetry contours shown in black and ADCP locations shown as black circles.

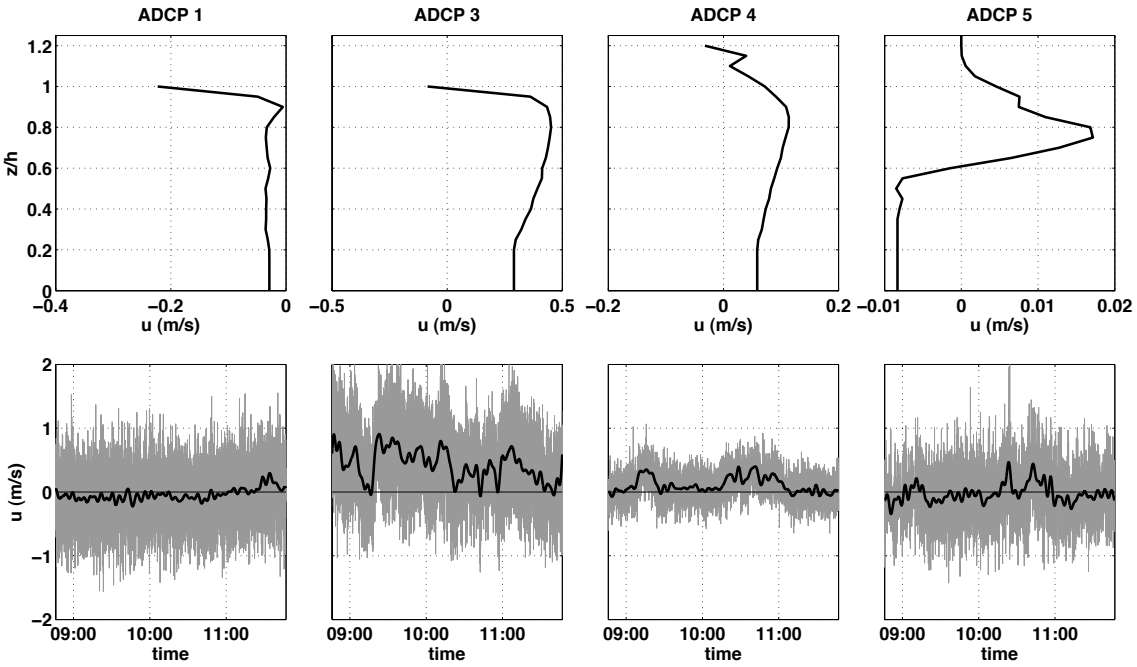

Figure 29. Eulerian velocity measurements at each ADCP (columns) during the drifter deployment on yearday 132, showing (top) the depth-relative mean vertical profile averaged over the duration of the drifter deployment, and (bottom) the surface cross-shore velocity (gray) and low-pass filtered ($f < 0.004$ Hz) surface cross-shore velocity (black), representing VLF rip current pulsations, where ADCPs 3 and 4 were located at the surfzone boundary inside the rip channel. Note the variable velocity scales in the top plots.

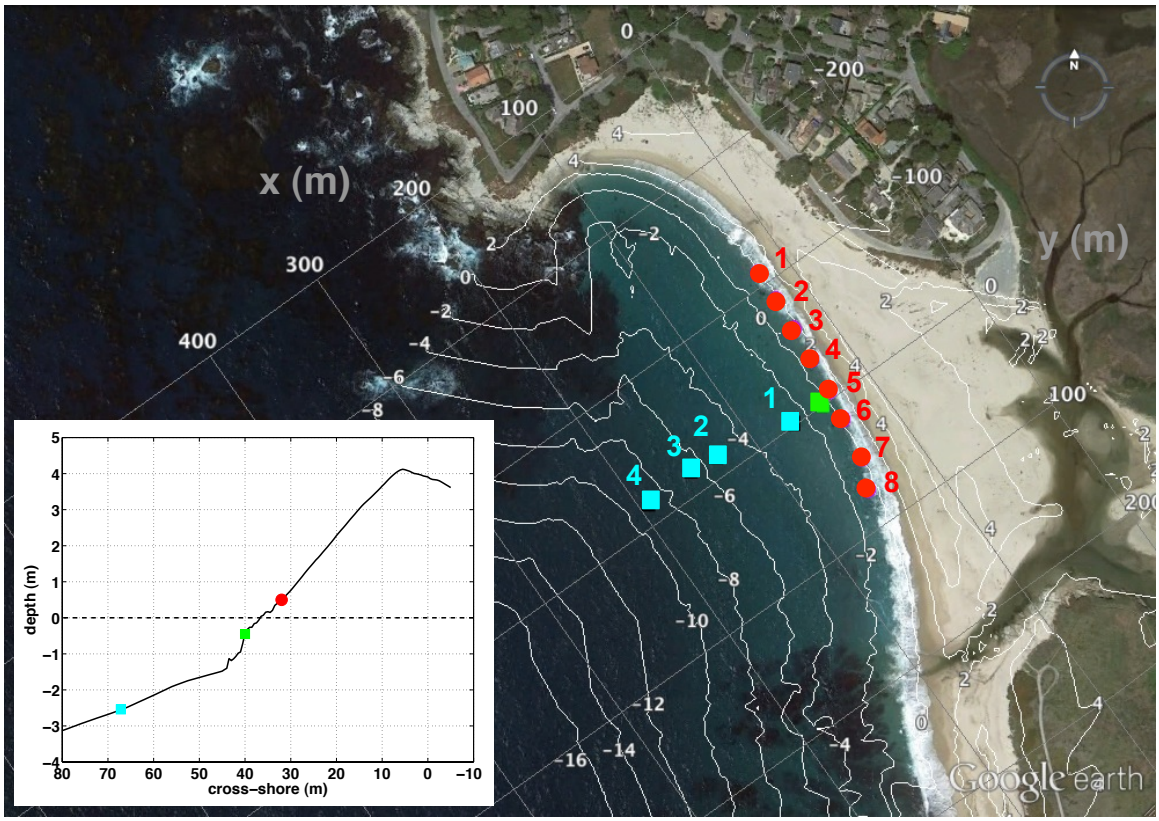

Figure 30. Carmel River State Beach, California, field site shown with a Google Earth image and bathymetry contours in meters overlaid in white. The inset shows the mean cross-shore beach profile, relative to mean sea level. Red dots represent the alongshore array of stationary dye sensors, cyan squares represent the cross-shore array of ADCPs, and the green square represents the location of the EMCM array. The local coordinate system is shown, where positive is offshore and to the south.

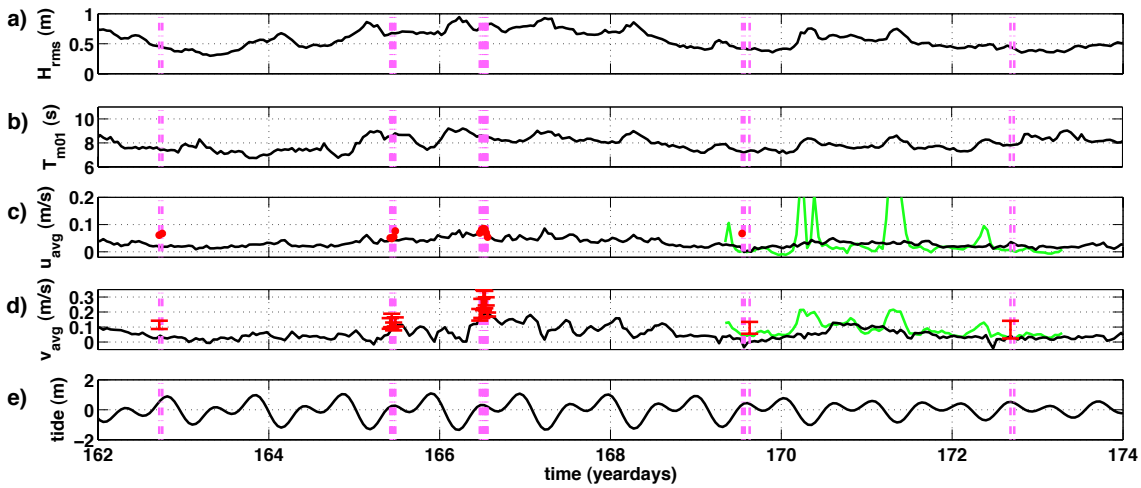

Figure 31. Hourly-mean (a) root-mean square wave height, H_{rms}, (b) mean wave period, T_{m01}, (c) depth-averaged cross-shore velocity, (d) depth-averaged alongshore velocity, and (e) tidal elevation measured at ADCP1 in 3 m water depth. Red dots and error bars in (c) and (d) represent surfzone currents estimated with the dye. Green lines in (c) and (d) represent depth-averaged velocities measured by the EMCM array in 0.4 m water depth. Vertical dashed magenta lines represent times of dye releases. Velocities are in the local coordinate system where positive is offshore and to the south.

Figure 32. Photos showing examples of (a) the initial dye slug release, (b) the well-mixed surf/swash zone shortly after the dye release, and (c-e) a dye sensor attached near the sea-bed on a pole (shown by the green arrows) in the surf zone, highlighting the intermittency of the dye observations as the sensor is alternately submerged and not submerged.

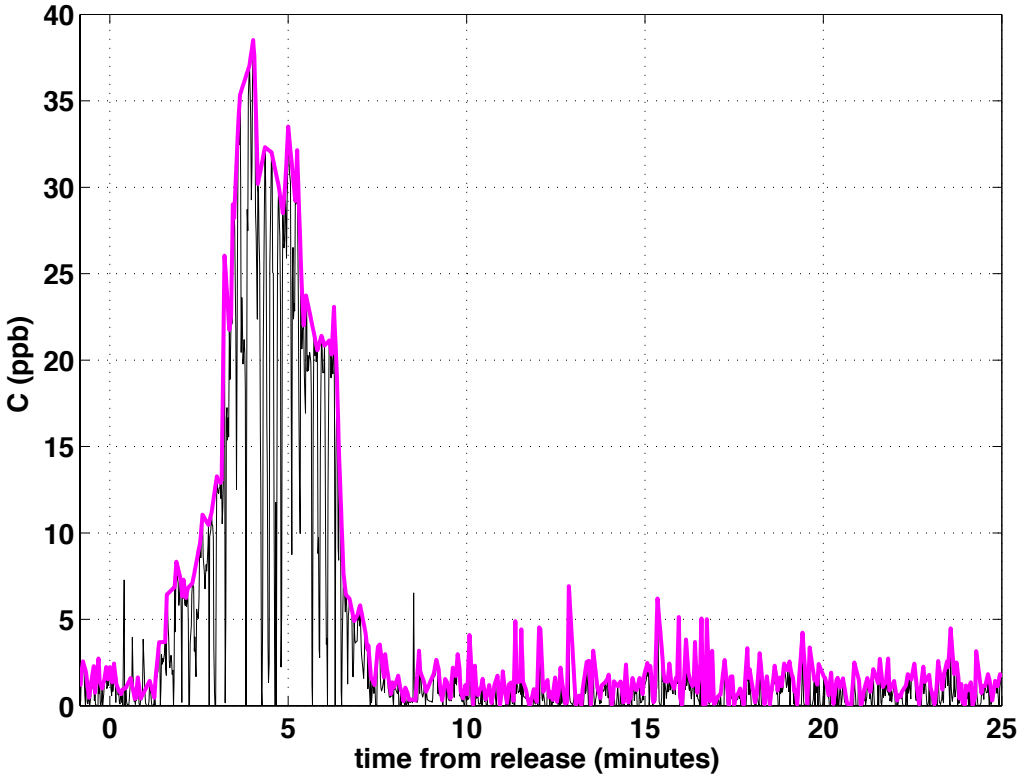

Figure 33. Example of measured dye concentration as a function of time (black) and the dye envelope fit to the measurements (magenta).

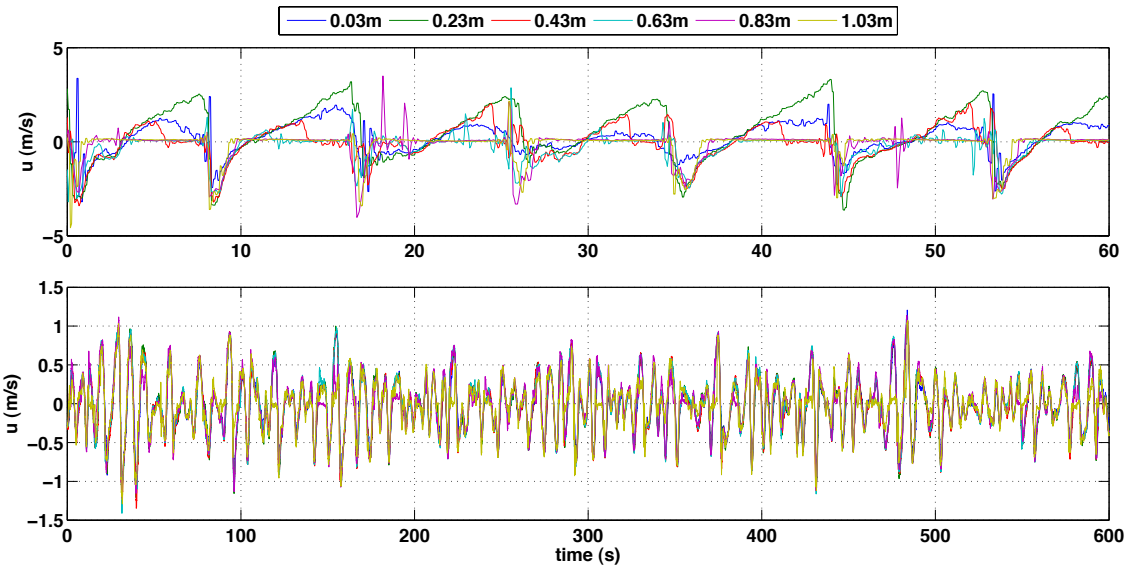

Figure 34. Example of cross-shore velocities measured by the EMCM array for times when the EMCM array was (top) inside the surf zone and (bottom) outside the surf zone. Cross-shore velocity is in the local coordinate system where positive is offshore. The height of each EMCM sensor above the sea-bed is given in the legend.

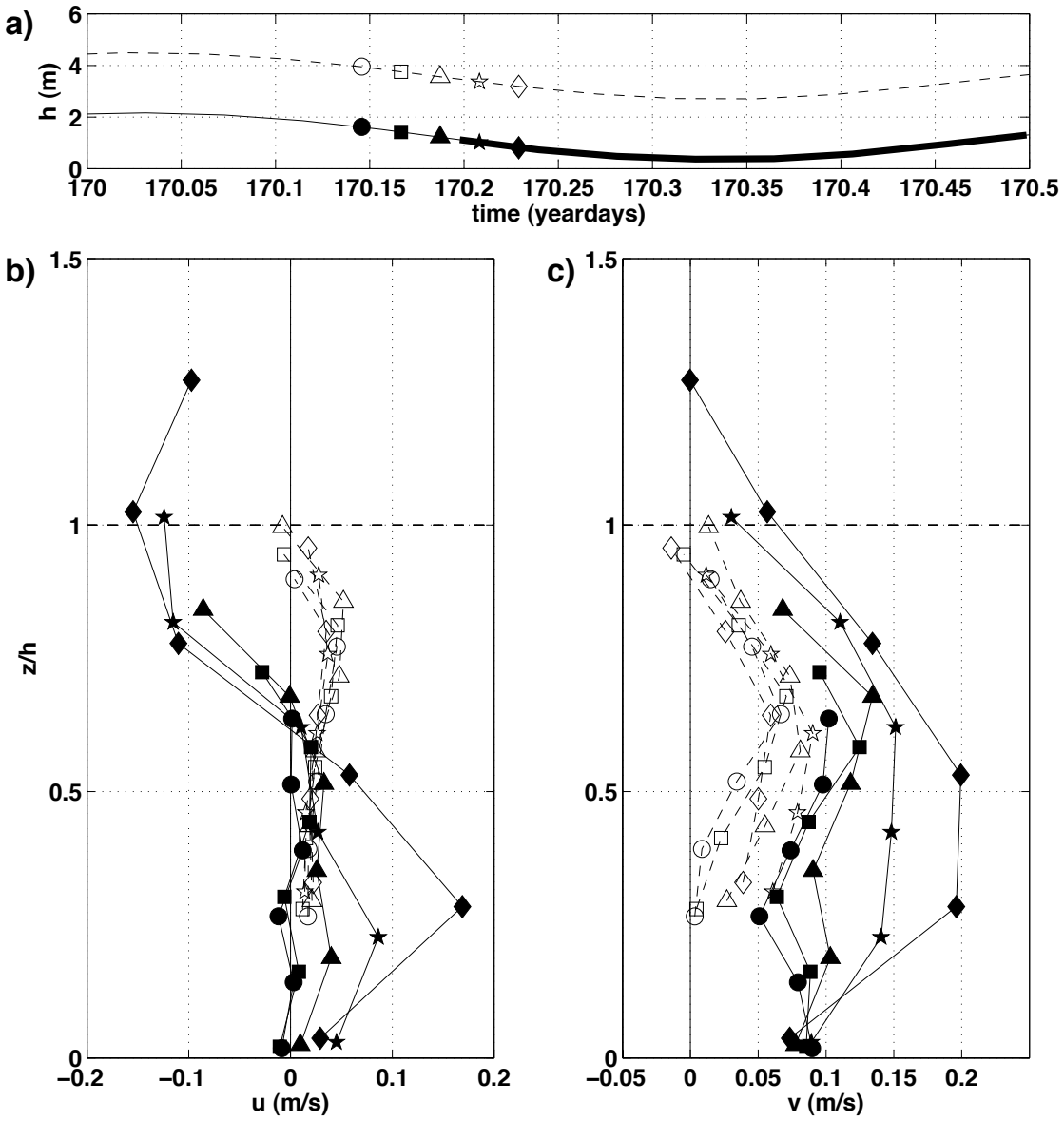

Figure 35. (a) Water depth measured at ADCP1 (dashed line) and at EMCM array (solid line), with times when the EMCM array was inside of the surf zone shown by the thick black line, (b) half-hour mean cross-shore velocity profiles measured by ADCP1 (open symbols) and EMCM array (solid symbols), and (c) half-hour mean alongshore velocity profiles measured by ADCP1 (open symbols) and EMCM array (solid symbols), as a function of depth-normalized height above the sea-bed. Symbols in the velocity profiles correspond to times in the water depth time series. Velocities are in the local coordinate system where positive is offshore and to the south.

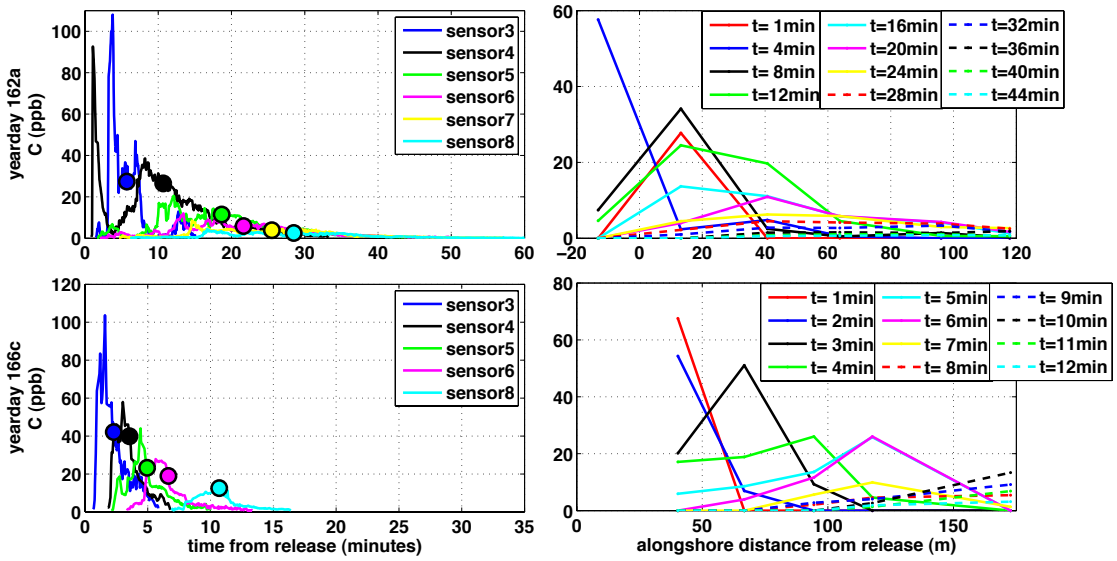

Figure 36. Dye concentration as a function of time (left) and as a function of alongshore distance from the dye release (right) measured by the alongshore array of stationary dye sensors for (top) yearday 162a during weak alongshore current conditions, and (bottom) yearday 166c during strong alongshore current conditions. Colored circles in left plots represent t_{m01} computed with Equation (14).

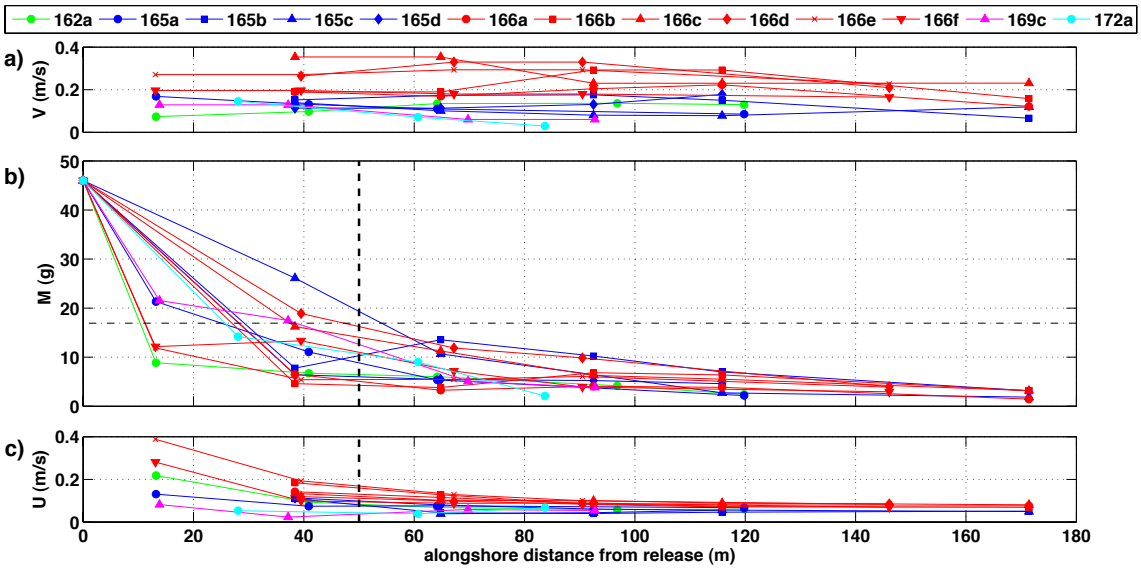

Figure 37. Estimates based on the dye concentration time series measured by the alongshore stationary dye sensor array of (a) the surfzone averaged alongshore current V using Equation (13), (b) the alongshore decay of dye mass $M(y)$ using Equation (15), and (c) the surfzone averaged cross-shore current U using Equation (12), as a function of alongshore distance y from the dye release. In (b) the horizontal black dashed-dotted line represents where M_0 decreases by $1/e$, and the in (b) and (c) the vertical black dashed lines represent the division between the near-field and far-field regions of the flow.

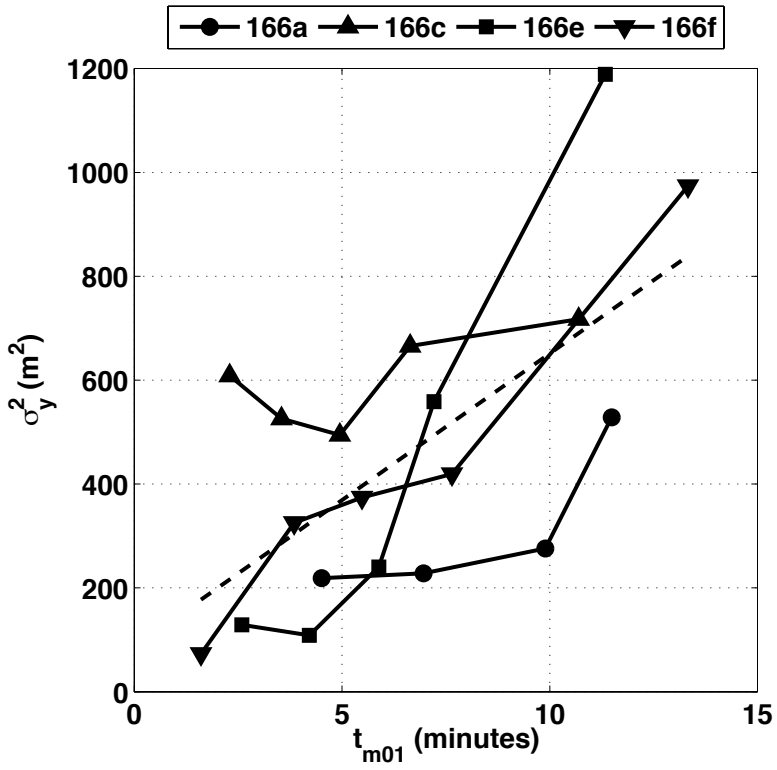

Figure 38. Dye dispersion inside of the surf zone measured with the alongshore array of stationary sensors as a function of weight-mean concentration time t_{m01}. The dashed line represents the line of best-fit for all measurements on yearday 166, which has an $r^2 = 0.44$ and is significant in the 95% confidence interval. The alongshore diffusivity κ_y is equal to half of the slope of the best-fit line.

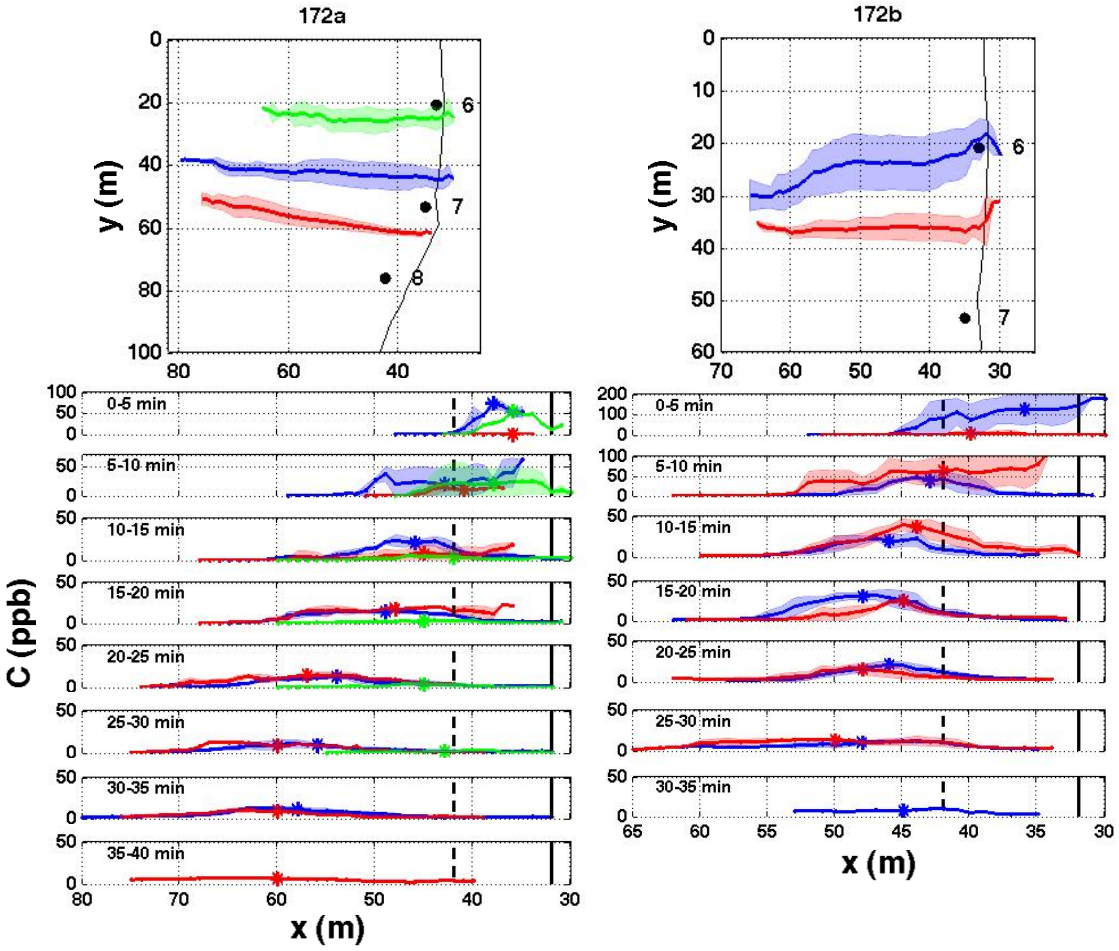

Figure 39. Example of data collected by swimmers for dye releases (left) 172a and (right) 172b. (top) Repeated cross-shore transects performed by different swimmers, and (bottom) the corresponding mean dye concentration profiles as a function of cross-shore distance for 5 minute time windows. Each color represents a different swimmer, and solid lines represent their mean cross-shore transect with ± one standard deviation represented by shaded areas. In bottom plots, solid vertical black lines represent approximate location of the shoreline, dashed vertical black lines represent approximate edge of surf zone, and asterisks indicate the first moment of the dye concentration profile representing the cross-shore location of the dye plume μ_x. The local coordinate system is used where positive is offshore and to the south.

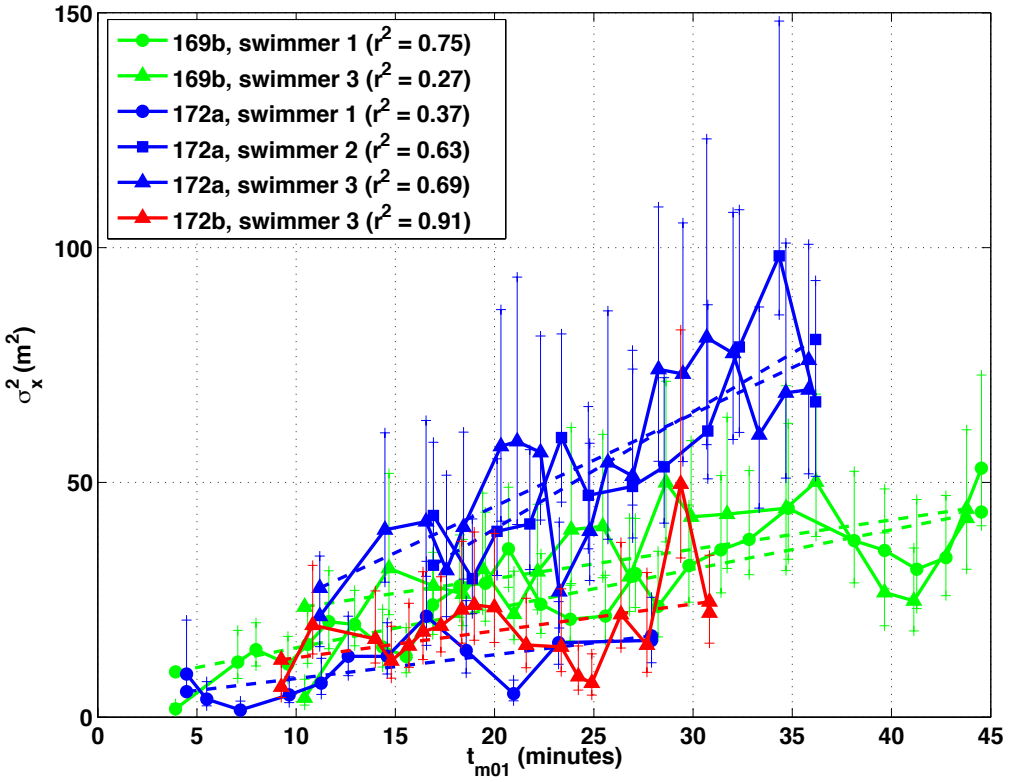

Figure 40. Dye dispersion outside the surf zone measured with the cross-shore swimmer transects as a function of weight-mean concentration time t_{m01}, with error bars representing the 95% confidence levels for the dispersion estimates for each transect. Solid lines of each color represent the dispersion estimates from the swimmer data for that dye release. Dashed lines of each color represent the lines of best-fit for the swimmer data for that dye release. Coefficients of determination are given for each swimmer, with all being significant in the 95% confidence interval. The cross-shore diffusivity κ_x outside the surf zone is equal to half of the slope of the best-fit line.

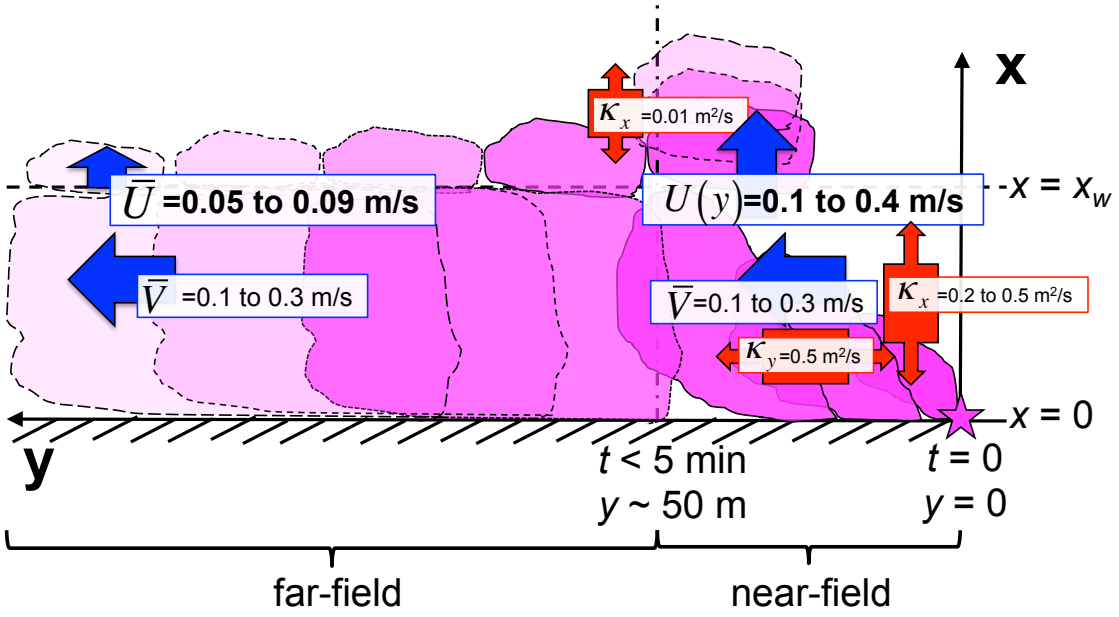

Figure 41. A conceptual diagram of the mixing and transport of dye (pink) that was observed on the sandy, steep beach at CRSB. Dye released as an instantaneous point source at the shoreline (star at $t = 0$, $x = 0$, $y = 0$), which is assumed to be rapidly vertically well-mixed, initially dispersed in two dimensions in the near-field ($t < 5$ min, $y < 50$ m), where advection and diffusion processes were important; then when the dye was completely mixed across the surf zone, the dye was transported due to advection in the far-field ($t > 5$ min, $y > 50$ m). In the near-field, the dye spread in the cross-shore (κ_x) by turbulent diffusion due to breaking waves and spread in the alongshore (κ_y) due to shear in the alongshore current, while also being advected downstream with the surfzone averaged alongshore current ($\bar{V}$) and also being advected offshore, resulting in a relatively large amount of cross-shore exchange ($U(y)$). In the far-field, the dye was advected downstream with the surfzone averaged alongshore current ($\bar{V}$) and the cross-shore transport leveled off to a constant ($\bar{U}$). Outside the surfzone ($x > x_w$), the dye moved as a constant patch, with a small amount of cross-shore spreading.

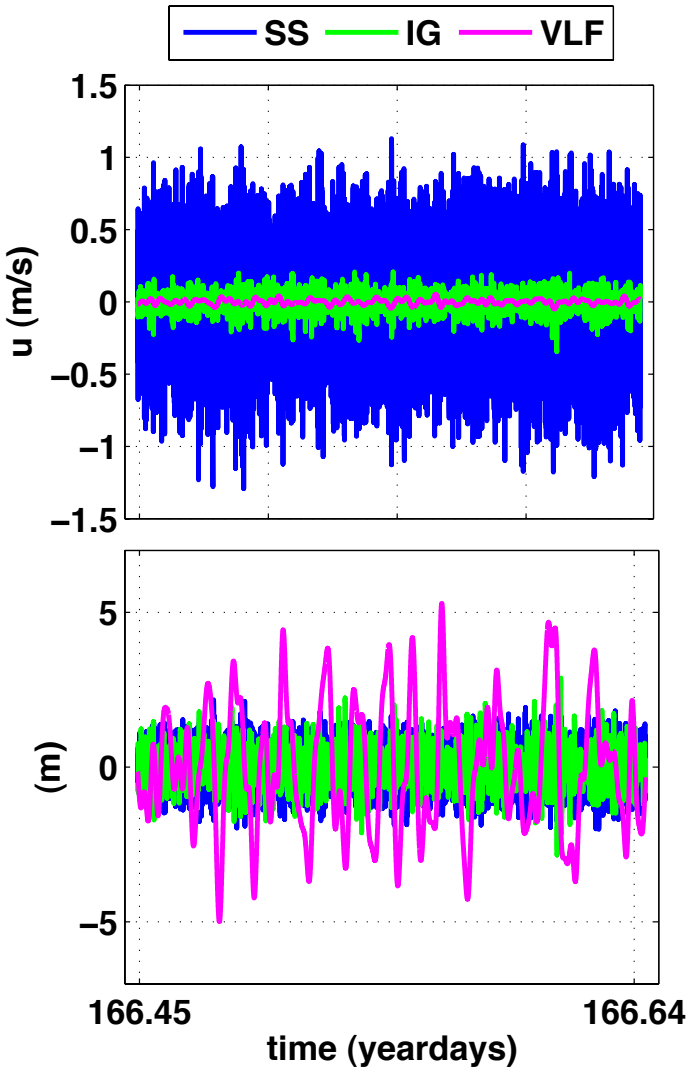

Figure 42. Frequency band-passed (top) cross-shore velocities and (bottom) excursion lengths computed from the time-integration of cross-shore velocity, measured at ADCP1 for the given frequency bands.

LIST OF REFERENCES

Aagard, T., B. Greenwood, and J. Nielsen, 1997: Mean currents and sediment transport in a rip channel. *Mar. Geol.*, **140**, 25–45.

Anderson, D.M., 2009: Approaches to monitoring, control and management of harmful algae blooms (HABs). *Ocean & Coastal Management*, **52**, 342–347.

Austin, M., T. Scott, J. W. Brown, J. A. Brown, J. MacMahan, G. Masselink, and P. Russell, 2010: Temporal observations of rip current circulation on a macro-tidal beach. *Cont. Shelf Res.*, **30**, 1149–1165.

Battjes, J. A., 1975: Modeling of turbulence in the surf zone, paper presented at Symposium on Modeling Technology. Am. Soc. of Civ. Eng., San Francisco, CA.

Boehm, A. B., 2003: Model of microbial transport and inactivation in the surf zone and application to field measurements of total coliform in northern Orange County, California. *Environ. Sci. Technol.*, **37**, 5511–5517.

Bowen, A. J., 1969: Rip currents: 1. Theoretical investigations. *J. Geophys. Res.*, **74**, 5467–5478.

Brander, R. W., and A. D. Short, 2000: Morphodynamics of a large-scale rip current system at Muriwai Beach, New Zealand. *Mar. Geol.*, **165**, 27–39.

Brander, R. W., and A. D. Short, 2001: Flow kinematics of low-energy rip current systems. *J. Coastal Res.*, **17**, 468–481.

Brown, J. W., J. H. MacMahan, A. J. H. M. Reniers, and E. B. Thornton, 2009: Surf zone diffusivity on a rip-channeled beach. *J. Geophys. Res.*, **114** (C11015), doi:10.1029/2008JC005158.

Brown, J. A., J. H. MacMahan, A. J. H. M. Reniers, and E. B. Thornton, 2014: Field observations of surf zone-inner shelf exchange on a rip-channeled beach. *J. Phys. Oceanogr.*, submitted.

Bruneau, N., B. Castelle, P. Bonneton, and R. Pedreros, 2009: Very low frequency motions of a rip current system: observations and modeling. *J. Coast. Res.*, **SI 56**, 1731–1735.

Castelle, B., H. Michallet, V. Marieu, F. Leckler, B. Dubardier, A. Lambert, C. Bemi, P. Bonneton, E. Barthelemy, and F. Bouchette, 2010: Laboratory experiment on rip current circulations over a moveable bed: Drifter measurements. *J. Geophys. Res.*, **115** (C12008), doi:10.1029/2010JC006343.

Clark, D. B., F. Feddersen, M. M. Omand, and R. T. Guza, 2009: Measuring fluorescent dye in the bubbly and sediment-laden surfzone. *Water, Air, Soil Pollut.*, **204**, 103–115.

Clark D. B., F. Feddersen, and R. T. Guza, 2010: Cross-shore surfzone tracer dispersion in an alongshore current. *J. Geophys. Res.*, **115** (C10035), doi:10.1029/2009JC005683.

Clark, D. B., F. Feddersen, and R. T. Guza, 2011: Modeling surf zone tracer plumes: 2. Transport and dispersion. *J. Geophys. Res.*, **116** (C11028), doi:10.1029/2011JC007211.

Clark, D. B., S. Elgar, and B. Raubenheimer, 2012: Vorticity generation by short-crested wave breaking. *Geophys. Res. Lett.*, **39** (L24604), doi:10.1029/2012GL054034.

Clarke, L. B., D. Ackerman, and J. Largier, 2007: Dye dispersion in the surfzone: Measurements and simple models. *Cont. Shelf Res.*, **27**, 650–669.

Cudaback, C. N., L. Washburn, and E. Dever, 2005: Subtidal inner-shelf circulation near Point Conception, California. *J. Geophys Res.*, **110** (C10007), 1–12.

Culliton, T. J., 1998: Population: distribution, density and growth. *NOAA's State of the Coast Report*, Natl. Oceanic and Atmos. Admin. (NOAA), Silver Spring, MD.

Dean, R. G., and R. A. Dalrymple, 1984: *Water Wave Mechanics for Engineers and Scientists*. World Scientific, 368.

Dronen, N., H. Karunarathna, J. Fredsoe, B. M. Sumer, and R. Deigaard, 2002: An experimental study of rip channel flow. *Coast. Eng.*, **45**, 223–238.

Falkowski, P. G., R. T. Barber, and V. Smetacek, 1998: Biogeochemical controls and feedbacks on ocean primary production. *Science*, **281**, 200–206.

Feddersen, F., 2007: Breaking wave induced cross-shore tracer dispersion in the surfzone: Model results and scalings. *J. Geophys. Res.*, **112** (C09012), doi:1029/2006JC 004006.

Feddersen, F., 2012: Scaling surf zone turbulence. *Geophys. Res. Lett.*, **39** (L18613), doi: 10.1029/2012GL052970.

Fewings, M., S. J. Lentz, and J. Fredericks, 2008: Observations of cross-shelf flow driven by cross-shelf winds on the inner continental shelf. *J. Phys. Oc.*, **38**,d2358–2378.

Fischer, H. B., E. J. List, R. C. Y. Koh, J. Imberger, and N. H. Brooks, 1979: *Mixing in Inland and Coastal Waters*. Academic Press, 483.

Fujimura, A., A. J. H. M. Reniers, C. B. Paris, A. L. Shanks, J. H. MacMahan, and S. G. Morgan, 2013: Slope-dependent Biophysical Modeling of Surf Zone Larva Transport. *Proc. Coastal Dynamics 2013*, Arcachon, France, Bordeaux University, 661-670.

Fujimura, A., A. J. H. M. Reniers, C. Paris, A. L. Shanks, J. H. MacMahan, and S. G. Morgan, 2014: Numerical simulations of larval transport into a rip-channeled surf zone. *Limnol. Oceanogr.*, **59** (4), 1434–1447.

Garcez Faria, A. F., E. B. Thornton, T. C. Lippmann, and T. P. Stanton, 2000: Undertow over a barred beach. *J. Geophys. Res.*, **105** (C7), 16999–17010.

Given, S., L. H. Pendleton, and A. B. Boehm, 2006: Regional public health cost estimates of contaminated coastal waters: A case study of gastroenteritis at Southern California beaches. *Environ. Sci. Technol.*, **40**, 4851–4858.

Grant, S. B., B. F. Sanders, A. B. Boehm, J. A. Redman, J. H. Kim, R. D. Mrse, A. K.Chu, M. Gouldin, C. D. McGee, N. A. Gardiner, B. H. Jones, J. Svejkovsky, G. V. Leipzig, and A. Brown, 2001: Generation of enterococci bacteria in a coastal saltwater marsh and its impact on surf zone water quality. *Environ. Science and Tech.*, **35** (12), 2407–2416.

Grant, S. B., J. H. Kim, B. H. Jones, S. A. Jenkins, J. Wasyl, and C. Cudaback, 2005: Surf zone entrainment, along-shore transport, and human health implications of pollution from tidal outlets. *J. Geophys. Res.*, **110**, C10025, doi:10.1029/2004JC002401.

Guza, R. T., and E. B. Thornton, 1980: Local and shoaled comparisons of sea surface elevations, pressures, and velocities. *J. Geophys. Res.*, **85** (C3), 1524–1530.

Haas, K. A., and I. A. Svendsen, 2002: Laboratory measurements of the vertical structure of rip currents. *J. Geophys. Res.*, **107** (C5), doi:10.1029/2001JC000911.

Haines, J. W., and A. H. Sallenger Jr., 1994: Vertical structure of mean cross-shore currents across a barred surf zone. *J. Geophys. Res.*, **99**, 14223–14242.

Haller, M. C., and R. A. Dalrymple, 2001: Rip current instabilities. *J. Fluid Mech.*, **433**, 161–192.

Haller, M. C., R. A. Dalrymple, and I. A. Svendsen, 2002: Experimental study of nearshore dynamics on a barred beach with rip channels. *J. Geophys. Res.*, **107**(C6), 3061, doi:10.1029/2001JC000955.

Harris, T. F. W., J. M. Jordan, W. R. McMurray, C. J. Verwey, and F. P. Anderson, 1963: Mixing in the surf zone. *Int. J. Air Water Pollut.*, **7**, 649–667.

Hasselmann, K., 1970: Wave-driven inertial oscillations. *Geophys Fluid Dyn.*, **1**, 463–502.

Hendrickson, J., and J. H. MacMahan, 2009: Diurnal sea breeze effects on inner-shelf cross-shore exchange. *Cont. Shelf Res.*, **29**, 2195–2206.

Herbers, T. H. C., S. Elgar, and R. T. Guza, 1999: Directional spreading of waves in the nearshore. *J. Geophys. Res.*, **104** (C4), 7683–7693.

Inman, D. L, F. J. Tait, and C. E. Nordstrom, 1971: Mixing in the surfzone. *J. Geophys. Res.*, **76**, 3493–3514.

Inman, D. L., and B. M. Brush, 1973: Coastal challenge. *Science*, **181**, 20–32.

Johnson, D., and C. Pattiaratchi, 2004a: Application, modeling and validation of surfzone drifters. *Coastal Eng.*, **51**, 455–471.

Johnson, D., and C. Pattiaratchi, 2004b: Transient rip currents and nearshore circulation on a swell-dominated beach. *J. Geophys. Res.*, **109** (C02026), doi:10.1029/2003JC001798.

Johnson , D., and C. Pattiaratchi, 2006: Boussinesq modeling of transient rip currents. *Coast. Eng.*, **53**, 419–439.

Kirincich, A. R., J. A. Barth, B. A. Grantham, B. A. Menge, and J. Lubchenco, 2005: Wind-driven inner-shelf circulation off central Oregon during summer. *J. Geophys. Res.*, **110** (C10S03), doi:10.1029/2004JC002611.

Kirincich, A. R., S. J. Lentz, and J. A. Barth, 2009: Wave-driven inner-shelf motions on the Oregon coast. *J. Phys. Oceanogr.*, **39**, 2942–2956.

Kundu, P. K., 1976: Ekman veering observed near the ocean bottom. *J. Phys. Oceanogr.*, **6**, 238–242.

Large, W. G., and S. Pond, 1981: Open Ocean Momentum Flux Measurements in Moderate to Strong Winds. *J. Phys. Oceanogr.*, **11**, 324–336.

Lentz, S. J., 1994: Current dynamics over the northern California inner shelf. *J. Phys. Oceanogr.*, **24**, 2461–2478.

Lentz, S. J., M. Fewings, P. Howd, J. Fredericks, and K. Hathaway, 2008: Observations and a model of undertow over the inner continental shelf. *J. Phys. Oceanogr.*, **38**, 2341–2357.

Long, J. W., and H. T. Ozkan-Haller, 2009: Low-frequency characteristics of wave group-forced vorticies. *J. Geophys. Res.*, **114** (C08004), doi:10.1029/2008JC004894.

MacMahan, J. H., 2001: Hydrographic surveying from a personal watercraft. *J. Surv. Eng.*, **127**, 12–24.

MacMahan, J. H., A. J. H. M. Reniers, E. B. Thornton, and T. P. Stanton, 2004a: Infragravity rip current pulsations. *J. Geophys. Res.*, **109** (C01033), doi:10.1029/2003JC002068.

MacMahan, J. H., A. J. H. M. Reniers, E. B. Thornton, and T. P. Stanton, 2004b: Surf zone eddies coupled with rip current morphology. *J. Geophys. Res.*, **109** (C07004), doi:10.1029/2003JC002083.

MacMahan, J. H., E. B. Thornton, T. P. Stanton, and A. J. H. M. Reniers, 2005: RIPEX: Observations of a rip current system. *Mar. Geol.*, **218**, 113–134.

MacMahan, J. H., E. B. Thornton, and A. J. H. M. Reniers, 2006: Rip current review. *Coast. Eng.*, **53**, 191–208.

MacMahan, J. H., J. W. Brown, and E. B. Thornton, 2009: Low-cost handheld Global Positioning System for measuring surf-zone currents. *J. Coast. Res.*, **25**, 744–754.

MacMahan, J. H., J. W. Brown, J. A. Brown, E. B. Thornton, A. J. H. M. Reniers, T. P. Stanton, M. Henriquez, E. Gallagher, J. Morrison, M. J. Austin, T. M. Scott, and N. Senechal, 2010a: Mean Lagrangian flow behavior on an open coast rip-channeled beach: A new perspective. *Mar. Geol.*, **268**, 1–15.

MacMahan, J. H., A. J. H. M. Reniers, and E. B. Thornton, 2010b: Vortical surf zone velocity fluctuations with *O*(10) min period. *J. Geophys. Res.*, **115** (C06007), doi:10.1029/2009JC005383.

Monismith, S. G., E. A. Cowen, H. M. Nepf, J. Magnaudet, and L. Thais, 2007: Laboratory observations of mean flows under surface gravity waves. *J. Fluid Mechanics*, **573**, 1310147.

Ohlmann, J. C., M. R. Fewings, and C. Melton, 2012: Lagrangian observations of inner-shelf motions in Southern California: Can surface waves decelerate shoreward-moving drifters just outside the surf zone? *J. Phys. Oceanogr.*, **42**, 1313–1326.

Peregrine, D. H., 1998: Surf zone currents. *Theor. Comput. Fluid Dyn.*, **10**, 295–309.

Putrevu, U., and I. A. Svendsen, 1993: Vertical structure of the undertow outside the surf zone. *J. Geophys. Res.*, **98** (C12), 22707–22716.

Reniers, A. J. H. M, J. A. Roelvink, and E. B. Thornton, 2004a: Morphodynamic modeling of an embayed beach under wave group forcing. *J. Geophys. Res.*, **109** (C01030), doi: 10.1029/2002JC001586.

Reniers, A. J. H. M., E. B. Thornton, T. P. Stanton, and J. A. Roelvink, 2004b: Vertical flow structure during Sandy Duck: observations and modeling. *Coastal Eng.*, **51**, 237–260.

Reniers, A. J. H. M., J. H. MacMahan, E. B. Thornton, and T. P. Stanton, 2007: Modeling of very low frequency motions during RIPEX. *J. Geophys. Res.*, **112** (C07013), doi:10.1029/2005JC003122.

Reniers, A. J. H. M., J. H. MacMahan, E. B. Thornton, T. P. Stanton, M. Henriquez, J. W. Brown, J. A. Brown, and E. Gallagher, 2009: Surf zone surface retention on a rip-channeled beach. *J. Geophys. Res.*, **114** (C10010), doi:10.1029/2008JC005153.

Reniers, A. J. H. M., J. H. MacMahan, F. J. Beron-Vera, and M. J. Olascoaga, 2010: Rip-current pulses tied to Lagrangian coherent structures. *Geophys. Res. Lett.*, **37** (L05605), doi:10.1029/2009GL041443.

Rutherford, J. C., 1994: *River Mixing*. Wiley, 347.

Schiff, K. C., M. J. Allen, E. Y. Zeng, and S. M. Bay, 2000: Southern California. *Mar. Pollut. Bull.*, **41** (1-6), 76–93.

Shepard, F. P., 1936: Undertow, rip tide, or "rip current". *Science*, **84**, 181–182.

Shepard, F. P., K. O. Emery, and E. C. LaFond, 1941: Rip currents: a process of geological importance. *J. Geol.*, **4**, 337–269.

Shepard, F. P., and D. L. Inman, 1950: Nearshore circulation related to bottom topography and wave refraction. *Eos Trans. AGU*, *31*, 555–565.

Sheremet, A., R. T. Guza, S. Elgar, and T. H. C. Herbers, 2002: Observations of nearshore infragravity waves: Seaward and shoreward propagating components. *J. Geophys. Res.,* **107** (C8), doi:10.1029/2001JC000970.

Smart, P. L., and I. M. S. Laidlaw, 1977: Evaluation of some fluorescent dyes for water tracing. *Water Resour. Res.*, **13**, 15–33.

Smith, J. A., 2006: Wave-current interactions in finite depth. *J. Phys. Oceanogr.*, **36**, 1403–1419.

Smith, J. A., and J. L. Largier, 1995: Observations of nearshore circulation-rip currents. *J. Geophys. Res.*, **100**, 10967–10975.

Sonu, C. J., 1972: Field observations of nearshore circulation and meandering currents. *J. Geophys. Res.*, **77**, 3232–3247.

Spydell, M., F. Feddersen, R. Guza, and W. Schmidt, 2007: Observing surf-zone dispersion with drifters. *J. Phys. Oceanogr.*, **37**, 2920–2939.

Spydell, M. S., and F. Feddersen, 2012: A Lagrangian stochastic model of surf zone drifter dispersion. *J. Geophys. Res.*, **117** (C03041), doi:10.1029/2011JC007701.

Stokes, G. G., 1847: On the theory of oscillatory waves. *Trans. Cambridge Philos. Soc.*, **8**, 441–455.

Svendsen, I. A., 1984: Mass flux and undertow in a surf zone. *Coast. Eng.*, **8**, 347–365.

Svendsen, I., and U. Putrevu, 1994: Nearshore mixing and dispersion. *Proc. R. Soc. London, Ser. A.*, **545**, 561–576.

Talbot, M. M. B., and G. C. Bate, 1987: Rip current characteristics and their role in the exchange of water and surf diatoms between the surf zone and inner shelf. *Estuarine, Coastal Shelf Sc.*, **25** (6), 707–720.

Taylor, G. I., 1922: Diffusion by continuous movements. *Proc. London Math. Soc.*, **20**, 196–212.

Thornton, E. B., and R. T. Guza, 1982: Energy saturation and phase speeds measured on a natural beach. *J. Geophys. Res.*, **87**, 9499–9508.

Thornton, E. B., and R. T. Guza, 1983: Transformation of wave height distribution. *J. Geophys. Res.*, **88**, 5925–5938.

Uchiyama, Y., J. C. McWilliams, A. F. Shchepetkin, 2010: Wave-current interaction in an oceanic circulation model with a vortex-force formalism: Application to the surf zone. *Oc. Model.*, **34**, 16–35.

Wright, L. D., 1982: Field observations of long-period surf zone oscillations in relation to contrasting beach morphologies. *Aust. J. Mar. Freshwater Res.*, **33**, 181–201.

Yu, J., and D. N. Slinn, 2003: Effects of wave-current interaction on rip currents. *J. Geophys. Res.*, **108** (C3), 3088, doi:10.1029/2001JC001105.

Xu, Z., and A. J. Bowen, 1994: Wave- and wind-driven flow in water of finite depth. *J. Phys. Oceanogr.*, **24**, 1850–1866.

THIS PAGE INTENTIONALLY LEFT BLANK

INITIAL DISTRIBUTION LIST

1. Defense Technical Information Center
   Ft. Belvoir, Virginia

2. Dudley Knox Library
   Naval Postgraduate School
   Monterey, California